AD-A161 513 TWO METHODS FOR VISCOUS AND INVISCID FREE-WAKE ANALYSIS 1/2
OF HELICOPTER ROT..(U) BOSTON UNIV MA CENTER FOR
COMPUTATIONAL AND APPLIED DYNAMICS.. L MORINO ET AL.
UNCLASSIFIED AUG 85 CCAD-TR-85-2 ARO-19797.3-EG F/G 20/4 NL

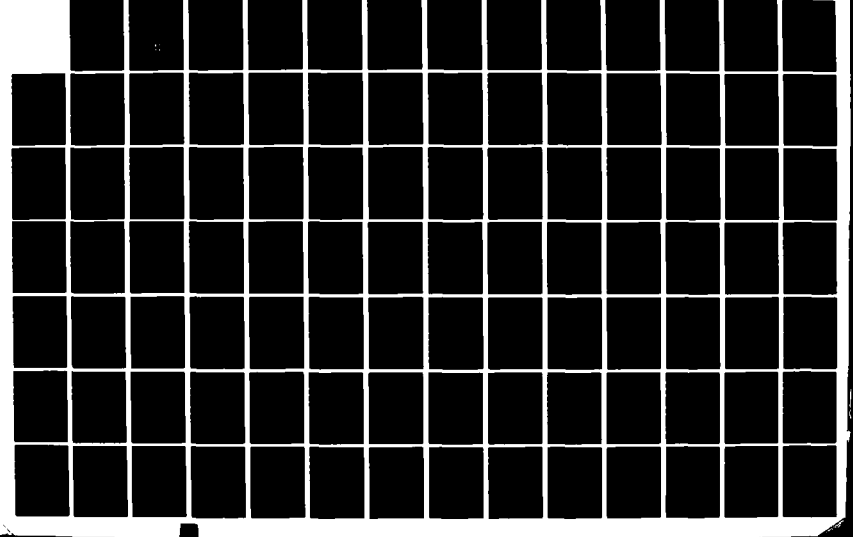

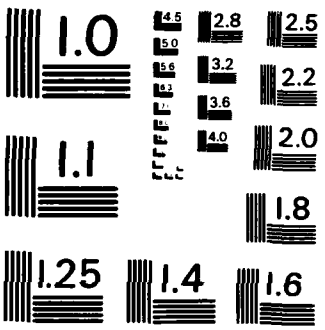

MICROCOPY RESOLUTION TEST CHART
NATIONAL BUREAU OF STANDARDS - 1963 - A

BOSTON UNIVERSITY

TWO METHODS FOR VISCOUS AND INVISCID FREE-WAKE ANALYSIS OF HELICOPTER ROTORS

by

L. Morino and B. Bharadvaj

DEPARTMENT OF AEROSPACE ENGINEERING
COLLEGE OF ENGINEERING
BOSTON, MASSACHUSETTS

MASTER COPY - FOR REPRODUCTION PURPOSES

UNCLASSIFIED
SECURITY CLASSIFICATION OF THIS PAGE (When Data Entered)

REPORT DOCUMENTATION PAGE	READ INSTRUCTIONS BEFORE COMPLETING FORM
1. REPORT NUMBER: ARO 19797.3-EG	2. GOVT ACCESSION NO.: N/A (AD A161 513)
	3. RECIPIENT'S CATALOG NUMBER: N/A
4. TITLE (and Subtitle): Two Methods for Viscous and Inviscid Free-Wake Analysis of Helicopter Rotors	5. TYPE OF REPORT & PERIOD COVERED: Final Report 2/15/83 to 4/14/85
	6. PERFORMING ORG. REPORT NUMBER: CCAD-TR-85-2
7. AUTHOR(s): L. Morino and B. Bharadvaj	8. CONTRACT OR GRANT NUMBER(s): DAAG29-83-K-0050
9. PERFORMING ORGANIZATION NAME AND ADDRESS: Boston University, Boston, MA 02215	10. PROGRAM ELEMENT, PROJECT, TASK AREA & WORK UNIT NUMBERS: N/A
11. CONTROLLING OFFICE NAME AND ADDRESS: U. S. Army Research Office, Post Office Box 12211, Research Triangle Park, NC 27709	12. REPORT DATE: August 1985
	13. NUMBER OF PAGES: 131
14. MONITORING AGENCY NAME & ADDRESS (if different from Controlling Office)	15. SECURITY CLASS. (of this report): Unclassified
	15a. DECLASSIFICATION/DOWNGRADING SCHEDULE

16. DISTRIBUTION STATEMENT (of this Report)

Approved for public release; distribution unlimited.

17. DISTRIBUTION STATEMENT (of the abstract entered in Block 20, if different from Report)

NA

18. SUPPLEMENTARY NOTES

The view, opinions, and/or findings contained in this report are those of the author(s) and should not be construed as an official Department of the Army position, policy, or decision, unless so designated by other documentation.

19. KEY WORDS (Continue on reverse side if necessary and identify by block number)

Helicopter-Rotor Aerodynamics, Free-Wake Analysis, Wake Dynamics, Scalar-Vector Potential Decomposition, Time Domain Analysis, Trailing Edge, Steady State.

20. ABSTRACT (Continue on reverse side if necessary and identify by block number)

Two integral equation methods for the free wake analysis of helicopter rotors (for potential and rotational flows, respectively) have been presented. The rotational flow formulation is based upon Helmholtz scalar/vector-potential decomposition. The advantages of the rotational flow formulation over the potential flow formulation have been discussed. The

DD FORM 1 JAN 73 1473 EDITION OF 1 NOV 65 IS OBSOLETE

UNCLASSIFIED
SECURITY CLASSIFICATION OF THIS PAGE (When Data Entered)

numerical equivalence of the two methods have been demonstrated. It should be noted that (whereas in the potential flow problem viscosity may be introduced only as artificial viscosity) in the rotational-flow formulation the presence of viscosity is consistent with the formulation. Therefore, this formulation is applicable to the solution of time-averaged Navier-Stokes equations: in particular, a simplified thin-wake analysis with an elementary eddy-viscosity model for turbulence is used in the numerical applications.

Results obtained indicate that, for appropriate values of emperical parameters (e.g., thickness of the wake at the trailing edge, eddy Reynolds number, intensity of the far wake sink disk) the solution reaches steady-state, with the wake converging to a smooth geometry and the sectional lift distribution in good agreement with the numerical results of Rao and Schatzle and, indirectly, the experimental ones of Bartsch. Ground effect results are also included. However, a sensitivity analysis over the effects of these parameters indicates that the results were not always as good. For some values of these parameters, the solution may reach a steady state but the sectional lift distribution does not necessarily show a marked improvement as the wake rolls up. For other values of these parameters, the solution may be completely unstable. The main reason for this sensitivity to the values of the empirical parameters is attributed to the fact that concentrated vortices are used for the discretization of the formulation. Additional work is needed to address these issues.

Analysis of the computer times indicates that the new formulation presented here (for rotational flows) has much broader applicability than the formulation for potential flows, while requiring approximately the same amount of computer time.

ACKNOWLEDGEMENTS

This work was supported by contract DAAG29-83-K-0050 from U.S. Army Research Office, Research Triange Park to Boston University. Dr. Robert E. Singleton acted as the technical monitor for this contract. Dr. Chee Tung, Aeromechanics Laboratory, USARTL (AVRADCOM), Ames Research Center, Moffet Field, CA and Mr. John C. Wilson, Structures Laboratory, USARTL (AVRADCOM), NASA Langley Research Center, Hampton, VA acted as Scientific Liaison representatives on this contract. The authors wish to thank Dr. Singleton, Dr. Tung and Mr. Wilson, as well as Dr. Slobodan Sipcic of Sarajevo University, for the valuable suggestions they offered during this project. They also with to thank Keith B. Meredith, Sonia Gulbankian, Masoud Mohammadi, John R. Zaleski, and Mark J. Downey for their help in generating the numerical results and editing this report.

A-1

LIST OF SYMBOLS

$\mathbf{a}_\alpha$ = base vectors on a surface

$\mathbf{a}^\alpha$ = contravariant base vectors on a surface

$\mathbf{A}$ = vector potential

c = chord

C_T = thrust coefficient

$E(\mathbf{x})$ = see Eq. 3.21

$\mathbf{g}_\alpha$ = material base vectors

$\mathbf{g}^\alpha$ = material contravariant base vectors

$\mathbf{n}$ = normal to σ

p = pressure

$\mathbf{r} = \mathbf{y} - \mathbf{x}$

$r = \mathbf{y} - \mathbf{x}$

R = rotor radius

t = time

$\mathbf{v}$ = velocity

x_1, x_2, x_3 = space coordinates

$\mathbf{x}$ = point having coordinates x_1, x_2, x_3

$\mathbf{y}$ = dummy point of integration

γ = surface distribution of vorticity

Γ = vortex intensity

δ_α^β = Kronecker delta (1 if $\alpha = \beta$, and 0 otherwise)

$\Delta\phi$ = discontinuity of ϕ across the wake

ρ = density

σ_{bw} = surface surrounding body and wake

σ_b = surface of body

σ_w = surface of wake

φ = velocity potential

ϕ = scalar potential

v = normal wash

$\boldsymbol{\omega}$ = vorticity

Ω = angular velocity

Special Symbols

∇ = grad

$\nabla\cdot$ = div

$\nabla\times$ = curl

∇^2 = Laplacian

∇_y = gradient with respect to **y**

$\nabla_y\cdot$ = divergence with respect to **y**

$\nabla_y\times$ = curl with respect to **y**

∇_y^2 = Laplacian with respect to **y**

∇_t = surface gradient

$\frac{\partial}{\partial n} = \mathbf{n}\cdot\nabla_y$

Subscripts

b = body

te = trailing edge

w = wake

∞ = infinity

TABLE OF CONTENTS

SECTION 1

INTRODUCTION

1.1 Motivation and Objectives

Two computational methods for the free wake aerodynamic analysis of a helicopter rotor are presented in this report.

The availability of these methods considerably enhances the computational capability in this area. This capability is needed in many aspects of the helicopter design, such as performance, structural analysis, and evaluation of generalized forces for flutter analysis.

In all of these cases the wake geometry is an essential aspect of the problem. The approaches used in the past can be classified under three broad groups:

A. classical-wake analysis

B. generalized-wake analysis

C. free-wake analysis

In the classical rotor-wake formulation, the wake for a hovering rotor is described as a spiral (helicoidal) surface which is obtained from the assumption of uniform vertical flow. This method is not only limited to the hovering case, but is also not sufficiently accurate for the aerodynamic analysis of helicopter rotors.

On the other hand, a generalized-wake analysis consists in an analytical description of the wake geometry in terms of a few parameters which are evaluated by interpolation of experimental results. The generalized-wake analysis may be used for both hover and forward flight, yields accurate results and is not necessarily more expensive than the classical-wake analysis. However, currently it requires the use of expensive wind tunnel experiments for the generation of the generalized-wake model.

Finally, the free-wake analysis consists in calculating, step-by-step, the

location of a wake point at a given time step from its location at the preceding time step: the drawback with this approach is that the free-wake analysis is quite expensive in terms of computer time. However, it could be used, instead of the much more expensive wind-tunnel experiments in order to generate a generalized wake model for hover, forward-flight and maneuvering.

1.2 Relation of Work with State of the Art

Two methods for the free-wake analysis of rotors in incompressible flows are presented here. The first one, for potential flows is an extension of the work by Morino, Kaprielian and Sipcic (Refs. 1, 2 and 3). The wake is treated as a doublet layer (fully equivalent to a zero-thickness vortex layer). By definition of potential flows, the formulation is limited to zero-thickness wake. [Artificial viscosity is often introduced as a numerical approximation to eliminate numerical instabilities, but is difficult to justify from a theoretical point of view since the wake is treated inconsistently: as zero-thickness in the integral equation for the evaluation of the potential on the surface, and as finite-thickness in the evaluation of the velocity field]. Therefore, the method is not expected to yield good results (at least without the use of some ad-hoc numerical scheme, such as artificial vorticity) in those cases for which the zero-thickness assumption is too drastic. Examples include: a rotor in ground effect (which is the specific problem addressed here), but also wake-fuselage interaction, blade-vortex interaction, blade slapping and tip vortex breakdown.

The second method presented here addresses this issue: distributed vorticity is allowed in the flow field. In this case the flow field is not potential and the first method is not applicable. The second method is based on the Helmholtz decomposition of a vector field into a solenoidal part and al irrotational part. Special attention is given in this report to the relationship between the two methods. In particular it is shown how the rotational-flow approach relates to the potential-flow approach for the case of inviscid initially-irrotational flows. It is also shown how the method can be extended to study viscous flows: this yields an understanding of when, why and how Euler equations are a good approximation to Navier Stokes equations.

A detailed summary of this report is given in Section 1.3 after a review of the state of the art. We feel that the unsteady analysis is the main strength of the methods presented here over other existing methods. Therefore particular emphasis is given in this review to the unsteady-flow analysis.

An excellent review on aerodynamic technology for advanced rotorcraft was presented by Landgrebe, Moffitt, and Clark in Refs. 4 and 5. Additional reviews on the specific issues of rotor wakes are presented in Refs. 1 and 6-10. Therefore only works which are particularly relevant to the objective and the motivation of this work are included in this brief review, which is not to be considered, by any means, complete. Also, only works dealing with free-wake analysis of rotors in incompressible flows are considered here. (The effects of compressibility are dealt with in a separate report (Ref. 11) and therefore not included in this review. A review on the use of panel methods for rotor aerodynamic analysis, also not included here, may be found in Ref. 1.)

The essence of the state of the art in incompressible rotor aerodynamics is briefly summarized here. As mentioned above, the various aerodynamic analyses of the rotor fall into one of the three following types:

A. Classical wake, i.e., a wake geometry described by a helicoidal spiral with the pitch obtained by assuming uniform flow.

B. Generalized wake, i.e., a wake geometry obtained by interpolating experimental data in terms of a few parameters.

C. Free wake, i.e., a wake geometry obtained computationally as an integral part of the solution.

Generalized-wake models for predicting the geometry of the rotor wake were developed from experimental data by Landgrebe (Ref. 12 and 13), Crews, Hohenemser and Ormiston (Ref. 14) and Kocurek (Ref. 15). Landgrebe's model was used by Rao and Schatzle (Ref. 7) in their lifting-surface theory: their work is particularly significant here because it shows that whereas the classical-wake formulation is not sufficiently accurate, a considerable improvement in the comparison with experimental results of Ref. 16 can be obtained simply by using Landgrebe's generalized-wake geometry. Free-wake analyses are considered for instance by Scully (Ref. 17), Pouradier and Horowitz (Ref. 18) and Summa (Refs. 6, 19 and 20). All these works indicate that the algorithms used are unstable unless special constraints (such

as specified contraction ratio or over-relaxation) are introduced. Another important issue is the one of simplified algorithms which can be used for instance to model the far wake: several models are available for the hover case (see e.g., Refs. 19-21). However none of these models is applicable to the case of the arbitrary motion considered in this report. The fast-wake formulation which Miller (Ref. 21.) introduced for modelling the whole wake is also an excellent candidate for the far-wake: this formulation could be extended to forward flight or more arbitrary motion. Additional works on wake dynamics which should be mentioned include those by Kandil (see e.g., Ref. 8) and Morino and Suciu (Refs. 9 and 10). The formulation of Refs. 9 and 10 is extended to helicopter rotors in Ref. 1 and is the basis of the potential methods presented here.

1.3 Summary of Work

As mentioned above, this report includes two different approaches to study the flow field around a helicopter rotor. The first one (see Section 2) is for potential flows and is similar to that of Refs. 1-3. [The discussion of the boundary condition on the wake and of the trailing edge conditions are more rigorous than that of Refs. 1-3]. This formulation is based upon an integral equation developed by Morino (Refs. 22-240) with applications to aircraft (Refs. 25-27) and rotors (Refs. 28-29). The wake is treated as a doublet layer (fully equivalent to a zero-thickness vortex layer).

The second formulation, presented in Section 3 is for incompressible rotational flows. The formulation is based on Helmholtz scalar/vector-potential decomposition (Refs. 30-32) and yields the following computational procedure: given the vorticity distribution at time t, evaluate the velocity according to Biot and Savart law, then use the scalar-potential contribution to satisfy the normal boundary conditions, and finally use the vorticity evolution equation to evaluate the vorticity at time $t - dt$. A novel approach (based on the use of material curvilinear coordinates) is used to solve the vorticity evolution equation with emphasis on a thin wake approximation. The formulation is presented for both inviscid and viscous flows (with a very simple eddy-viscosity modelling for turbulence).

Section 4 deals with the comparison between the two formulations. In particular, it is shown how in the limiting case of zero-thickness wake. the rotational-flow formulation reduces to a potential-flow formulation closely related to that of Section 2.

Finally, numerical results are presented in Section 5, and conclusions in Section 6.

SECTION 2

POTENTIAL-FLOW FORMULATION

A general formulation for the analysis of potential flows is presented in this section. Special emphasis is given to the issues related to the wake transport, which were first introduced in Ref. 1. This section includes some refinements with respect to the formulation of Ref. 1 (i.e., the formulation of the wake condition and of the trailing edge conditions) and is included here essentially for the sake of completeness. The differential formulation (including a detailed analysis of the wake condition) is presented first (Sections 2.1 to 2.4), followed by the integral formulation (Sections 2.5 to 2.9). The wake generation (trailing edge conditions) is discussed in Section 2.10, and the conditions at infinity are examined in Section 2.11.

2.1 Governing Equations

In this report we will assume that the frame of reference is connected with the undisturbed air. We also assume that the fluid is inviscid and incompressible. Hence, the phenomenom is governed by the continuity equation for incompressible fluids (conservation of mass)

$$\nabla \cdot \mathbf{v} = 0 \tag{2.1}$$

(where $\mathbf{v}$ is the velocity vector) and by Euler's equations (conservation of momentum)

$$\frac{D\mathbf{v}}{Dt} = -\frac{1}{\rho} \nabla p \tag{2.2}$$

where p is the pressure, ρ the density (constant for incompressible fluid), and t the time, whereas

$$\frac{D}{Dt} = \frac{\partial}{\partial t} + \mathbf{v} \cdot \nabla \tag{2.3}$$

is the material or substantial derivative. Equations 2.1 and 2.2 form a system of four partial differential equations in four unknowns v_1, v_2, v_3, and p.

In order to complete the formulation of the problem, the boundary conditions at infinity, on the body and on the wake must be obtained. Recalling that the frame of reference has been assumed to be connected with the undisturbed air, the boundary conditions at infinity are

$$\mathbf{v} = 0 \tag{2.4}$$

and

$$p = p_\infty \tag{2.5}$$

On the surface of the body (rotor in our case) we assume that the surface is impermeable. This implies that the normal components of the velocity $\mathbf{v}$ of the fluid, and of the velocity $\mathbf{v}_b$ of the body coincide at point $\mathbf{x}$ on the surface σ_b of the body:

$$(\mathbf{v} - \mathbf{v}_b) \cdot \mathbf{n} = 0 \qquad (\text{for } \mathbf{x} \text{ on } \sigma_b) \tag{2.6}$$

where $\mathbf{n}$ is the normal to σ_b at $\mathbf{x}$.

The boundary conditions on the wake are discussed in Section 2.3 after introducing the concept of potential wake.

2.2 Wakes in Irrotational Flows

The basis of the discussion on wake dynamics is the well known Kelvin's theorem which states that the circulation

$$\Gamma = \oint_C \mathbf{v} \cdot d\mathbf{x} \tag{2.7}$$

over a material contour C (i.e., a contour which is made up of material particles) remains constant in time ($d\Gamma/dt = 0$). As shown for instance in Ref. 30, this theorem is an immediate consequence of the definition of Γ, of Euler equations (Eq. 2.1) and of the fact that the density is constant (or, in general, that the fluid is barotropic).

Next assume that the flow field is irrotational at time 0. Then according to Stokes theorem

$$\oint_C \mathbf{v} \cdot d\mathbf{x} = \iint_\sigma \nabla \times \mathbf{v} \cdot \mathbf{n} \, d\sigma(\mathbf{x}) \tag{2.8}$$

(where C is the contour of σ), Γ is initially equal to zero for any contour C connected with a surface σ fully inside the fluid volume. Hence, for all these contours, Γ remains identically equal to zero. This implies that

$$\nabla \times \mathbf{v} = 0 \tag{2.9}$$

for almost all the fluid points at all times: the only points to be excluded are those material points which come in contact with the solid boundaries (since a contour surrounding any of these points in general is not completely inside the fluid region and therefore Kelvin's theorem cannot be used in this case). In order to simplify the discussion of this issue, let us focus on the case of an isolated blade with a sharp trailing edge and consider only those flows for which the fluid leaves the surface of the blade at the trailing edge (this issue is further discussed later in Section 2.9). These flows are called *attached flows*. For these flows the points which come in contact with the rotor are only those emanating from the trailing edge and therefore form a surface: such a surface is called the *wake*. Equation 2.9 does not apply to points of the wake. [Note that if the trailing edge is fixed with respect to the frame of reference, the wake is a *streak surface* (Ref. 32). Since the trailing edge, in general, moves we say that the wake is a *generalized streak surface*.]

We may conclude that for an inviscid and incompressible fluid, if a flow field is initially irrotational, it remains irrotational at all times except for those points which come in contact with the surface of the body. If the flow is attached (i.e., by definition if the fluid leaves the body only at the points of a line which is called the *trailing edge*) then the locus of these points forms a generalized streak surface which is called a wake.

It may be worth emphasizing that the result of zero-thickness wake is a direct consequence of the hypothesis of incompressible (in general, barotropic) inviscid flow and of the definition of attached flows, and does not require additional assumptions (the assumption of initially irrotational flows is not essential for the thickness of the wake to be zero).

2.3 Boundary Conditions on Wake

In order to be able to solve the mathematical problem, we need a bound-

ary condition on the wake. This condition may be obtained from the result shown above that the wake has zero thickness, and hence, is a surface of discontinuity; therefore, the principles of conservation of mass and momentum across a surface of discontinuity may be used to obtain the wake boundary conditions.

Let subscripts u and l indicate the two sides of the wake, let $\mathbf{n}$ be the outward normal on side u and let

$$\Delta f = f_u - f_l \tag{2.10}$$

denote the discontinuity of any function f across the wake surface. [For the classical wing-wake, u and l correspond to upper and lower sides respectively, $\mathbf{n}$ is the upper normal and $\Delta f = f_{upper} - f_{lower}$. In the case of a rolled-up rotor wake, it is still convenient to use the subscripts u and l: they should be understood to mean the sides of the wake that are the continuation of the upper and lower sides of the blade respectively.]

The equations of conservation of mass and momentum across a possible surface of discontinuity (e.g., a shock wave or a wake) are given by (Ref. 30)

$$\Delta\, \rho(v_n - v_s) = 0 \tag{2.11}$$

$$\Delta\, \rho(v_n - v_s)\mathbf{v} - p\mathbf{n} = \rho(v_n - v_s)\Delta\mathbf{v} + \Delta p\, \mathbf{n} = 0 \tag{2.12}$$

where $v_n = \mathbf{v} \cdot \mathbf{n}$ is the normal component of the velocity $\mathbf{v}$, and v_s is the velocity of the surface (by definition, in the direction of the normal $\mathbf{n}$). Note that

$$\Delta v_s = 0 \tag{2.13}$$

In the case of incompressible flows, $\Delta\rho = 0$ and hence, Eqs. 2.11 and 2.13 yield

$$\Delta v_n = 0 \tag{2.14}$$

and the only possible surfaces of discontinuity are waves. (Surfaces of discontinuity with $\Delta v_n \neq 0$ are called shocks, and are not possible in incompressible flows). Then the normal component of Eq. 2.12 yields

$$\Delta p = 0 \tag{2.15}$$

Hence using Eq. 2.15, Eq. 2.12 reduces to

$$\rho(v_n - v_s)\Delta \mathbf{v} = 0 \tag{2.16}$$

This implies either $\Delta \mathbf{v} = 0$ (i.e., the surface under consideration is not a surface of discontinuity) or, if there is a discontinuity (i.e., on a wake surface),

$$v_n = v_s \tag{2.17}$$

which indicates that the fluid does not penetrate the surface of the wake.

2.4 Potential Flow; Potential Wakes

Next consider a well known theorem from vector field theory which states that if a vector field $\mathbf{v}$ is irrotational, then there exists a function, φ, called velocity potential such that

$$\mathbf{v} = \nabla \varphi \tag{2.18}$$

If the region is simply connected (as in the case considered here), then φ is single-valued.

Hence, the results of Section 2.3 may be restated as follows: for an inviscid incompressible fluid, a flow field which is attached and initially irrotational is potential at all times and at all points, except at the points of wake.

If the flow is potential, i.e., if $\mathbf{v}$ is given by Eq. 2.18, Eq. 2.1 may be rewritten as

$$\nabla^2 \varphi = 0 \tag{2.19}$$

where ∇^2 is the Laplacian operator.

Similarly, Eq. 2.4 may be rewritten as

$$\varphi = 0 \qquad (\text{for } \mathbf{x} \text{ at } \infty) \tag{2.20}$$

whereas Eq. 2.6 becomes

$$\frac{\partial \varphi}{\partial n} = \mathbf{v}_t \cdot \mathbf{n} \qquad (\text{for } \mathbf{x} \text{ on } \sigma_b) \tag{2.21}$$

Furthermore, Eq. 2.2 may be integrated to yield Bernoulli's theorem

$$\frac{\partial \varphi}{\partial t} - \frac{1}{2}\nabla \varphi^2 - \frac{p}{\rho} = \frac{1}{\rho} p_\infty \tag{2.22}$$

(taking the gradient of Eq. 2.22 and using Eq. 2.18 one obtains Eq. 2.2: the constant on the right hand side of Eq. 2.22 is obtained from the boundary conditions at infinity.)

Next, in order to obtain a convenient condition on the wake, combine Bernoulli's theorem (Eq. 2.22) with the wake condition, $\Delta p = 0$ (Eq. 2.15). This yields

$$\frac{\partial \varphi_u}{\partial t} - \frac{\partial \varphi_l}{\partial t} - \frac{1}{2}(\mathbf{v}_u \cdot \mathbf{v}_u - \mathbf{v}_l \cdot \mathbf{v}_l) = 0 \tag{2.23}$$

that is,

$$\frac{\partial \varphi_u}{\partial t} - \frac{\partial \varphi_l}{\partial t} + \frac{1}{2}(\mathbf{v}_u - \mathbf{v}_l) \cdot (\mathbf{v}_u - \mathbf{v}_l) = \frac{\partial \varphi_u}{\partial t} - \frac{\partial \varphi_l}{\partial t} + \frac{1}{2}(\mathbf{v}_u - \mathbf{v}_l) \cdot \Delta \mathbf{v} = 0 \tag{2.24}$$

[Note that Eq. 2.14 implies in particular that only the tangential components of the velocity are discontinuous across the surface of the wake, that is (using local coordinates ξ^1, ξ^2 and ξ^3 with ξ^1 and ξ^2 on the surface of the wake and ξ^3 in the direction of the normal $\mathbf{n}$)

$$\begin{aligned}\Delta \mathbf{v} &= \Delta(v_1 \mathbf{g}^1 - v_2 \mathbf{g}^2 + v_3 \mathbf{n}) = \Delta(v_1 \mathbf{g}^1 + \Delta v_2 \mathbf{g}^2) \\ &= \Delta\left(\frac{\partial \varphi}{\partial \xi^1}\mathbf{g}^1 + \frac{\partial \varphi}{\partial \xi^2}\mathbf{g}^2\right) = \Delta \frac{\partial \varphi}{\partial \xi^1}\mathbf{g}^1 - \Delta \frac{\partial \varphi}{\partial \xi^2}\mathbf{g}^2 \\ &= \frac{\partial \Delta\varphi}{\partial \xi^1}\mathbf{g}^1 - \frac{\partial \Delta\varphi}{\partial \xi^2}\mathbf{g}^2 = \nabla_t(\Delta\varphi)\end{aligned} \tag{2.25}$$

where v_α are the covariant components of $\mathbf{v}$, whereas $\mathbf{g}^\alpha$ are the contravariant base vector, related to the covariant base vector

$$\mathbf{g}_\alpha = \frac{\partial \mathbf{x}}{\partial \xi^\alpha} \tag{2.26}$$

by the relationship $\mathbf{g}_\alpha \cdot \mathbf{g}^\beta = \delta_\alpha^\beta$ where δ_α^β is the Kronecker delta. In addition

$$\nabla_t f = \frac{\partial f}{\partial \xi^1}\mathbf{g}_1 + \frac{\partial f}{\partial \xi^2}\mathbf{g}_2 \tag{2.27}$$

is the *tangential portion* of the vector ∇f. It is important to note that $\nabla(\Delta\varphi)$ is a meaningless expression since $\Delta\varphi$ is defined only over the surface of the wake.]

Also, it is possible to write

$$\frac{\partial \varphi_u}{\partial t} - \frac{\partial \varphi_l}{\partial t} = \left(\frac{\partial}{\partial t} + v_n \frac{\partial}{\partial n}\right)\Delta\varphi \tag{2.28}$$

The right hand side of Eq. 2.28 is meaningful (time derivative for an observer moving with the surface in the direction of the normal to the surface), even though $\partial\Delta\varphi/\partial t$ and $\partial\Delta\varphi/\partial n$ individually are not.

Therefore, introducing the concept of a wake point $\mathbf{x}_w$ as a point having velocity

$$\mathbf{v}_w = \frac{1}{2}(\mathbf{v}_u + \mathbf{v}_l) \tag{2.29}$$

and using Eqs. 2.25 and 2.28, Eq. 2.24 may be rewritten as

$$\frac{D_w}{Dt}(\Delta\varphi) = 0 \tag{2.30}$$

where

$$\frac{D_w}{Dt} = \frac{\partial}{\partial t} - \mathbf{v}_w \cdot \nabla = \frac{\partial}{\partial t} + v_w^1 \frac{\partial}{\partial \xi^1} + v_w^2 \frac{\partial}{\partial \xi^2} + v_n \frac{\partial}{\partial n} \tag{2.31}$$

is the material time derivative for a function defined only over a surface. Equation 2.2 may be integrated to yield

$$\Delta\varphi = \text{constant in time} \tag{2.32}$$

following a wake point $\mathbf{x}_w$ which has velocity $\mathbf{v}_w$ given by Equation 2.29. The value of $\Delta\varphi$ is equal to the value that it had when the point $\mathbf{x}_w$ left the trailing edge.

Note that v_u^1 and v_u^2 are the average values of the contravariant tangential components of $\mathbf{v}_u$ and $\mathbf{v}_l$ (recall that the tangential components of $\mathbf{v}$ are discontinuous across the wake), whereas $v_w^3 = v_n = v_s$ (see Eq. 2.17) since v_n is continuous across the wake. It may be worth noting that v_u^3 does not appear in Equation 2.24. However the fact that $\mathbf{v}_w$ has normal velocity equal to v_n stems from the use of Equation 2.28.

2.5 Summary of Differential Formulation

In summary, if the flow field of an inviscid incompressible fluid is initially irrotational, it remains irrotational at all times except for the points of the wake, and therefore except for those points, may be expressed as

$$\mathbf{v} = \nabla\varphi \tag{2.33}$$

Then (see Eq. 2.11), φ satisfies Laplace's equation

$$\nabla^2\varphi = 0 \tag{2.34}$$

with condition at infinity (see Eq. 2.20)

$$\varphi = 0 \tag{2.35}$$

whereas the boundary condition on the rotor blade is given by (see Eq. 2.21)

$$\frac{\partial \varphi}{\partial n} = \mathbf{v}_b \cdot \mathbf{n} \tag{2.36}$$

On the other hand, for points on the wake, the velocity is given by (see Eq. 2.29)

$$\mathbf{v} = \frac{1}{2}(\nabla\varphi_u - \nabla\varphi_l) \tag{2.37}$$

whereas, (see Eq. 2.32)

$$\Delta\varphi = \text{constant in time} \tag{2.38}$$

following $\mathbf{x}_w$.

Equations 2.34 to 2.38, with the addition of the trailing-edge condition (see Section 2.10), may be used to obtain the solution for φ. Once φ is known, the velocity may be evaluated using Eq. 2.33. Then the pressure may be evaluated using Bernoulli's theorem (see Eq. 2.22)

$$\frac{\partial \varphi}{\partial t} - \frac{1}{2}|\mathbf{v}|^2 + \frac{p}{\rho} = \frac{p_\infty}{\rho} \tag{2.39}$$

2.6 Green's Theorem for Laplacian Operator

The integral equation used in this work is a particular case of that introduced by Morino (Refs. 22-24: see also Refs. 25-29 for applications to airplanes and rotors) for the general case of potential compressible flows for bodies having arbitrary shapes and motions. The derivation of such an equation is presented here for the specific case of interest, incompressible potential flow around a helicopter rotor having arbitrary shape and motion. The integral equation is based on the Green's function method, outlined in the following.

The basis for the method used here is the second Green's identity

$$\iiint_V (f\nabla_y^2 g - g\nabla_y^2 f)dV(\mathbf{y}) = -\oint\!\!\!\oint_\sigma \left(f\frac{\partial g}{\partial n} - g\frac{\partial f}{\partial n}\right) d\sigma(\mathbf{y}) \tag{2.40}$$

where $f = f(\mathbf{y})$, $g = g(\mathbf{y})$, and

$$\frac{\partial}{\partial n} = \mathbf{n} \cdot \nabla_y \tag{2.41}$$

Equation 2.40 is easily obtained by combining Gauss theorem.

$$\iiint_V \nabla_y \cdot \mathbf{a}\, dV(\mathbf{y}) = -\iint_\sigma \mathbf{a} \cdot \mathbf{n}\, d\sigma(\mathbf{y}) \tag{2.42}$$

where σ surrounds V and $\mathbf{n}$ is the inward directed normal. with the identity

$$\nabla_y \cdot (f\nabla_y g - g\nabla_y f) = f\nabla_y^2 g - g\nabla_y^2 f \tag{2.43}$$

The essence of the method consists in choosing for g the Green's function, G, defined by

$$\nabla_y^2 G = \delta(\mathbf{y} - \mathbf{x}) \tag{2.44}$$

where δ is the Dirac delta function defined by

$$\iiint_{-\infty}^{\infty} f(\mathbf{y})\delta(\mathbf{y})dV(\mathbf{y}) = f(\mathbf{0}) \tag{2.45}$$

The boundary condition at infinity for Eq. 2.44 is

$$G = 0 \tag{2.46}$$

The solution to Eqs. 2.44 and 2.46 is the well known potential for the unit source

$$G = -\frac{1}{4\pi r} \tag{2.47}$$

where

$$r = \mathbf{y} - \mathbf{x} \tag{2.48}$$

Introducing the function

$$\begin{aligned} E(\mathbf{y}) &= 1 \qquad \mathbf{y} \text{ inside } \sigma \\ &= 0 \qquad \mathbf{y} \text{ outside } \sigma \end{aligned} \tag{2.49}$$

Equation 2.46 implies

$$\iiint_V f(\mathbf{y})\delta(\mathbf{y})dV(\mathbf{y}) = \iiint_{-\infty}^{\infty} E(\mathbf{y})f(\mathbf{y})\delta(\mathbf{y})dV(\mathbf{y}) = E(\mathbf{0})f(\mathbf{0}) \tag{2.50}$$

Combining Eqs. 2.40. 2.44. 2.47 and 2.50 yields the elegant formula

$$E(\mathbf{x})f(\mathbf{x}) = \iint_{\sigma} \left[\frac{\partial f}{\partial n} \frac{-1}{4\pi r} - f \frac{\partial}{\partial n} \left(\frac{-1}{4\pi r} \right) \right] d\sigma(\mathbf{y}) - \iiint_{V} \frac{1}{4\pi r} \nabla_y^2 f \, dV(\mathbf{y}) \qquad (2.51)$$

Equation 2.51. the key to the method presented here, does not usually have a name associated with it (except as being the key to Greens's function method): we will refer to it as Green's theorem for the Laplacian operator.

2.7 Green's Theorem for Incompressible Potential Aerodynamics

In order to obtain Green's theorem for incompressible aerodynamics. we identify the function f in Eq. 2.51 with the velocity potential. Hence the volume V must exclude the volume V_b of the rotor as well as a thin layer, V_w. which includes the wake surface σ_w (because the equation $\nabla^2\varphi = 0$ is not valid in V_b and on σ_w). Finally, the volume V must be bound by an outer surface σ_∞. Hence the surface σ (the boundary of the volume V) is formed by two surfaces: the surface σ_{bw} (which surrounds the rotor volume, V_b, and the wake volume, V_w: note that the inward normal for σ is outward for σ_{bw}), and the surface σ_∞ (which is a spherical surface of radius R and center $\mathbf{x}$).

Then, using Eq. 2.34. Eq. 2.51. for $f = \varphi$, reduces to

$$E(\mathbf{x})\varphi(\mathbf{x}) = \iint_{\sigma_{bw}+\sigma_\infty} \left[\frac{\partial \varphi}{\partial n} \frac{-1}{4\pi r} - \varphi \frac{\partial}{\partial n} \left(\frac{-1}{4\pi r} \right) \right] d\sigma(\mathbf{y}) \qquad (2.52)$$

Note that, under the conditions [it is verified *a posteriori* (Eqs. 2.79 - 2.80) that these conditions are satisfied]

$$\lim_{R\to\infty} \varphi = 0 \qquad (2.53)$$

$$\lim_{R\to\infty} R \frac{\partial \varphi}{\partial n} = 0 \qquad (2.54)$$

as the radius R of σ_∞ goes to infinity, one obtains

$$\lim_{R\to\infty} \iint_{\sigma_\infty} \left[\frac{\partial \varphi}{\partial n} \frac{-1}{4\pi r} - \varphi \frac{\partial}{\partial n} \left(\frac{-1}{4\pi r} \right) \right] d\sigma = 0 \qquad (2.55)$$

Therefore, as R tends to infinity. Eq. 2.52 becomes

$$E(\mathbf{x})\varphi(\mathbf{x}) = \iint_{\sigma_{bw}} \left[\frac{\partial \varphi}{\partial n} \frac{-1}{4\pi r} - \varphi \frac{\partial}{\partial n} \left(\frac{-1}{4\pi r} \right) \right] d\sigma(\mathbf{y}) \qquad (2.56)$$

Next let the two sides of the surface σ'_w surrounding the wake become infinitesimally close to the surface of the wake. Note that in this process, the closed surface σ'_w of the wake is replaced by the two sides of an open surface σ_w. Let $\mathbf{n}$ be the normal on the side u of σ_w. In the limit, one obtains

$$\oiint_{\sigma'_w} \frac{\partial \varphi}{\partial n} \frac{1}{4\pi r} \, d\sigma = \iint_{\sigma_w} \Delta \left(\frac{\partial \varphi}{\partial n} \right) \frac{1}{4\pi r} \, d\sigma = 0 \tag{2.57}$$

(since, see Eq. 2.14, $\Delta(\partial\varphi/\partial n) = \Delta \mathbf{v}_n = 0$), whereas

$$\oiint_{\sigma'_w} \varphi \frac{\partial}{\partial n} \left(\frac{1}{4\pi r} \right) d\sigma = \iint_{\sigma_w} \Delta\varphi \frac{\partial}{\partial n} \left(\frac{1}{4\pi r} \right) d\sigma \tag{2.58}$$

Therefore, in the limit, Eq. 2.52 reduces to

$$E(\mathbf{x})\varphi(\mathbf{x}) = \oiint_{\sigma_b} \left[\frac{\partial \varphi}{\partial n} \frac{-1}{4\pi r} - \varphi \frac{\partial}{\partial n} \left(\frac{-1}{4\pi r} \right) \right] d\sigma(\mathbf{y}) - \iint_{\sigma_w} \Delta\varphi \frac{\partial}{\partial n} \left(\frac{-1}{4\pi r} \right) d\sigma(\mathbf{y}) \tag{2.59}$$

where σ_b is the (closed) surface of the rotor blade and σ_w is the (open) surface of the wake of the rotor blade. Furthermore (see Eq. 2.14), $\Delta\varphi = \varphi_u - \varphi_l$, where $\mathbf{n}$ is the normal on the side u of the wake. Note that $\Delta\varphi$ on σ_w is evaluated from Eq. 2.38. Note also that the vortex-layer wake of the rotor is represented as a doublet layer. The proof of the equivalence of doublet layers and vortex layers is given, for instance, in Reference 31.

2.8 Integral Equation

Equation 2.54 may be used to obtain the value of φ at any point in the field if the value of φ and $\partial\varphi/\partial n$ on the surface of the rotor and the value of $\Delta\varphi$ on its wake are known. Note that $\partial\varphi/\partial n$ is known from the boundary condition on the rotor, Eq. 2.36, whereas $\Delta\varphi$ may be calculated from the boundary condition on the surface of the wake, Eq. 2.38.

Hence, in order to be able to use Eq. 2.59, one must have an equation for evaluating φ on the surface: such an equation is obtained by noting that if $\mathbf{x}$ approaches a point on the surface of the rotor, then the value of $\varphi(\mathbf{x})$ approaches the value of φ on the surface of the rotor. In order to perform this limit, it is convenient to interpret the doublet integral in terms of solid angles. Note that (see Figure 1),

$$\frac{\partial}{\partial n} \left(\frac{-1}{4\pi r} \right) d\sigma(\mathbf{y}) = \mathbf{n} \cdot \mathbf{r} \frac{d\sigma(\mathbf{y})}{4\pi r^3} = \frac{1}{4\pi} \cos\alpha \frac{d\sigma(\mathbf{y})}{r^2} = \frac{1}{4\pi} d\Omega(\mathbf{y}) \tag{2.60}$$

where $\mathbf{r} = \mathbf{y} - \mathbf{x}$, and

$$d\Omega(\mathbf{y}) = \frac{d\sigma(\mathbf{y}) \cos \alpha}{r^2}$$

is the elementary solid angle, i.e., the surface element that $d\sigma$ projects upon the unit sphere. Hence

$$\iint_{\sigma} \frac{\partial}{\partial n} \left(\frac{-1}{4\pi r} \right) d\sigma(\mathbf{y}) = \frac{1}{4\pi} \iint_{\Omega} d\Omega(\mathbf{y}) = \frac{1}{4\pi} \Omega(\mathbf{x}) \tag{2.61}$$

Note that, as is well known

$$\begin{aligned} \Omega(\mathbf{x}) &= 4\pi \qquad \text{for } \mathbf{x} \text{ inside } \sigma_b \\ &= 2\pi \qquad \text{for } \mathbf{x} \text{ on } \sigma_b \text{ (regular point)} \\ &= 0 \qquad \text{for } \mathbf{x} \text{ outside } \sigma_b \end{aligned} \tag{2.62}$$

(where a regular point is a point where σ_b has a unique tangent plane). Comparing Eqs. 2.46 and 2.62 yields, for $\mathbf{x}$ both inside and outside σ,

$$E(\mathbf{x}) = 1 - \frac{\Omega(\mathbf{x})}{4\pi} \tag{2.63}$$

Using Eqs. 2.61 and 2.63, Eq. 2.53 may be rewritten as

$$\begin{aligned} \varphi(\mathbf{x}) = \iint_{\sigma_b} \frac{\partial \varphi}{\partial n} \frac{-1}{4\pi r} \, d\sigma(\mathbf{y}) - \iint_{\sigma_b} \varphi(\mathbf{y}) - \varphi(\mathbf{x}) \frac{\partial}{\partial n} \left(\frac{-1}{4\pi r} \right) d\sigma(\mathbf{y}) \\ - \iint_{\sigma_w} \Delta\varphi \, \frac{\partial}{\partial n} \left(\frac{-1}{4\pi r} \right) d\sigma(\mathbf{y}) \end{aligned} \tag{2.64}$$

The advantage of Equation 2.64 over Equation 2.59 is that each term is continuous (as $\mathbf{x}$ crosses σ_b) and therefore is valid in particular even if $\mathbf{x}$ is on σ_b. This implies that Eq. 2.63 is also valid even if $\mathbf{x}$ is on σ_b (whether $\mathbf{x}$ is a regular point of σ_b or not). In particular, if $\mathbf{x}$ is a regular point of σ_b, then $\Omega = 2\pi$ and $E = 1/2$. Equation 2.47 may thus be generalized as

$$\begin{aligned} E(\mathbf{x}) = 1 - \Omega(\mathbf{x}) \; 4\pi &= 1 \qquad \mathbf{x} \text{ outside } \sigma_b \\ &= \frac{1}{2} \qquad \mathbf{x} \text{ on } \sigma_b \text{ (regular point)} \\ &= 0 \qquad \mathbf{x} \text{ inside } \sigma_b \end{aligned} \tag{2.65}$$

In any event, for $\mathbf{x}$ on σ_b, Eq. 2.59 (with E given by Eq. 2.65) is an integral equation relating the unknown values of the velocity potential on the surface

of the rotor, to the values of $\partial\varphi/\partial n$ (prescribed by the boundary condition on the surface of the blade) and the values of the potential discontinuity on the wake (known from the preceding time history).

2.9 Velocity Field: Wake Transport

Once φ on the surface is known, Eq. 2.59 may be used to calculate φ anywhere in the field, and hence the velocity at any point in the field as, (see Eq. 2.33)

$$\mathbf{v} = \nabla\varphi \tag{2.66}$$

Noting that

$$\nabla\left(\frac{1}{r}\right) = \frac{\mathbf{r}}{r^3} \tag{2.67}$$

where

$$\mathbf{r} = \mathbf{y} - \mathbf{x} \tag{2.68}$$

one obtains

$$\mathbf{v}(\mathbf{x}) = \iint_{\sigma_b}\left[\frac{\partial\varphi}{\partial n}\frac{-\mathbf{r}}{4\pi r^2} - \varphi\,\frac{\partial}{\partial n}\left(\frac{-\mathbf{r}}{4\pi r^3}\right)\right]d\sigma(\mathbf{y}) - \iint_{\sigma_w}\Delta\varphi\,\frac{\partial}{\partial n}\left(\frac{-\mathbf{r}}{4\pi r}\right)d\sigma(\mathbf{y}) \tag{2.69}$$

This equation may also be used to calculate the velocity of the points of the wake if the contribution of the wake integral in an infinitesimal neighborhood of the wake point is excluded from the calculation: such a contribution is responsible for the velocity discontinuity across the wake and its exclusion automatically yields the semi-sum between the two values on the two sides of the wake.

2.10 Wake Generation; Trailing Edge Condition

In this section the issue of the wake generation is analyzed. First the analytical results of Section 2.8 are interpreted from a physical point of view. Next, the trailing edge condition is introduced, and then the mechanism of wake generation is discussed.

In order to discuss the problem of wake generation, it is convenient to consider the problem of a rotor subject to a sudden start, i.e., the case of a rotor which for $t < 0$ is at rest, and is surrounded by a fluid which is also a rest. At time 0^+, the rotor is assumed to have finite velocity.

Since for time $t < 0$, the fluid was at rest, the wake has not yet had time to develop. Therefore $\Delta\varphi = 0$ everywhere in the field and the solution to the problem at time 0^- is obtained by solving Equation 2.59 with $\Delta\varphi = 0$, that is

$$E(\mathbf{x})\varphi(\mathbf{x}) = -\iint_{\sigma_t} \left[\frac{\partial\varphi}{\partial n}\frac{1}{4\pi r} - \varphi\frac{\partial}{\partial n}\left(\frac{1}{4\pi r}\right)\right] d\sigma \tag{2.70}$$

with E given by Equation 2.65.

This corresponds to the solution of the Laplace equation without wake contribution and, as well known (for instance from conformal mapping solution in two dimensional flows), this yields a separation point which in general is different from the trailing edge, and hence causes infinite velocity at the trailing edge. In turn, this indicates the presence of a vortex at the trailing edge: this manifests itself by the fact that $\Delta\varphi_{te} \neq 0$.

It is known that (since our potential is single valued) the solution to the exterior Neumann problem for Laplace equation is unique. (Multi-valued potential functions occur in multiply-connected regions).

[The proof is easily obtained, (see, e.g. Ref. 31), by integrating the identity

$$\nabla \cdot (u\nabla u) = u\nabla^2 u - \nabla u \cdot \nabla u \tag{2.71}$$

to obtain

$$\iint_\sigma u\frac{\partial u}{\partial n} d\sigma = \iiint_V u\nabla^2 u \; dV - \iiint_V \nabla u^2 dV \tag{2.72}$$

The difference, u, between two solutions to the Neumann problem satisfies the Laplace equation with homogeneous boundary conditions on σ. Therefore, the first two integrals in Eq. 2.72 are equal to zero. This implies $\nabla u = 0$, i.e., the difference, u, between two solution is a constant, which is equal to zero because of the condition at infinity: in other words the solution is unique.]

This is in sharp conflict with the classical two-dimensional result in which a suitable vortex can be added inside an airfoil to obtain smooth flow at the trailing edge. The mathematical reason for the difference is that the flow region around an airfoil is doubly connected, whereas that around a rotor (as well as most three dimensional shapes of aerodynamic interest) is simply connected. From an intuitive point of view, we can say that in a doubly connected region, it is possible to add a vortex of arbitrary intensity

inside an airfoil (or inside a doughnut-shaped object, which also corresponds to a doubly-connected flow-region). Then, adding a suitable single-valued solution, one may obtain a nontrivial solution to the homogeneous Neumann exterior problem for the Laplace equation. This solution can always be added to the solution of the airfoil problem, which is therefore, not unique. It should be noted that the potential corresponding to a vortex is multivalued and the above proof of uniqueness fails for multivalued potential functions.

In the case of a rotor, it is possible to add a vortex inside the rotor-surface: however, it is not possible to have a contour which is 'interlocked' with the vortex without penetrating the rotor surface (this is true, by definition, for any simply connected region). The potential flow is then single-valued and is impossible to generate a nontrivial solution. The solution to the rotor problem is thus unique.

In order to clarify the issue of the trailing edge conditions, we will call the *Kutta-Joukowski condition* as that smooth flow trailing edge condition which is used to eliminate the issue of a nonunique solution (see Refs. 33 and 34). This condition is required for two-dimensional steady flows, but not in three-dimensional flows, unless the region is multiply connected, nor, for that matter, for two dimensional unsteady flows.

In unsteady flows, the wake generation is responsible for the elimination of singularities at the trailing edge. The correct trailing edge condition for unsteady flows, we believe, that concentrated vortices typically do not form at the trailing edge.

More precisely, we introduce the following assumption: if, at certain discrete times, $t = T_i$, concentrated vortices form at the trailing edge (this may happen because of any time-discontinuity in the velocity distribution on the surface of the rotor, i.e., infinite acceleration as in the case of the sudden start discussed above), then these vortices are immediately shed. (This condition must be satisfied if we want the solution to our problem to be the limiting case of the solution of Navier-Stokes equations). At any other time (when the acceleration is finite), there are no concentrated vortices at the trailing edge. The implication of this assumption is that (except at $t = T_i$) the value of $\Delta\varphi$ is continuous at the trailing edge: for the well known equivalence between doublet and vortex layers (Ref. 31) indicates a discontinuity in the doublet

intensity implies the presence of a concentrated vortex. In other words, if $\mathbf{x}_w$ is a point on the wake and $\mathbf{x}_{te}$ is a point on the trailing edge.

$$\lim_{\mathbf{x}_w \to \mathbf{x}_{te}} \Delta\varphi(\mathbf{x}_w) = \Delta\varphi_{te} \tag{2.73}$$

where $\Delta\varphi_{te}$ is the difference in the values of the potential as the points on upper and lower surfaces of the rotor blade approach a point of the trailing edge.

At the times $t = T_i$ where the acceleration is infinite. Eq. 2.73 may be generalized as

$$\lim_{\epsilon \to 0} \Delta\varphi_w(t_i^+ + \epsilon) = \Delta\varphi_{te}(t_i^+) \tag{2.74}$$

and

$$\lim_{\epsilon \to 0} \Delta\varphi_w(t_i^- - \epsilon) = \Delta\varphi_{te}(t_i^-) \tag{2.75}$$

which expresses that the intensity of $\Delta\varphi$ on the wake has a discontinuity. The implication is that a vortex is shed at $t = T_i$, and is convected with the wake.

Note that without this asumption, the solution si not unique.; there exist at least two solutions: that considered here, and another in which the vortex remains at the trailing edge. It would be desirable to prove that under the trailing edge condition proposed, there exists a theorem of existence and uniqueness for the equation of potential flows.

2.11 Conditions at Infinity

In this subsection, Eqs. 2.53 and 2.54 are verified. Note as r goes to infinity, Equation 2.56 yields

$$\begin{aligned}\varphi(\mathbf{x}) &= \iint_{\sigma_{bw}} \left[\frac{\partial\varphi}{\partial n}\left(\frac{-1}{4\pi r}\right) - \varphi\frac{\partial}{\partial n}\left(\frac{-1}{4\pi r}\right)\right] d\sigma(\mathbf{y}) \\ &= \frac{1}{4\pi r}\iint_{\sigma_{bw}} \frac{\partial\varphi}{\partial n} d\sigma(\mathbf{y}) - \frac{1}{4\pi r^2}\iint_{\sigma_{bw}} \varphi\frac{\mathbf{r}\cdot\mathbf{n}}{r} d\sigma(\mathbf{y})\end{aligned} \tag{2.76}$$

Even if the flux through σ_{bw} is not equal to zero, i.e.,

$$\iint_{\sigma_{bw}} \frac{\partial\varphi}{\partial n} d\sigma(\mathbf{y}) \neq 0 \tag{2.77}$$

(this is the case, for instance, if the body is deforming with change in volume), noting that

$$\lim_{\mathbf{x}\to\infty} \iint_{\sigma_{body}} \varphi \frac{\mathbf{r}\cdot\mathbf{n}}{r} d\sigma(\mathbf{y}) = \text{finite} \tag{2.78}$$

Eq. 2.76 implies

$$\varphi = O(r^{-1}) \tag{2.79}$$

and

$$\frac{\partial \varphi}{\partial n} = O(r^{-2}) \tag{2.80}$$

at infinity.

SECTION 3

ROTATIONAL-FLOW FORMULATION

The formulation for incompressible rotational flows is presented in this Section. Following the classical approach of Prandtl, the flow region is divided into two regions: an inner one (i.e., the boundary layer region, near the boundary surface) and an outer one. The emphasis is on the outer region (the inner one is assumed to be solved by a boundary layer code or, if necessary, by a thin-layer Navier-Stokes formulation). The formulation is based on Helmholtz scalar/vector-potential decomposition. Whereas the derivation is strictly *mathematical*, the resulting formulation may be restated in *physical* terms as follows. If the vorticity at time t is known, then, using Biot and Savart law (Section 3.3), one obtains the velocity "induced by the vorticity"; then the scalar-potential contribution is added to satisfy the normal boundary condition between inner and outer region. The two above steps allow to evaluate the velocity field from the vorticity field. Once the velocity field at time t is known, the loop may be closed by evaluating the vorticity field at time $t - dt$ (from that at time t) by using the vorticity evolution equation.

A new approach for solving the vorticity-evolution equation is used here. For the sake of clarity, the formulation for inviscid flows is presented first (the formulation is extended to include diffusion, via a very simple eddy-viscosity turbulence modelling, in Section 3.9). As shown by Morino (Refs. 35 and 36), for inviscid flows, the material contravariant components (i.e., the contravariant components in a curvilinear coordinate system which moves with the material points, Section 3.5) of the vorticity remain constant in time (Section 3.6). In particular, for thin-wake approximation, this implies that the wake-thickness remains constant (Section 3.7). This result is used for the numerical solution of the vorticity evolution equation: given the velocity field, one may evaluate the new location of the wake; from this, one evaluates

the base vectors and the new values of the vorticity, as a linear combination of the (time-independent) material contravariant components of the vorticity and their corresponding base vectors (see Eq. 3.35). As mentioned above, the formulation is then extended to the ensemble-averaged Navier-Stokes equations (with a simple eddy-viscosity modelling for turbulence): the evolution equation for the contravariant material components is obtained and used to derive the expression for the time-evolution of the wake thickness. [Actual numerical calculations indicate that the effect of the thickness change may be important in avoiding numerical instabilities (see Section 5)].

3.1 Governing Equations

The assumption of incompressible flow is used throughout this report. However, it is important to differentiate between incompressible *fluids* and incompressible *flows*. An incompressible fluid has zero compressibility, while in an incompressible flow (of a compressible fluid), the effects of compressibility may be assumed to be equal to zero. For instance, the assumption of incompressible air flow is acceptable when the local Mach number is much less than one.

Similarly, the *flow* of a viscous *fluid* may be assumed to be inviscid within a certain region when effects of the viscosity are negligible in that region. Following Prandtl, the flow may be decomposed into a boundary layer (a region near the solid surface, i.e., the surface of the rotor in our case) where the viscosity is important, and an outer region where the effects of viscosity may be negligible: we will concentrate on the outer region, and initially assume that the flow is inviscid in that region. [However, as mentioned above, the issue of the validity of the inviscid-flow assumption in the region of the wake may be too restrictive in our case: this point is addressed at the end of this section, where we will use the ensemble-averaged Navier-Stokes equations to discuss how the formulation may be modified to include the presence of eddy-viscosity.]

Under the above assumptions of inviscid incompressible flow, the phenomenon is governed by the continuity equation (conservation of mass) for

incompressible flows

$$\nabla \cdot \mathbf{v} = 0 \tag{3.1}$$

and Euler equations (conservation of momentum)

$$\frac{D\mathbf{v}}{Dt} = -\frac{1}{\rho}\nabla p \tag{3.2}$$

3.2 Helmholtz Decomposition

The method used here is based on the classical Helmholtz decomposition (see Ref. 30) of the flow field into an irrotational part and a solenoidal part

$$\mathbf{v} = \nabla\phi + \nabla \times \mathbf{A} \tag{3.3}$$

In Equation 3.3 ϕ is the scalar potential and $\mathbf{A}$ is the vector potential, which satisfies the condition

$$\nabla \cdot \mathbf{A} = 0 \tag{3.4}$$

and the equation

$$\nabla^2\mathbf{A} = -\boldsymbol{\omega} \tag{3.5}$$

where

$$\boldsymbol{\omega} = \nabla \times \mathbf{v} \tag{3.6}$$

is the vorticity.

[In order to prove Eq. 3.1, note that for any vector $\mathbf{a}$

$$\nabla \times \nabla \times \mathbf{a} = \nabla(\nabla \cdot \mathbf{a}) - \nabla^2\mathbf{a} \tag{3.7}$$

Hence, using Eqs. 3.4 (which may always be satisfied by using $\mathbf{A} = \mathbf{A}_0 + \nabla\chi$ with $\nabla^2\chi = -\nabla \cdot \mathbf{A}_0$ to 3.7, one obtains

$$\nabla \times (\mathbf{v} - \nabla \times \mathbf{A}) = \boldsymbol{\omega} - \nabla(\nabla \cdot \mathbf{A}) - \nabla^2\mathbf{A} = 0 \tag{3.8}$$

which indicates that there exists a potential function ϕ such that

$$\mathbf{v} - \nabla \times \mathbf{A} = \nabla\phi \tag{3.9}$$

in agreement with Eq. 3.3.]

Note that combining Eqs. 3.1 and 3.3, one obtains that, for incompressible flows,

$$\nabla^2 \phi = 0 \tag{3.10}$$

3.3 Biot-Savart Law

If $\boldsymbol{\omega} = 0$, a particular solution of Eq. 3.5 is (see Eq. 2.51 applied to the infinite space)

$$\mathbf{A}(\mathbf{x}) = \iiint_V \frac{\boldsymbol{\omega}(\mathbf{y})}{4\pi r} dV(\mathbf{y}) \tag{3.11}$$

where

$$r = |\mathbf{y} - \mathbf{x}| \tag{3.12}$$

[Note that

$$\begin{aligned} \nabla \cdot \mathbf{A} &= \iiint_V \boldsymbol{\omega} \cdot \nabla \left(\frac{1}{4\pi r} \right) dV(\mathbf{y}) = - \iiint_V \boldsymbol{\omega} \cdot \nabla_y \left(\frac{1}{4\pi r} \right) dV(\mathbf{y}) \\ &= \iiint_V \nabla_y \cdot \boldsymbol{\omega} \frac{1}{4\pi r} dV(\mathbf{y}) - \oiint_\sigma \boldsymbol{\omega} \cdot \mathbf{n} \frac{1}{4\pi r} d\sigma(\mathbf{y}) \end{aligned} \tag{3.13}$$

where $\mathbf{n}$ is the outer normal to σ. Noting that

$$\nabla \cdot \boldsymbol{\omega} = \nabla \cdot \nabla \times \mathbf{v} \equiv 0 \tag{3.14}$$

we can see that Eq. 3.4 (used in Eq. 3.8) is not satisfied unless

$$\boldsymbol{\omega} \cdot \mathbf{n} = 0 \qquad \text{on } \sigma \tag{3.15}$$

If this condition is not satisfied, then as shown in Ref. 30, a distribution of vorticity may be added inside σ to generate a combined solenoidal vorticity field in the whole space such that Eq. 3.4 is automatically satisfied: the last term in Eq. 3.13 does not exist in this case.]

It should be noted that Eq. 3.11 is fully equivalent to the classical Biot-Savart law. In order to show this, let us consider a very thin vortex tube. In this case, we have that the velocity induced by the vortex tube is given by (note that $dV = d\sigma ds$, where $d\sigma$ is an element of a cross-section of the vortex tube, normal to $\boldsymbol{\omega}$, and ds is an arclength parallel to $\boldsymbol{\omega}$, so that $\boldsymbol{\omega} ds = \omega d\mathbf{y}$)

$$\begin{aligned} \mathbf{v}(\mathbf{x}) = \nabla \times \iiint_V \frac{\boldsymbol{\omega}}{4\pi r} dV(\mathbf{y}) &= \iiint_V \nabla \frac{1}{4\pi r} \times \boldsymbol{\omega} \, d\sigma ds \\ &= \iiint_V \frac{\mathbf{y} - \mathbf{x}}{4\pi r^3} \times \omega \, d\sigma d\mathbf{y} = \int_C \left(\oiint_{\sigma(s)} \frac{\mathbf{y} - \mathbf{x}}{4\pi r^3} \omega \, d\sigma \right) \times d\mathbf{y} \end{aligned} \tag{3.16}$$

Assuming that σ is infinitesimally small (so that $(\mathbf{y}-\mathbf{x})/r^3$ may be taken outside of the surface integral) and noting that the intensity of the vortex tube

$$\Gamma = \iint_{\sigma} \omega d\sigma \tag{3.17}$$

is independent of s, one obtains Biot-Savart law:

$$\mathbf{v}(\mathbf{x}) = \Gamma \int_{C} \frac{\mathbf{y}-\mathbf{x}}{4\pi r^3} \times d\mathbf{y} \tag{3.18}$$

Hence, Eq. 3.11 may be considered as the Biot-Savart law for continuous distribution of vorticity.

3.4 Method of Solution

The Helmholtz decomposition theorem and Biot-Savart law for distributed vorticity may be combined to yield

$$\mathbf{v} = \nabla\phi + \mathbf{w} \tag{3.20}$$

where $\mathbf{w}$ is the velocity induced by the vorticity and is given by

$$\mathbf{w}(\mathbf{x}) = \nabla \times \iiint_{V} \frac{\boldsymbol{\omega}}{4\pi r} dV(\mathbf{y}) \tag{3.21}$$

(with $\boldsymbol{\omega} \cdot \mathbf{n} = 0$ on the boundary of V, see Eq. 3.15), whereas ϕ satisfies Laplace's equation

$$\nabla^2\phi = 0 \tag{3.22}$$

The condition at infinity is $\phi = 0$. Therefore, ϕ satisfies Eq. 2.59, without the wake term since ϕ is continuous in the whole field:

$$E(\mathbf{x})\phi(\mathbf{x}) = \iint_{\sigma_b} \left[\frac{\partial\phi}{\partial n} \frac{-1}{4\pi r} - \phi \frac{\partial}{\partial n}\left(\frac{-1}{4\pi r}\right) \right] d\sigma(\mathbf{y}) \tag{3.23}$$

Next, a boundary condition on $\partial\phi/\partial n$ is needed. In order to impose this boundary condition, we follow the classical approach of Lighthill (Ref. 37) and introduce a "transpiration velocity" (i.e., "equivalent sources" of Ref. 37): this velocity is such that an inviscid flow around a permeable surface (with flow-through defined by such transpiration velocity) is equal to the outer flow region of the actual viscous flow around an impermeable surface.

The transpiration velocity for three-dimensional flows was introduced by Lighthill (Ref. 37) and is given by Eq. 25 of Ref. 37, or, using our notations,

$$v_{tr} = \nabla_t \cdot \int_0^{\delta} (\mathbf{u}(\delta) - \mathbf{u}(\varsigma))\, d\varsigma \tag{3.24}$$

where $\nabla_t \cdot$ is the surface divergence, δ is the boundary layer thickness, and ς is an arclength normal to the boundary surface.

In this work, we will assume that the transpiration velocity is known (using, for instance, a boundary-layer code or a thin-layer Navier-Stokes code). The boundary condition is then given by $\mathbf{v} \cdot \mathbf{n} = \mathbf{v}_b \cdot \mathbf{n} + v_{tr}$, or

$$\frac{\partial \phi}{\partial n} = -\mathbf{w} \cdot \mathbf{n} - \mathbf{v}_b \cdot \mathbf{n} + v_{tr} \tag{3.25}$$

[In the actual numerical calculations, the transpiration-velocity contribution is neglected: in this case, Eq. 3.25 is equivalent to Eq. 2.6.]

It is apparent that in order to complete the formulation, we need an equation for $\boldsymbol{\omega}$ (as well as suitable initial and boundary conditions). The differential equation for $\boldsymbol{\omega}$ is immediately obtained by taking the curl of the Euler equations. By using the identities

$$(\mathbf{v} \cdot \nabla)\mathbf{v} = \nabla\left(\frac{v^2}{2}\right) - \boldsymbol{\omega} \times \mathbf{v} \tag{3.26}$$

and

$$\nabla \times (\mathbf{a} \times \mathbf{b}) = -(\mathbf{a} \cdot \nabla)\mathbf{b} + (\mathbf{b} \cdot \nabla)\mathbf{a} + \mathbf{a}(\nabla \cdot \mathbf{b}) - \mathbf{b}(\nabla \cdot \mathbf{a}) \tag{3.27}$$

one obtains the Helmholtz vorticity equation (Ref. 30, p. 152)

$$\frac{D\boldsymbol{\omega}}{Dt} = (\boldsymbol{\omega} \cdot \nabla)\mathbf{v} \tag{3.28}$$

The solution of Eq. 3.25 as well as the initial and boundary conditions are discussed in Sections 3.6 and 3.7.

3.5 Material Contravariant Components

The objective of the next three sections is to introduce the concept of material (or convected) contravariant components of vorticity (that is, the

contravariant components of the vorticity in a system of curvilinear coordinates that are convected by the fluid flow), in order to facilitate the integration of the vorticity transport equation. In particular, it will be shown that, for inviscid incompressible flows, the material contravariant components of the vorticity are constant following a material point. This result is used to obtain a simple but powerful computational scheme for the solution of Helmholtz vorticity equation. The formulation presented here is based on the results obtained in Refs. 35 and 36 for compressible flows.

In order to introduce the concept of material contravariant components, consider a system of material (or convected) coordinates, ξ^α,[4] i.e., a system of curvilinear coordinates that are convected with the material particles.

As in the classical formulation, a given material particle is identified by the material coordinates ξ^α and, at any time its location is determined by the Cartesian coordinates x_i, functions of the material coordinates and time

$$x_i = x_i(\xi^\alpha, t) \tag{3.29}$$

Equation 3.29 gives the Lagrangian description of the fluid motion. It may by noted that if the ξ^α's ($\alpha = 1,2,3$) are kept constant, then $x_i = x_i(t)$ represents the trajectory of a fluid point. As a consequence, coordinate lines and coordinate surfaces (for instance, the surface $\xi^1 = \text{const}$) are always composed of the same particles, and therefore are material lines and material surfaces respectively.

It should be emphasized that the coordinates ξ^α are closely related to the classical Lagrangian coordinates Ξ^α (see Ref. 30, p. 128) which coincide with the Cartesian coordinates x_i at $t = 0$. The only difference between the Ξ^α-coordinates and the ξ^α-coordinates is that, in contrast with the classical approach, we will not assume that the ξ^α-coordinates coincide with the Cartesian coordinates at time $t = 0$. This not only emphasizes the curvilinear nature of the Ξ^α-coordinates and ξ^α-coordinates, but, more importantly,

[4] Note that Greek letters are used for curvilinear components (subscript for covariant and superscript for contravariant components). Latin letters (subscript) are used for Cartesian components. Einstein summation convention on repeated indices is used on both Greek and Latin indices.

yields an additional flexibility which allows for a convenient choice of the ξ^α-coordinates at $t = 0$ and facilitates the derivation, interpretation and extension of some useful classical results.

Next, some elementary concepts on curvilinear coordinates are briefly reviewed and applied to the specific case of material curvilinear coordinates. The velocity of a material point is given by

$$\mathbf{v} = \left.\frac{\partial \mathbf{x}}{\partial t}\right|_{\xi^\alpha} \tag{3.30}$$

(where ξ^α after a vertical bar indicates that the derivative is taken with ξ^α = constant). Next consider a quantity f, such as the density ρ, which is a function of space and time. The material (or substantial) derivative, Df/Dt (see Eq. 2.3), is the time derivative for an observer that moves with the fluid particle, i.e.,

$$\frac{Df}{Dt} \doteq \left.\frac{\partial f}{\partial t}\right|_{\xi^\alpha} = \left.\frac{\partial f}{\partial t}\right|_{\mathbf{x}} - \frac{\partial f}{\partial x_i}\left.\frac{\partial x_i}{\partial t}\right|_{\xi^\alpha} \tag{3.31}$$

or, using Eq. 3.30

$$\frac{Df}{Dt} = \frac{\partial f}{\partial t} - \mathbf{v}\cdot\nabla f \tag{3.32}$$

Next, for any given time, t, introduce the base vectors

$$\mathbf{g}_\alpha = \frac{\partial \mathbf{x}}{\partial \xi^\alpha} \tag{3.33}$$

which are tangent to the coordinate lines. Recalling that the ξ^α-lines are material lines, we see that the vectors $\mathbf{g}_\alpha$ are always tangent to the same material line. Note that

$$\frac{D\mathbf{g}_\alpha}{Dt} = \frac{\partial}{\partial t}\left(\frac{\partial \mathbf{x}}{\partial \xi^\alpha}\right)\Bigg|_{\xi^\beta} = \frac{\partial}{\partial \xi^\alpha}\left(\left.\frac{\partial \mathbf{x}}{\partial t}\right|_{\xi^\beta}\right) = \frac{\partial \mathbf{v}}{\partial \xi^\alpha} \tag{3.34}$$

This relationship is the key to the interpretation of the vortex stretching term in the vorticity evolution equation.

Next, recall that any vector, in particular the vorticity $\boldsymbol{\omega}$ may be expressed as

$$\boldsymbol{\omega} = \omega^\alpha \mathbf{g}_\alpha \tag{3.35}$$

where the ω^α's are known as contravariant components of the vorticity vector $\boldsymbol{\omega}$. In order to emphasize that the ξ^α's are material curvilinear coordinates, we will refer to the ω^α's as material contravariant components of the vorticity.

3.6 Vorticity Transport in Material Contravariant Components

Combining Eqs. 3.28 and 3.35, we obtain

$$\frac{D}{Dt}(\omega^\alpha \mathbf{g}_\alpha) - \omega^\alpha \frac{\partial \mathbf{v}}{\partial \xi^\alpha} = 0 \tag{3.36}$$

The second term in Eq. 3.36 is known as the vortex-stretching term: using Eq. 3.34, we may see that the vortex-stretching term may be reinterpreted as representing the stretching of the material base vectors. Combining Eqs. 3.34 and 3.36, one obtains

$$\frac{D\omega^\alpha}{Dt} = 0 \tag{3.37}$$

which shows that, for inviscid incompressible flows, the material contravariant components of the vorticity are constant following a material point. Hence, in general, the vorticity is given by

$$\boldsymbol{\omega}(\xi^\beta, t) = \omega^\alpha(\xi^\beta, t_0)\ \mathbf{g}_\alpha(\xi^\beta, t) \tag{3.38}$$

[If ξ^α coincide with the coordinate Ξ^α, (i.e., coincides with the Cartesian coordinates x_i at $t = 0$) then Equation 3.38 coincides with Eq. 17.5 of Ref. 30, p. 152: a result obtained by Cauchy in 1815.]

The above results are used here as the basis of the computational method for rotational flows. For incompressible inviscic flows, the vorticity is given by Eq. 3.38 at all times: assume that we know the vorticity field at time $t = t_0$ and the functions $\mathbf{x}(\xi^\alpha, t)$ at time t_0 and at time t_1; it should be emphasized that whereas these pieces of information are not sufficient to evaluate the velocity field, nontheless they are sufficient to evaluate the vorticity field at time t_1. Indeed, from $\mathbf{x}(\xi^\alpha, t_0)$ we may evaluate the vectors $\mathbf{g}_\alpha$ at $t = t_0$ and hence, the contravariant components $\omega^\alpha(\xi^\beta, t_0)$. On the other hand, the knowledge of $\mathbf{x}(\xi^\alpha, t_1)$ allows for the evaluation of $\mathbf{g}_\alpha$ at $t = t_1$ and hence, of the vorticity field at time $t = t_1$, via Eq. 3.38.

In particular, for the helicopter rotor wake problem of interest here, once the locations of material gridpoints on the wake are evaluated at a given time step, the direction and intensity of the vorticity field can be evaluated immediately using Eq. 3.38. Once the vorticity is known, the velocity field is evaluated using the formulation presented in Section 3.4.

It may be worth noting that some classical vortex theorems may be obtained (more directly than in the classical approach, Ref. 30) as an immediate consequence of Eq. 3.38. The first (and most relevant here) is that, for inviscid incompressible flows, a vortex line is a material line. In order to prove this, let us choose the coordinates ξ^α such that the ξ^1-lines (and hence, the base vectors $\mathbf{g}_1$) are parallel to the vorticity field at time $t = t_0$. This implies $\omega^2 = \omega^3 = 0$ at $t = t_0$ and according to Eq. 3.37, $\omega^2 = \omega^3 = 0$ at all times, or

$$\boldsymbol{\omega}(\xi^\beta, t) = \omega^1(\xi^\beta, t_0)\ \mathbf{g}_1(\xi^\beta, t) \tag{3.39}$$

Hence, $\boldsymbol{\omega}$ is always parallel to the ξ^1-lines, which, as pointed out above, are by definition material lines: therefore, vortex lines are material lines (in agreement with Ref. 30, p.152).

[Another classical result that is easily obtained from Eq. 3.38 is related to vortex stretching. Using Eq. 3.39, one obtains

$$\frac{\boldsymbol{\omega}}{\boldsymbol{\omega}_0} = \kappa \tag{3.40}$$

where

$$\kappa = \mathbf{g}_1 / \mathbf{g}_{1|0} = d\mathbf{x} / d\mathbf{x}_0 \tag{3.41}$$

is the stretching factor of the vortex line at the given material point. Finally, it may be worth noting that if we introduce a small material cylinder around an element $d\mathbf{x}$ of a vortex line, having a cross-section dA and a constant mass $dm = \rho dA\ d\mathbf{x} = \rho dA_0\ d\mathbf{x}_0$, one obtains, using Eqs. 3.41 and 3.42,

$$\boldsymbol{\omega}\, dA = \boldsymbol{\omega}_0\, dA_0 \tag{3.42}$$

in agreement with Kelvin's theorem, (see Eqs. 2.7 and 2.8).

As mentioned above, all these results are valid for compressible isentropic flows as well (see Ref. 36).]

3.7 Thin Wake Approximation

In this section, we will show how the formulation can be simplified in the case of a thin wake, i.e., in the case in which the vorticity in the outer region may be assumed to be approximately equal to zero everywhere, except for a thin (but finite-thickness) layer. In this case, the velocity induced by the vorticity is given by Eq. 3.21, or

$$\mathbf{w}(\mathbf{x}) = \nabla \times \iiint_V \frac{\boldsymbol{\omega}}{4\pi r} dV(\mathbf{y}) = \nabla \times \int_{-\delta/2}^{\delta/2} \left(\oiint_\sigma \frac{\boldsymbol{\omega}}{4\pi r} d\sigma(\mathbf{y}) \right) d\varsigma \tag{3.43}$$

where σ is a vortical surface (i.e., $\boldsymbol{\omega}$ is tangent to σ), and ς is an arclength in the direction normal to σ. The origin of ς is "in the middle of the layer," and is defined precisely later (see Eq. 3.47). The thickness δ is such that, in any case, $|\boldsymbol{\omega}| = 0$ for $|\varsigma| > \delta$. If the wake is thin, then Eq. 3.43 may be approximated with

$$\mathbf{w}(\mathbf{x}) = \nabla \times \oiint_\sigma \frac{\boldsymbol{\gamma}}{4\pi r} d\sigma(\mathbf{y}) \tag{3.44}$$

where

$$\boldsymbol{\gamma} = \int_{-\delta/2}^{\delta/2} \boldsymbol{\omega} \, d\varsigma \tag{3.45}$$

and σ is the midsurface ($\varsigma = 0$) of the wake-layer.

Next, let us choose the material coordinates so that the ξ^1-lines are parallel to the vorticity field. Then $\omega^2 = \omega^3 = 0$ and $\boldsymbol{\omega}$ is given by Eq. 3.39. Also, the ξ^2-lines are chosen so that the surface σ is composed of a network of ξ^1-lines and ξ^2-lines (i.e., σ is given by $\xi^3 = 0$). The lines ξ^3 are such that at time $t = t_0$, they are normal to σ. Combining Eq. 3.39 with Eq. 3.45, one obtains

$$\boldsymbol{\gamma} = \int_{-\delta/2}^{\delta/2} \omega^1 \mathbf{g}_1 \, d\varsigma \tag{3.46}$$

Next let us choose the origin of ς so that

$$\int_{-\delta/2}^{\delta/2} \omega^1 \varsigma \, d\varsigma = 0 \tag{3.47}$$

and assume that $\mathbf{g}_1$ is approximately given by $\mathbf{g}_1 = \mathbf{a}_1 + \varsigma \mathbf{b}_1 + O(\xi^2)$ (where $\mathbf{a}_1$ is the base vector $\mathbf{g}_1$ of the midsurface σ ($\varsigma = 0$), and $\mathbf{b}_1$ is an arbitrary vector).

Combining with Eqs. 3.46 and 3.47 and neglecting terms of order δ^2, one obtains

$$\boldsymbol{\gamma} = \gamma^1 \mathbf{a}_1 \tag{3.48}$$

where

$$\gamma^1 = \int_{-\delta/2}^{\delta/2} \omega^1 d\varsigma \tag{3.49}$$

Note that by definition of the wake thickness, $\omega^1 = 0$ at the extremes of integration. Therefore, applying Leibniz rule

$$\frac{d}{dt}\int_a^b f(x,t)dx = f(b,t)\frac{db}{dt} - f(a,t)\frac{da}{dt} - \int_a^b \frac{\partial f}{\partial t}dx \tag{3.50}$$

one obtains, using Eq. 3.37,

$$\begin{aligned}\frac{D\gamma^1}{Dt} &= \int_{-\delta/2}^{\delta/2} \frac{\partial \omega^1}{\partial t}\bigg|_{\xi^1,\xi^2,\xi^3=const} d\varsigma \\ &\simeq \int_{-\delta/2}^{\delta/2} \frac{\partial \omega^1}{\partial t}\bigg|_{\xi^1,\xi^2,\xi^3=const} d\varsigma = \int_{-\delta/2}^{\delta/2} \frac{D\omega^1}{Dt} d\varsigma = 0\end{aligned} \tag{3.51}$$

[Note that the $\simeq$ sign is due to the fact that the ς-lines are always normal to σ, whereas the ξ^3-lines, initally normal to σ, move with the flow, and to move away from the normal because of the shear-motion induced by the vorticity. However, this approximation used in Eq. 3.51 is acceptable if $\partial\omega^1/\partial\xi^2$ is small (compared, for instance, to $\omega^1|_{max}/\delta$).]

It may be worth noting that, at least in the case of a flat constant-thickness layer of constant vorticity, Eq. 3.45 gives the exact velocity distribution outside the layer. For instance, if $\boldsymbol{\omega} = \omega\mathbf{j}$ (with $\omega = const$) for $-\delta/2 < \varsigma < \delta/2$ and $\omega = 0$, otherwise, one obtains $\mathbf{v} = \omega i\delta/2$ for $\varsigma > \delta/2$. (Actually, Eq. 3.45 gives the exact result even if $\boldsymbol{\omega} = \omega(\varsigma)\mathbf{j}$ with $\omega = 0$ for $\varsigma > \delta/2$). Therefore, Eq. 3.45 is expected to give good results as long as the curvature is not too high. [This is not the case near at high tip vortices. However, in that case, one could use the analysis of Section 3.3 (Eq. 3.16 and 3.18) to reach similar conclusions about the validity of Eq. 3.45.]

Of course, the velocity obtained from Eq. 3.45 would be incorrect inside the wake layer. Therefore, it is important to obtain an equation that gives

the time-evolution of the wake thickness. Consider the second moment of vorticity

$$\hat{\boldsymbol{\gamma}} = \int_{-\delta/2}^{\delta/2} \varsigma^2 \boldsymbol{\omega}(\varsigma) d\varsigma = \hat{\gamma}^1 \mathbf{a}_1 \tag{3.52}$$

where

$$\hat{\gamma}^1 = \int_{-\delta/2}^{\delta/2} \varsigma^2 \omega^1(\varsigma) d\varsigma \tag{3.53}$$

and note that (with the same qualifying statement used for Eq. 3.51)

$$\frac{D\hat{\gamma}^1}{Dt} = 0 \tag{3.54}$$

In order to obtain an approximate equation for the evolution of the thickness, we will assume that, as the thickness changes, the shape of the function describing $\omega^1(\varsigma)$ does not change, i.e.,

$$\omega^1(\varsigma) = A(t) f\left(\frac{2\varsigma}{\delta(t)}\right) \tag{3.55}$$

[This expression may be thought of as the first term of a series expansion for $\omega^1(\varsigma)$.] For instance, one could use $f(u) = 0$ for $|u| > 1$ and $f(u) = 1 - 2u^2 + u^4$ [or $f(u) = (1 + \cos \pi u)/2$, or even $f(u) = 1$] for $|u| < 1$. In this case,

$$\frac{\hat{\gamma}^1}{\gamma^1} = \int_{-\delta/2}^{\delta/2} \varsigma^2 f(2\varsigma/\delta) d\varsigma \Big/ \int_{-\delta/2}^{\delta/2} f(2\varsigma/\delta) d\varsigma = \alpha\delta^2 \tag{3.56}$$

where

$$\alpha = \int_{-1}^{1} u^2 f(u) du \Big/ \int_{-1}^{1} f(u) du \tag{3.57}$$

is a factor independent of δ and time; if $f(u) = (1 - 2u^2 + u^4)$, then $\alpha = 1/7$ [if $f(u) = (1 + \cos \pi u)/2$, then $\alpha = \frac{1}{3} - \frac{2}{\pi^2}$; if $f(u) = 1$, then $\alpha = 1/3$]. Therefore using Eqs. 3.51 and 3.54, one obtains

$$\frac{D\delta}{Dt} = 0 \tag{3.58}$$

that is, that the wake thickness remains constant in time.

3.8 Summary of Formulation for Inviscid Rotational Flows

The solution of Euler equations in the region outside the boundary layer has been reduced to the solution of the vorticity transport equation. This may be studied by a Lagrangian analysis of the points of the vortical region (wake), i.e., by solving for the function $\mathbf{x} = \mathbf{x}(\xi^\alpha, t)$. From this function, one obtains the base vectors $\mathbf{g}_\alpha = \partial \mathbf{x}/\partial \xi^\alpha$ and hence, the vorticity $\boldsymbol{\omega} = \omega^\alpha \mathbf{g}_\alpha$, where ω^α is constant in time and equal to the value it had at time $t = 0$ or when the fluid particle left the inner region (at the trailing edge). From the distribution of $\boldsymbol{\omega}$, one may evaluate the velocity, $\mathbf{w}$, "induced" by the vorticity, according to Biot-Savart law. Then a potential component, $\nabla\phi$, is added to satisfy the normal boundary condition. This process yields a relationship

$$\frac{\partial}{\partial t}\mathbf{x}(\xi^\alpha, t) = \mathbf{v}[\mathbf{x}(\xi^\alpha, t), t] \tag{3.59}$$

which is a differential equation for the unknown function $\mathbf{x}(\xi^\alpha, t)$. This equation in general is solved numerically, using for instance the procedure outlined in Section 4.

For attached flows, one may use a thin-wake approximation in which only the geometry of the midsurface of the wake is required. This implies that, in Eq. 3.59 only two curvilinear coordinates are used (i.e., $\alpha = 1, 2$ instead of $\alpha = 1, 2, 3$). Then $\boldsymbol{\gamma}$ is obtained from $\boldsymbol{\gamma} = \gamma^\alpha \mathbf{a}_\alpha$, where $\mathbf{a}_\alpha$ are the surface base vectors (and α again ranges from 1 to 2). The velocity outside the wake layer is obtained using Biot-Savart law for a layer of vorticity (whereas a simple correction is required inside the wake layer, which, as shown above, has a thickness that remains constant in time).

3.9 Effect of Eddy-Viscosity - Navier-Stokes Equations

It seems natural at this point to ask ourselves whether the assumption that the effects of the viscosity are negligible is physically acceptable. More realistically, one should speak of the eddy-viscosity, since the wake is turbulent and typically the eddy-viscosity coefficient is much higher than the viscosity coefficient. In order to discuss this issue, it is convenient to see how the formulation may be modified by using the ensemble-averaged Navier-Stokes equations (instead of Euler equations) to study the region outside

the boundary layer (i.e., without the restrictive assumption of zero eddy-viscosity).

In this case, Euler equations, Eq. 3.2, are replaced by the ensemble-averaged Navier-Stokes equations*

$$\frac{D\mathbf{v}}{Dt} = \frac{1}{\rho}\nabla p - \nu_E \nabla^2 \mathbf{v} \tag{3.60}$$

where ν_E is the eddy-viscosity coefficient. Equations 3.3 and 3.24 are still valid whereas Eq. 3.25 is replaced by (assuming for simplicity that ν_E is constant)

$$\frac{D\boldsymbol{\omega}}{Dt} = (\boldsymbol{\omega} \cdot \nabla)\mathbf{v} - \nu_E \nabla^2 \boldsymbol{\omega} \tag{3.61}$$

[A less restrictive derivation of Eq. 3.61 (not requiring the assumption that ν_E is constant) may be obtained directly from the vorticity evolution equation for incompressible viscous fluids (i.e., Eq. 3.61 with ν instead of ν_E). It should be emphasized that this equation indicates that $\boldsymbol{\omega}$ is not destroyed, but only diffused by the presence of viscosity. Equation 3.61 is then obtained by averaging and setting* $\langle \boldsymbol{\omega}' \cdot \nabla \mathbf{v}' - \mathbf{v}' \cdot \nabla \boldsymbol{\omega}' \rangle + \nu \nabla^2 \boldsymbol{\omega} = \nu_E \nabla^2 \boldsymbol{\omega}$: this last assumption is justified by the fact that the term within $\langle\ \rangle$ does not destroy, but only convects (diffuses) vorticity.]

It should be emphasized that the presence of eddy-viscosity does not affect the method except for the equation of vorticity evolution. In this case, the analysis of Section 3.6 must be generalized to viscous flows. In particular, Eq. 3.36 becomes

$$\frac{D\omega^\alpha}{Dt}\mathbf{g}_\alpha = \nu_E \ \nabla^2 \boldsymbol{\omega} \tag{3.62}$$

or

$$\frac{D\omega^\alpha}{Dt} = \nu_E \ \mathbf{g}^\alpha \cdot \nabla^2 \boldsymbol{\omega} \tag{3.63}$$

where $\mathbf{g}^\alpha$ are the contravariant base vectors such that

$$\mathbf{g}^\alpha \cdot \mathbf{g}_\beta = \delta^\alpha_\beta \tag{3.64}$$

where δ^α_β is the Kronecker delta (an extension of Eq. 3.63 to compressible flows is given in Ref. 36).

---

* In this Section, $\mathbf{v}$ and $\boldsymbol{\omega}$ indicate ensemble-averaged values.

* Here $\mathbf{v}'$ and $\boldsymbol{\omega}'$ indicate perturbation from the ensemble-averaged values; $\langle\ \rangle$ indicates averaging.

Equation 3.63 indicates that the only effect of the viscosity in the outer region is that the material contravariant components of the vorticity are not simply convected, but also diffuse in the process of being convected.

A more quantitative result may be obtained for attached flows, under the assumption of thin wake. In this case, we may assume that the derivatives of $\boldsymbol{\omega}$ in the normal direction are much larger than those in the tangential direction, so that at any instant

$$\nabla^2 \boldsymbol{\omega} \simeq \frac{\partial^2}{\partial \varsigma^2}(\omega^\alpha \mathbf{g}_\alpha) \tag{3.65}$$

Using Eqs. 3.46, 3.63 and 3.65, and noting that (since $\partial \boldsymbol{\omega}/\partial \varsigma = 0$ outside the wake)

$$\int_{-\delta/2}^{\delta/2} \frac{\partial^2 \boldsymbol{\omega}}{\partial \varsigma^2} d\varsigma = \frac{\partial \boldsymbol{\omega}}{\partial \varsigma}\Bigg|_{-\delta/2}^{\delta/2} \equiv 0 \tag{3.66}$$

one obtains

$$\frac{D\gamma^1}{Dt} = 0 \tag{3.67}$$

i.e., that Eq. 3.51 is valid in presence of eddy-viscosity as well. This result should have been expected because: (i) the effect of eddy-viscosity is not to dissipate, but to diffuse the vorticity, and (ii) the only diffusion included in Eq. 3.65 is that in the direction ς, which does not affect $\boldsymbol{\gamma}$ (the integral of $\boldsymbol{\omega}$ in the ς direction, Eq. 3.45).

For the same reason, one should expect that the time evolution of the thickness of the wake is affected by the presence of eddy-viscosity. In order to show this, multiply Eq. 3.63 by ς^2 and integrate to obtain (choosing the ξ^1-lines parallel to $\boldsymbol{\omega}$, using Eq. 3.53 and neglecting higher order terms)

$$\frac{D\hat{\gamma}^1}{Dt}\mathbf{a}_1 = \nu_E \int_{-\delta/2}^{\delta/2} \varsigma^2 \frac{\partial^2 \boldsymbol{\omega}}{\partial \varsigma^2} d\varsigma \tag{3.68}$$

Noting the $\boldsymbol{\omega} = \partial \boldsymbol{\omega}/\partial \varsigma = 0$ outside the wake, one obtains (see Eqs. 3.45 and 3.48)

$$\int_{-\delta/2}^{\delta/2} \varsigma^2 \frac{\partial^2 \boldsymbol{\omega}}{\partial \varsigma^2} d\varsigma = -\int_{-\delta/2}^{\delta/2} 2\varsigma \frac{\partial \boldsymbol{\omega}}{\partial \varsigma} d\varsigma = 2\int_{-\delta/2}^{\delta/2} \boldsymbol{\omega}\, d\varsigma = 2\boldsymbol{\gamma} = 2\gamma^1 \mathbf{a}_1 \tag{3.69}$$

and hence, combining with Eq. 3.68,

$$\frac{D\hat{\gamma}^1}{Dt} = 2\,\nu_E\,\gamma^1 \tag{3.70}$$

Finally, using Eqs. 3.56 and 3.67, and recalling that $D\alpha/dt = 0$ (see Eq. 3.57), one obtains

$$\frac{D}{Dt}(\alpha\gamma^1\delta^2) = \alpha\gamma^1\frac{D\delta^2}{Dt} = 2\ \nu_E\ \gamma^1 \tag{3.71}$$

or, assuming for simplicity that ν_E is constant,

$$\delta(\xi^\beta, t) = (\delta_0^2 + 2\ \nu_E\ t/\alpha)^{\frac{1}{2}} \tag{3.72}$$

with

$$\delta_0 = \delta(\xi^\beta, 0) \tag{3.73}$$

where $t = 0$ is either the initial time or the time when the wake point left the inner region at the trailing edge.

The approximate formulation presented above indicates that (within the limits of the formulation) the only effect of eddy-viscosity is a growth of the wake thickness. If Re_E is the eddy-Reynolds number based upon the eddy viscosity coefficient, chord and tip speed ΩR

$$Re_E = \frac{c\Omega R}{\nu_E} \tag{3.74}$$

one obtains

$$\left(\frac{\delta}{\delta_0}\right)^2 - 1 = \frac{2}{\alpha}\left(\frac{c}{\delta_0}\right)^2\frac{R}{c}\ \Omega t\ \frac{1}{Re_E} \tag{3.75}$$

If δ_0 is of the order of the thickness of the blade, or $c/\delta_0 \sim 10$, using $\alpha = 1\ 7$ (see Eq. 3.57), one obtains that after one revolution (i.e., for $t = T = 2\pi\ \Omega$) the thickness increases by the factor

$$\frac{\delta_1}{\delta_0} = \sqrt{1 - 2800\ \pi\ \frac{R}{c}\ \frac{1}{Re_E}} \tag{3.76}$$

For an eddy Reynold's number of 5,000 and $R/c = 16$, we obtain that

$$\frac{\delta_1}{\delta_0} = \sqrt{1 + 28.15} = 5.4 \tag{3.77}$$

i.e., the thickness becomes more than five times larger during the first revolution.

In conclusion, the effect of the viscosity may be taken approximately into account by introducing a thickness growth that, while not extremely small, is sufficiently small to be evaluated using the simplified analysis presented in this section. It should be emphasized that the main effect of the wake thickness is "local." The effect upon distant points may still be evaluated using the zero-thickness approximation (see Eqs. 3.43 and 3.44).

SECTION 4

COMPARISON OF THE TWO FORMULATIONS: THE LIMITING CASE

The formulations for potential flows and for rotational flows have been presented in Sections 2 and 3, respectively. The first formulation is limited to zero-thickness wake, whereas the second one allows for finite-thickness wakes and may be used for both inviscid (Sections 3.1 to 3.8) and viscous flows (Section 3.9). It is apparent that the limiting case of the rotational-flow formulation as the wake thickness goes to zero (e.g., for inviscid fluids) should be fully equivalent to the potential-flow formulation. In this section, the equivalence between the two formulations (as the wake thickness goes to zero) is analized in detail. This analysis is not only useful for the theoretical clarification of the relationship between potential flows and rotational (inviscid and viscous) flows, but it also helps in indicating how the numerical scheme used for the potential-flow formulation may be modified to be applicable to the rotational-flow formulaltion.

4.1 Rotational Flows: Limiting Case

As the wake thickness goes to zero (i.e., the viscosity, and hence, the boundary-layer thickness go to zero, see Section 2) the formulation for rotational flows simplifies considerably. The velocity is given by (see Eqs. 3.20 and 3.44)

$$\mathbf{v} = \nabla\phi + \mathbf{w} \tag{4.1}$$

with

$$\mathbf{w}(\mathbf{x}) = \nabla \times \iint_{\sigma_w} \frac{\boldsymbol{\gamma}}{4\pi r} d\sigma(\mathbf{y}) \tag{4.2}$$

The scalar-potential ϕ satisfies the equation (Eq. 3.23)

$$E(\mathbf{x})\phi(\mathbf{x}) = -\iint_{\sigma_b}\left[\frac{\partial\phi}{\partial n}\frac{1}{4\pi r} - \phi\frac{\partial}{\partial n}\left(\frac{1}{4\pi r}\right)\right]d\sigma(\mathbf{y}) \tag{4.3}$$

with boundary conditions (see Eq. 3.25)

$$\frac{\partial\phi}{\partial n} = \mathbf{v}_b\cdot\mathbf{n} - \mathbf{w}\cdot\mathbf{n} \qquad \text{on } \sigma_b \tag{4.4}$$

The surface distribution of vortiticy γ, satisfies the equation (see Eq. 3.52)

$$\gamma^a = \text{constant in time} \tag{4.5}$$

following a wake point.

Because of the well known equivalence between doublet layers and vortex layers (Ref. 31), Eq. 4.2 may be rewritten as

$$\mathbf{w} = \nabla\iint_{\sigma_w}\Delta\phi_w\frac{\partial}{\partial n}\left(\frac{1}{4\pi r}\right)d\sigma = \nabla\phi_w \tag{4.6}$$

with $\Delta\phi_w$ such that

$$\gamma = \mathbf{n}\times\nabla_t(\Delta\phi_w) \tag{4.7}$$

(where ∇_t is the tangential gradient) and

$$\phi_w(\mathbf{x}) = \iint_{\sigma_w}\Delta\phi_w\ \frac{\partial}{\partial n}\left(\frac{1}{4\pi r}\right)d\sigma(\mathbf{y}) \tag{4.8}$$

Therefore, the rotational-flow formulation (in the limiting case of zero-wake thickness) may be restated as follows: the velocity is given by

$$\mathbf{v} = \nabla\phi + \nabla\phi_w \tag{4.9}$$

where ϕ satisfies Eq. 4.3, whereas ϕ_w is given by Eq. 4.8.

Using Bernoulli's theorem and noting that $\Delta\phi = 0$, one obtains (see Section 2.4)

$$\frac{D}{Dt}(\Delta\phi_w) = 0 \tag{4.10}$$

or

$$\Delta\phi_w = \text{constant in time} \tag{4.11}$$

following a wake point.

[Note that Eqs. 4.5 and 4.11 are equivalent. In order to show this, recall that, in general,

$$\nabla f = \mathbf{g}^1 \frac{\partial f}{\partial \xi^1} + \mathbf{g}^2 \frac{\partial f}{\partial \xi^2} + \mathbf{g}^3 \frac{\partial f}{\partial \xi^3} \tag{4.12}$$

where $\mathbf{g}^\alpha$ are the contravariant base vectors which are such that

$$\mathbf{g}^\alpha \cdot \mathbf{g}_\beta = \delta^\alpha_\beta \qquad (\alpha, \beta = 1, 2, 3) \tag{4.13}$$

This implies

$$\mathbf{g}^2 \times \mathbf{g}^3 = \mathbf{g}^1 \Big/ (\mathbf{g}_1 \times \mathbf{g}_2 \cdot \mathbf{g}_3)$$

$$\mathbf{g}^3 \times \mathbf{g}^1 = \mathbf{g}^2 \Big/ (\mathbf{g}_1 \times \mathbf{g}_2 \cdot \mathbf{g}_3) \tag{4.14}$$

In particular, (using $\mathbf{a}_1 = \mathbf{g}_1$, $\mathbf{a}_2 = \mathbf{g}_2$, $\mathbf{a}_3 = \mathbf{a}^3 = \mathbf{n} = \mathbf{a}_1 \times \mathbf{a}_2 / |\mathbf{a}_1 \times \mathbf{a}_2|$) one obtains

$$\begin{aligned} \boldsymbol{\gamma} &= \mathbf{n} \times \nabla_t (\Delta\phi_w) \\ &= \left(\mathbf{n} \times \mathbf{a}^1 \frac{\partial}{\partial \xi^1} + \mathbf{n} \times \mathbf{a}^2 \frac{\partial}{\partial \xi^2} \right) \Delta\phi_w \\ &= \left(-\frac{\partial(\Delta\phi_w)}{\partial \xi^2} \mathbf{a}_1 - \frac{\partial(\Delta\phi_w)}{\partial \xi^1} \mathbf{a}_2 \right) \Big/ |\mathbf{a}_1 \times \mathbf{a}_2| \\ &= \gamma^1 \mathbf{a}_1 + \gamma^2 \mathbf{a}_2 \end{aligned} \tag{4.15}$$

where

$$\gamma^1 = \frac{-1}{|\mathbf{a}_1 \times \mathbf{a}_2|} \frac{\partial(\Delta\phi_w)}{\partial \xi^2}$$

$$\gamma^2 = \frac{1}{|\mathbf{a}_1 \times \mathbf{a}_2|} \frac{\partial(\Delta\phi_w)}{\partial \xi^1} \tag{4.16}$$

Since $\Delta\phi_w$ is constant in time following a wake point (i.e., keeping ξ^1 and ξ^2 constant) one can see that the same is true for the material contravariant components γ^α if and only if

$$|\mathbf{a}_1 \times \mathbf{a}_2| = \text{constant in time} \tag{4.17}$$

following a wake particle. In order to show that Eq. 4.17 is correct, consider a small material wake-volume element $dV = d\sigma\delta$, where δ is the thickness of the wake and $d\sigma$ is the area of a midsurface element. Since the density is

constant and dV is a material volume, then dV is constant in time. But, as shown in Section 3, δ is constant in time for inviscid flows. Therefore,

$$d\sigma = |\mathbf{a}_1 \times \mathbf{a}_2| \, d\xi^1 d\xi^2 \tag{4.18}$$

is also constant in time, and hence, Eq. 4.17 is true (since $d\xi^1$ and $d\xi^2$ are constant for a material element).

It may be worth noting that from a physical point of view, Eq. 4.17 may be stated as saying that the area of a material element of the wake surface is constant in time.

In conclusion, the material contravariant components γ^α and $\Delta\sigma_u$ are related through Eq. 4.16 and therefore, because of Eq. 4.17, Eqs. 4.5 and 4.11 are equivalent.]

4.2 Relationship with Potential-Flow Formulation

Presented in this section is the relationship between: (i) the limiting case of the rotational-flow formulation (Eqs. 4.3 to 4.11), and (ii) the potential-flow formulation of Section 2.

In order to facilitate the discussion, consider Eq. 2.59 and note that, following Lamb (Ref. 32), this equation may be generalized by allowing a "fictitious" flow inside σ_b: this interiaor flow has a velocity $\mathbf{v}_I = \nabla\varphi_I$, where φ_I has an integral representation of the type

$$E_I\varphi_I = \iint_{\sigma_b} \left[\frac{\partial\varphi_I}{\partial n_I}\frac{-1}{4\pi r} - \varphi_I \frac{\partial}{\partial n_I}\left(\frac{-1}{4\pi r}\right)\right] d\sigma \tag{4.19}$$

This equation is obtained by following the same procedure used to obtain Eq. 2.52, but using the volume inside σ_b instead of that outside. As a consequence,

$$E_I = 1 - E \tag{4.20}$$

and

$$\mathbf{n}_I = -\mathbf{n} \tag{4.21}$$

Combining Eqs. 2.59 and 4.19 and using Eqs. 4.20 and 4.21, one obtains

$$E\varphi + (1-E)\varphi_I = -\iint_{\sigma_b}\left[\frac{\partial}{\partial n}(\varphi - \varphi_I)\,\frac{1}{4\pi r} - (\varphi - \varphi_I)\,\frac{\partial}{\partial n}\left(\frac{1}{4\pi r}\right)\right] d\sigma + \iint_{\sigma_w} \Delta\varphi\,\frac{\partial}{\partial n}\left(\frac{1}{4\pi r}\right) d\sigma \tag{4.22}$$

which is the generalized integral equation for potential flows. Note that φ_I satisfies Eq. 4.19 and is otherwise completely arbitrary (since $E_I \equiv 0$ outside σ_b).

On the other hand, Eqs. 4.3 and 4.9 may be combined to yield

$$E\phi - \phi_w = -\iint_{\sigma_b} \left[\frac{\partial \phi}{\partial n}\frac{1}{4\pi r} - \phi\frac{\partial}{\partial n}\left(\frac{1}{4\pi r}\right)\right] - \iint_{\sigma_w} \Delta\phi_u \frac{\partial}{\partial n}\left(\frac{1}{4\pi r}\right) d\sigma \tag{4.23}$$

Note that (see Eqs. 2.33 and 4.8) the velocity is given by

$$\mathbf{v} = \nabla\varphi = \nabla(\phi + \phi_w) \tag{4.24}$$

with (see Eqs. 2.36, 4.4 and 4.6)

$$\frac{\partial \varphi}{\partial n} = \frac{\partial \phi}{\partial n} - \frac{\partial \phi_w}{\partial n} = \mathbf{v}_b \cdot \mathbf{n} \tag{4.25}$$

Therefore, one expects that, at least outside σ

$$\varphi = \phi - \phi_w \tag{4.26}$$

Substituting this equation into Eq. 4.23, one obtains (note that $\Delta\phi = 0$ on the wake)

$$E\varphi - (1 - E)\phi_w = -\iint_{\sigma_b} \left[\frac{\partial}{\partial n}(\varphi - \phi_w)\frac{1}{4\pi r} - (\varphi - \phi_w)\frac{\partial}{\partial n}\left(\frac{1}{4\pi r}\right)\right] d\sigma$$
$$- \iint_{\sigma_w} \Delta\varphi \frac{\partial}{\partial n}\left(\frac{1}{4\pi r}\right) d\sigma \tag{4.27}$$

By comparing Eqs. 4.22 and 4.27, we may conclude that the limiting case of the rotational-flow formulation coincides with the potential-flow formulation as extended by adding an internal flow

$$\varphi_I = \phi_w \tag{4.28}$$

4.3 Comments

The results of Section 4.3 indicate that Eq. 2.59 (potential-flow formulation) and Eqs. 4.3, 4.4 and 4.6 (limiting case of the rotational-flow formulations) are fully equivalent. However, the second formulation has a

distinct advantage over the first one. In the potential-flow formulation, the wake is treated as a doublet layer, and hence, is restricted to zero thickness. In the limiting case of the rotational formulation, on the other hand, there is no way to ascertain whether the wake is treated as a doublet layer or as a vortex layer. This implies that the wake thickness does not have to be equal to zero, and therefore, the formulation can be used to introduce (in a *gradual* fashion!) the effects of viscosity and eddy-viscosity.

It may be worth pointing out that "artificial viscosity" may be introduced in the potential-flow formulation for the evaluation of the velocity of the wake points (via Eq. 2.69). As we will see in Section 5, this yields results that are practically indistinguishable from those obtained from the use of actual eddy-viscosity in the rotational flow: however, there is a big difference between the two cases. In the potential-flow formulation, "artificial viscosity" is just what it says: it is an artificial way to enhance the numerical stability by increasing the vortex size in the evaluation of the velocity of the wake points: this introduces an inconsistency in the way the wake is treated in the integral equation, Eq. 2.59 (zero-thickness doublet layer) and in the velocity calculation, Eq. 2.69 (vortex layer with a finite-thickness stemming from the artificial-viscosity approximation). The rotational-flow formulation, on the other hand, is fully consistent: the same (finite-thickness or zero-thickness) wake description is used for both the integral equation (Eq. 3.22) and in the velocity expression (Eq. 3.20 or Eq. 4.2 for finite-thickness and zero-thickness, respectively). Therefore, the effect of viscosity is not necessarly artificial, but may be the one actually provided by the turbulence model that is chosen to represent the phenomenon.

4.4 Discretization of Potential-Flow Formulation

In order to solve the problem, the integral formulations presented above must be discretized in space and time. In this section, we consider the discretization of the potential-flow formulation. The results of this section will then be modified to obtain the discretization of the rotational-flow formulation: in order to be able to motivate this modification, it is convenient to introduce a finite-element discretization process of arbitrary order (even

though a zeroth-order formulation is used in the actual computations).

Using general finite-element representation, with M nodes on the surface of the body and N nodes on the surface of the wake, it is possible to approximate φ,

$$\psi = \frac{\partial \varphi}{\partial n} \tag{4.29}$$

and $\Delta\varphi$ as

$$\varphi(\mathbf{x}, t) = \sum_{i=1}^{M} \varphi_i(t)\ M_i(\mathbf{x}) \tag{4.30}$$

$$\psi(\mathbf{x}, t) = \sum_{i=1}^{M} \psi_i(t)\ M_i(\mathbf{x}) \tag{4.31}$$

and

$$\Delta\varphi(\mathbf{x}, t) = \sum_{j=1}^{N} \Delta\varphi_j(t)\ N_j(\mathbf{x}) \tag{4.32}$$

where $\varphi_i(t) = \varphi(\mathbf{x}_i, t)$, $\psi_i(t) = \psi(\mathbf{x}_i, t)$ and $\Delta\varphi_j(t) = \Delta\varphi(\mathbf{x}_i, t)$, whereas $M_i(\mathbf{x})$ and $N_j(\mathbf{x})$ are prescribed finite-element shape functions,[*] which have the property

$$\begin{aligned} M_i(\mathbf{x}) = \delta_{ik} &= 1 \qquad \text{for } i = k \\ &= 0 \qquad \text{for } i \neq k \end{aligned}$$

(where δ_{ik} is the Kronecker delta). For instance, in the zeroth-order formulation used in Refs. 1-3, M_i and N_j are equal to one within an element of the surface (of the body and the wake) and equal to zero outside. For a first-order formulation, within a given quadrilateral element, φ may be described as (see, for instance, Ref. 26)

$$\begin{aligned} \varphi = {} & \varphi_{--} \frac{1}{4}(1 + \xi^1)(1 + \xi^2) - \\ & \varphi_{--} \frac{1}{4}(1 + \xi^1)(1 - \xi^2) - \\ & \varphi_{--} \frac{1}{4}(1 - \xi^1)(1 + \xi^2) - \\ & \varphi_{-} \frac{1}{4}(1 - \xi^1)(1 - \xi^2) \end{aligned} \tag{4.33}$$

[*] Note that, in order to avoid proliferation of symbols, the same shape functions are used for φ and ψ, although this is not essential to the method.

where φ_{++}, φ_{+-}, φ_{-+} and φ_{--} are the values of φ at the four corners of the element. (The geometry of the element itself may be described in a similar fashion.) Hence, M_{++}, M_{+-}, M_{-+} and M_{--}, the local shape function (which, assembled, yield the global shape function $M_j(\xi^1, \xi^2)$) are given by

$$M_{++}(\xi^1, \xi^2) = \frac{1}{4}(1 + \xi^1)(1 + \xi^2) \tag{4.34}$$

and similar expressions for the others.

Combining Eqs. 4.24 to 4.32 with Eq. 2.59, using the colocation method and setting the control points at the nodes of the elements, $\mathbf{x}_k$, one obtains (see e.g., Ref. 26)

$$E_k \varphi_k = \sum_{i=1}^{N} B_{ki} \psi_i + \sum_{i=1}^{N} C_{ki} \varphi_i + \sum_{j=1}^{M} F_{kj} \Delta\varphi_j \tag{4.35}$$

where $E_k = E(\mathbf{x}_k)$ and

$$B_{ki} = \iint_{\sigma_b} M_i(\mathbf{y}) \, \frac{-1}{4\pi |\mathbf{y} - \mathbf{x}_k|} d\sigma(\mathbf{y}) \tag{4.36}$$

$$C_{ki} = \iint_{\sigma_b} M_i(\mathbf{y}) \, \frac{\partial}{\partial n} \left(\frac{-1}{4\pi |\mathbf{y} - \mathbf{x}_k|} \right) d\sigma(\mathbf{y}) \tag{4.37}$$

and

$$F_{kj} = \iint_{\sigma_w} N_j(\mathbf{y}) \, \frac{\partial}{\partial n} \left(\frac{-1}{4\pi |\mathbf{y} - \mathbf{x}_k|} \right) d\sigma(\mathbf{y}) \tag{4.38}$$

At each time step, ψ_i are known from the boundary conditions, $\Delta\varphi_j$ are known from the preceding time step, and Eq. 4.35 may be solved for φ_k.

A similar discretization is used for Eq. 2.69 to obtain the velocity of the wake points in terms of ψ_i, φ_i and $\Delta\varphi_j$. Once the velocity $\mathbf{v}_j(t)$ is known, the new location of a wake point is obtained by

$$\mathbf{x}(t + \Delta t) = \mathbf{x}_j(t) + \mathbf{v}_j(t) \Delta t \tag{4.39}$$

Note that according to Eq. 2.38, $\Delta\varphi_j$ is constant in time (as long as j indicates the same material wake point). The trailing edge condition is used to obtain the values of $\Delta\varphi_i$ on the first row of elements from the values of φ_i at the trailing-edge points on the upper and lower surfaces. The process may then be repeated for the next time step.

For the zeroth-order formulation, the numerical algorithm is essentially identical to that of Refs. 1 to 3 (see these references for details). The main difference between the present formulation and that of Refs. 1 to 3 is that here the first wake element is rigidly connected with the rotor blade. This has two advantages: (i) it eliminates the unrealistic trend obtained for the first element in Refs. 1 to 3, and (ii) it does not require a matrix inversion at each time step (as needed in Refs. 1 to 3) because all the coefficients of the matrix that multiply φ_i are time independent.

4.5 Discretization of Rotational-Flow Formulation

The discretization for the rotational-flow formulation differs from that for potential-flow formulation only in the discretization of the vorticity (the integral equation may be discretized in the same way for both problems, yielding for Eq. 4.3 an approximation equal to Eq. 4.35, with $F_{kj} = 0$). One of the difficulties in discretizing the vorticity equation is to impose that the vorticity field is solenoidal. This problem does not arise in the potential-flow formulation because an arbitrary doublet distribution corresponds to a vorticity distribution that is always solenoidal (Ref. 31). The relationship between the two formulations may be exploited to extend the discretization for the potential-flow formulation to that for rotational flows.

In order to accomplish this, it is convenient to start from a zero-thickness formulation. In this case (see Eqs. 4.7 and 4.32) the vorticity may be expressed as

$$\boldsymbol{\gamma} = \sum_i \Delta\varphi_i \, \boldsymbol{\gamma}_i \tag{4.40}$$

where

$$\boldsymbol{\gamma}_i = \mathbf{n} \times \nabla N_i(\mathbf{x}) \tag{4.41}$$

is the surface distribution of vorticity corresponding to a doublet distribution $N_i(\mathbf{x})$. Note that if N_i is continuous, $\boldsymbol{\gamma}_i$ will not include concentrated vorticies. This is true, for instance, for the first-order formulation which yields (see Eqs. 4.15 and 4.16)

$$\boldsymbol{\gamma}_{+-} = -\frac{1}{4}(1-\xi^1)\mathbf{a}_1 \Big/ \mathbf{a}_1 \times \mathbf{a}_2$$

$$-\frac{1}{4}(1-\xi^2)\mathbf{a}_2 \Big/ |\mathbf{a}_1 \times \mathbf{a}_2 \tag{4.42}$$

This is an elementary "vortex sheet" with vortex lines parallel to the lines N_{--} = constant. For the zeroth-order formulation, on the other hand, Eq. 4.41 yields a quadrilateral vortex filament.

In order to extend this formulation to distributed vorticity (limiting ourselves, for the sake of simplicity, to the case of a thin wake) we may use the concepts introduced in Section 3.7, Eq. 3.55, and set

$$\boldsymbol{\omega}_{--+}(\xi^1, \xi^2, \varsigma) = \frac{1}{\delta} F(2\varsigma/\delta)\ \mathbf{n} \times \nabla_t N(\xi^1, \xi^2) \tag{4.43}$$

(with $\int_{-1}^{1} F(u)du = 1$) which also automatically satisfies the solenoidality condition (the function $F(u)$ may be obtained from the expression for $f(u)$ given in Section 3.7). Equation 4.43 represents a thin "blob" of vorticity which automatically satisfies the solenoidality condition and automatically adjusts the intensity to take into account the vortex stretching. For the zeroth-order formulation, we are back to the expressions for finite-core vortex filaments (see, for instance, Ref. 1).

SECTION 5

NUMERICAL RESULTS

In order to assess their validity and efficiency, the two formulations presented in Sections 2 and 3 have been coded using the discretization outlined in Section 4. As mentioned before, only the zeroth-order formulation (i.e., concentrated vortices or equivalent constant-strength doublet panels) has been implemented. Numerical results have been obtained. Detailed presentation of the results is given in Ref. 38, which is meant to serve as a collection of results and will be continuously updated as new results become available. Only those results that are needed for the assessment of the formulations are included here.

All the results presented here are for the test case considered by Morino, Kaprielian and Sipcic (Refs. 1 to 3) and by Rao and Schatzle (Ref. 7) for which the experimental results of Bartsch (Ref. 16) are available. The main reason for this choice is the fact that we are familiar with this problem and prefered to work on familiar grounds while developing a new formulation and a new computer program. It is understood that additional results on different test cases are needed. They are currently being obtained and will be included in Ref. 38. However, even if only one test case is presented here, the results presented are quite extensive because of the many issues which had to be addressed.

5.1 Preliminary Remarks

The test case presented here is a rotor with tip radius $R = 17.5$ ft, root cut-out radius $r_0 = 2.33$ ft, chord $c = 1.083$ ft, collective pitch angle $\theta_r = 10.61^c$ and twist angle $\theta_1 = -5^c$. The angular velocity is $\Omega = 355$ rpm.

Some preliminary studies were made (using a single-bladed rotor with a prescribed wake) in order to assess the rate of convergence. These results are

presented in Ref. 38. The main conclusion is that the two formulations yield very similar results although the rate of convergence of the rotational-flow formulation is not as fast as that of the potential-flow formulation in terms of the number of elements on the blade. In any event, sufficiently accurate results are obtained for both formulations using 7 elements in the radial direction, 3 elements in the chordwise direction and a five-spiral wake with 12 elements per spiral. All the results presented in this Section use the above values. Because of its broader applicability (i.e., from potential to viscous flows) the emphasis here is on the rotational-flow formulation; the potential-flow formulation is only used to assess the accuracy and the efficiency of the rotational-flow formulation.

The results of Ref. 1 show that, because of the wake truncation the last few wake spirals tend to move outward and upward due to the lack of the suction effect caused by the portion of the wake that was ignored in the computational model. As already pointed out, for instance by Summa (Ref. 20), this problem may be corrected by introducing an intermediate and a far-wake model. Extensive preliminary studies (presented in Ref. 38) were made in order to assess several intermediate and far-wake models. The restrictions that we imposed on the selection of the model were: (i) the results should be reasonably insensitive to the far-wake model employed and (ii) the intermediate wake model should be eventually developed directly from the computational results themselves.

In trying to develop an intermediate wake model, we were not able to infer the shape of the wake from the computer data as they were generated. However, we noticed that the velocity of points of the wake were quite predictably regular and could be inferred from the velocity of the wake points of the preceding spirals. Therefore, we chose an intermediate wake model in which the velocity (not the positions) are assumed. Note that the only function of the intermediate wake spirals is to enable the last few spirals of the wake to move with the physically expected behaviour: thus, the results obtained for the sectional lift distribution are quite insensitive to the velocity assumed in the intermediate wake spirals because the exact geometry of the last few spirals is not as important as the preventing of their divergence: also, only the roll-up in the first one or two spirals is crucial in predicting

the blade loading. For the results presented here (except for the rotor in ground-effect) the velocity assumed for the intermediate spirals is the one that would generate a Landgrebe wake, even for the single-bladed rotor for which the Landgrebe model is not necessarily valid. (For the rotor in ground-effect, the velocity for the intermediate wake is described in Section 5.4.) It is acknowledged that an approach less dependent on experimental data is desirable, and eventually a self-correcting model (i.e., one with parameters that are updated during the running of the code) should be developed.

The far-wake model for the rotor out of ground-effect is needed to compensate for the wake truncation. It is known (see for instance Summa, Ref. 20) that a uniform vorticity distribution over a semi-infinite cylinder induces (outside of the cylinder) exactly the same velocity as a sink disk located at the end of the cylinder, provided the flux into the sink is equal to the flux through a cross-section of the cylinder. Since the flux through the far wake is equal to the flux through the rotor, the total flux into the sink must be equal to $\pi R^2 u_0$, where u_0 is the velocity at the rotor disk. An estimate for u_0 can be obtained from the actuator disk theory (for a rotor in hover) according to which $u_0 = \Omega R \sqrt{C_T/2}$. This point is discussed further in Section 5.2 where numerical results obtained using different estimates for the flux are presented.

Next, consider the issue of the initial geometry of the wake. In order to assess the robustness of the code, the initial wake was assumed to have little resemblance to the expected final result, i.e., a modified classical wake with a pitch $\Delta z = 2\pi R \sqrt{C_T/2}$ and C_T prescribed (see the following subsections for numerical values). The modifications are outlined in the following. After some experimentation, it was observed at the first time-step that the tip vortex would move upward (as it should), but the vortex filament nearest to the tip vortex would move downward and take a long time to recover from this position. Therefore, in all the results presented here, the initial classical wake was modified by moving the tip vortex upward by one-fourth of the pitch (but not higher than the blade tip). Moreover, a radial contraction of the wake was employed (using Landgrebe's expressions even for the case of a single-bladed rotor for which they are not strictly applicable.)

In addition to the initial geometry of the wake, there is the issue of the initial vorticity distribution on the wake. In order to avoid the well-known problems of the start-up vortex (see, e.g., Summa, Ref. 6) in all our studies, computations for the first N time-steps were performed with the wake frozen in the initial position. (Here N is obtained from the number of elements along a vortex filament, by adding two, e.g., $N = 62$ for five spirals and twelve elements per spiral.) This enables "loading" of the wake with a vorticity distribution very close to that of the frozen-wake steady-state solution and ensures that any start-up vorticity spike is washed-out from the wake.

Another issue that we addressed in the preliminary studies, not included here (see Ref. 38), is that of the vortex at the root cut-out. The vortex sheet tends to roll-up at the root just as it does at the tip. It is necessary to employ small elements at the root region in order to calculate this roll-up. However, it is well-known (see e.g., Miller, Ref. 21) that this region is not crucial to the overall phenomenon. Therefore, we used large elements near the root. As a consequence, the vortex sheet does not roll-up, but tends to move upward and generate disturbances that eventually propagate to the entire wake. In order to avoid this, the first vortex of the wake sheet has a prescribed velocity (i.e., we use the same methodology employed for the intermediate wake.)

Before discussion of the results, a few words about the way they are presented are in order. The figures included here are of two types. In the first type, we present the radial cross-sections of the wakes. Four cross-sections per wake spiral, 90° apart from each other, are shown: i.e., the topmost line corresponds to the blade trailing edge, the second line is the cross-section of the wake 90° behind the blade, the third line is 180° behind and the fourth is 270° behind the trailing edge. The fifth line is 360° or one revolution behind the trailing edge and is therefore approximately on the same plane as the trailing edge (as are the ninth line, the thirteenth line, and so on). In the second class of figures, we present the sectional lift coefficient as a function of the dimensionless radius r/R for different time-steps or different cases.

5.2 Parametric Study

A few parameters in the formulation are empirical. These include on the one hand, both the initial size of the vortex-filament core and its growth in time (see Section 3.9), and on the other hand, the intermediate wake model (which depends on C_T) and the far wake model which depends on the estimate of the flux through the rotor. The effects of these parameters were studied (results presented below) in order to gain a better understanding of their significance. In all the results presented here, the value of the radius of the vortex filaments at the trailing edge is set equal to 0.3249, which corresponds to 30% of the chord. In view of the fact that the wake is represented by discrete vortices, we estimate that this corresponds to $\delta_0/c = 0.2$ (the estimate is based upon the velocity induced by a finite-thickness vortex sheet and its approximation with finite-core vortex filaments) and seems to be a barely acceptable upper estimate for the boundary layer thickness. Lower sizes for the vortex filament core appear desirable; different values were explored but it appears that this value is necessary for the robustness of the solution.

An appreciation for the effects of the size of the vortex-filament core is obtained from the analysis of the rate of growth of the core size. Two cases were considered for the analysis of Section 3.9. In one, the growth was assumed to be such that the core size doubled during the first wake spiral. For the thin-wake analysis presented in Section 3.9 one obtains $Re_E = 11,845$ (see Eq. 3.76 with $\delta_1/\delta_0 = 2$ and $R/c = 17.5/1.083$). The other case is that for which the core size quadruples in the first blade revolution: this corresponds to $Re_E = 2,435$. We feel that these values are realistic and bracket the actual values for Re_E.

As far as the intermediate and far-wake modeling are concerned, the following were used. For all the runs, five wake spirals were used. Unless stated otherwise, only the first wake spiral was treated as being free whereas the other four were treated as the intermediate wake (i.e., with prescribed velocity). This means that at each time step the locations were recalculated for all points of the wake, and the contributions of all the spirals were taken into account in evaluating the velocity at the nodes of the first spiral. Of course, all the five spirals were taken into account in solving the integral

equation.

The intensity of the sink disk was evaluated from the velocity at the rotor plane obtained from the actuator disk theory as

$$u_0 = \Omega R \sqrt{C_T / 2}$$

This value corresponding to an infinite blade analysis might be too low: in view of the fact that the numerical results indicate a very smooth transition between the free portion and the intermediate portion of the wake, the intermediate wake expression might be a better way to estimate the flux through the rotor. Assessing u_0 from the expressions used for the intermediate wake (see Landgrebe, Ref. 12), we obtained

$$u_0 = 2.156 \Omega R \sqrt{C_T / 2}$$

The intensity of the disk is 31 ft/s with the former model and 66.7 ft/s the latter. In both cases, the disk was located at $z = -17.5$ ft ($z = 0$ corresponds to the plane of the rotor) and has a radius of 14.0 ft (this is the estimated location of the tip vortex after five revolutions).

In conclusion, initially, four cases were analyzed as indicated below (other cases are discussed later): unless otherwise specified, all the cases are for rotational-flow formulation.

Case #	Strength	δ_1 / δ_0
1	31.0	2
2	31.0	4
3	66.7	2
4	66.7	4

Case 1 shown in Figure 2 is one of the most interesting cases we have encountered and we would classify it as a 'borderline' case between stable and unstable runs. For this reason, we present an extensive representation of the time history. The evolution of the wake is shown by means of the plots of the geometry at every six iterations (or time steps starting from the time step in which the wake is 'unfrozen,' see Section 5.1). [It may be pointed out that for all the runs in this report, the number of time steps per revolution is equal to the number of elements per spiral, i.e., 12. Therefore six

time steps correspond to one half revolution of the rotor.] One may observe that after two revolutions, the wake seems to go into a limit cycle, i.e., it oscillates radially with a periodic motion without apparently 'going wild.' The period of the oscillation appears to be approximately two revolutions (compare iterations #24 with #48, #30 with #54 and #36 with #60). We can also describe the phenomenon as traveling waves with a wavelength of twice the pitch. It is not clear to us how these results should be interpreted and how close to physical reality they are.

Case 2 (same disk strength but lower eddy-Reynolds number, i.e., $\delta_1/\delta_0 = 4$) is shown in Figure 3 and indicates a much more stable wake. Only four time steps during the last (approximately the fourth) revolution that was obtained are presented. It is apparent that the top portion is completely stabilized and the initial irregularities are being 'washed out,' i.e., convected by the prescribed velocity used for the intermediate wake. [It is apparent that the model used for the intermediate wake velocity (from the Landgrebe model) is not realistic for the tip-vortex region: the tip vortex has a lower velocity and therefore the vortex sheet 'catches up' with it, yielding an unrealistic crossing. However, the crossing does not cause any problem since the velocity of these points are prescribed.] It may be worth noting that one of the points of the wake spiral underneath the blade (fifth line from the top) actually touches the blade itself. However this does not seem to introduce anomalies in the motion of the wake sheet. Again, this is unrealistic and is probably due to the effect of viscosity (it may be worth emphasizing again that in the rotational flow, we do not consider the viscosity as an 'artificial' one but as an 'eddy viscosity,' i.e., as a crude modeling of turbulent flow). On the other hand, the sectional lift coefficient presented in Figure 4 shows an anomaly where the vortex touches the blade. In addition, it does not indicate a trend to form a spike near the tip of the blade as expected to occur as the wake rolls up.

The results for Case 3 shown in Figure 5 are extremely stable: as mentioned above, this corresponds to a disk strength of 66.7 ft/s (obtained from the flux through the disk as evaluated from Landgrebe's model) and a δ_1/δ_0 of 2 ($Re_E = 11.845$). It is apparent that the increase in the strength of the sink has had the effect of stabilizing the results obtained in Case 1. On the

other hand, the results appear to be even smoother than in Case 2 for which we used higher viscosity (but lower sink strength). It may be worth noting that increasing the strength to 100 ft/s (Case 3A, not shown here) does not seem to affect the wake motion within plotting accuracy. The sectional lift distribution is shown in Figure 6 and again no spike seems to be present indicating that the solution obtained for the wake geometry might be too smooth.

In Case 3B which is the same as Case 3 except that the potential-flow formulation is used instead of the rotational-flow formulation (as pointed out above, in this case the viscosity may be introduced only as artificial viscosity). The results, shown in Figure 7, are extremely similar to those of Figure 5. Similar analogy was encountered in all the runs that we made for the potential-flow formulation, indicating the computational equivalence (not the conceptual one) of the two methods.

Next, consider Case 4, shown in Figure 8. The effect of the increase in viscosity over Case 3 appears to be a sharper turning of the wake vortex sheet. In fact, this trend is very similar to that of Case 2 (compare Figure 5D to Figure 3C, both corresponding to the 48th time step). The effect of the higher suction in Case 4 has the predictable effect of increasing the distance of the tip vortex corresponding to the first spiral, from the blade (in Case 2, the tip vortex of the first spiral, fifth line from the top, was touching the blade). Surprisingly enough, Case 4 has a higher value of the sectional or local lift coefficient (see Fig. 9) than Case 2 (Figure 4), where the vortex was touching the blade.

In all of the above results, only the first spiral is free. In order to assess the effect of using only one free wake, consider Case 5, which is similar to Case 4, but with the first two wake spirals being free (with velocity calculated at each time step), while the intermediate wake is composed of the last three wake spirals. This is the longest run that we made - eighty time steps, or almost seven revolutions. The transient behaviour of the wake, shown in Figure 10, is similar to that presented in Ref. 1. The wake geometry becomes very messy in the region of the second spiral around the 24th time step. Around the 36th time step, the first two spirals are smoother and eventually the solution converges (which was not the case in Ref. 1 because

of the lack of intermediate and far-wake models). The time history of the loading distribution is shown in Figure 11. The spike is more pronounced than in Case 4 (one free spiral).

As apparent from Figure 12, comparison with the results of Rao and Schatzle (Ref. 7) and Morino, Kaprielian and Sipcic (Ref. 1) show that Case 4 (one free spiral) and Case 5 (two free spirals) are in good agreement with the results of Rao and Schatzle (who show excellent agreement with experimental results for the case of a four-bladed rotor, see Section 5.3). It should be noted that Rao and Schatzle obtained results by a generalized wake analysis (using Landgrebe model for the wake geometry) whereas our results are obtained using a free-wake analysis. Also shown in the figure are the results of our own generalized wake analysis (also using a modified Landgrebe wake) which are in good agreement with the two-free-spiral free-wake analysis.

5.3 Multi-Bladed Rotor

The results presented in Section 5.2 are all for a single bladed rotor. In order to have an assessment on more realistic configurations, two-bladed and four-bladed rotors have been investigated. Results from a prescribed wake analysis are given for a two-bladed and a four-bladed rotor, while the free wake analysis is limited to the case of a two-blade case.

Consider Case 6, i.e., the free-wake analysis for a two-bladed rotor. The data used for Case 6 are very similar to that of Case 4 with the number of blades increased to two: the number of free spirals is retained as one. The wake geometry after 45 iterations for Case 6 are shown in Figure 13. One may observe the strong similarity between this and the wake of Case 4 for the corresponding time-step. If the computations are continued for additional time-steps, we expect the wake to stabilize as for the single-bladed rotor. The sectional lift distribution is shown in Figure 14 along with results from our own generalized wake analysis. Again, the results are in good agreement. This gave us sufficient confidence in our own generalized-wake analysis to use it for an indirect assessment of the method (the free-wake analysis for the four-bladed rotor has not yet been attempted): the results

for the generalized-wake analysis for a four-bladed rotor are compared in Figure 14A with the numerical results of Rao and Schatzle (Ref. 7) and the flight test data presented by Bartsch (Ref. 16) for a XH-51A helicopter rotor.

5.4 Ground Effect

The final problem considered here is the case of a single-bladed rotor in ground effect. Contrary to our expectations, as we lowered the rotor-plane to the ground, the problems we encountered were not in the region near the ground, but were in the region near the rotor. We were able to explain this with the fact that as the image became closer to the rotor, it had the effect of a source (negative sink): the spirals got closer and the effect of the concentrated vortex discretization became more pronounced. [As a point gets close to a vortex sheet, the velocity induced is tangential to the sheet. On the other hand, if a point gets close to a series of of concentrated vortices simulating the vortex sheet, the velocity is tangential to the sheet only if the point approaches a vortex along the normal to the vortex sheet through that vortex. Very strong normal components arise from any deviation from that line.] Therefore, we limited our analysis to a rotor which is sufficiently close to the ground to experience ground effect, but not so close that the above described effect of concentrated vortex discretization would require extremely high viscosity to 'stabilize' the solution.

The results presented here, Case 7, are for the same problem as Case 4, except for ground effect. The initial wake geometry is the same as that for the out-of ground-effect test cases. The prescribed velocity in the intermediate wake is such that the wake generated would have to go to zero exponentially with ψ, the azimuth angle, whereas the radius would go exponentially to infinity (see Ref. 38 for details). The far-wake model is a distribution of sinks over a cylinder of 20 ft radius. The intensity is obtained for the flow through the rotor as evaluated from the actuator disk theory.

The wake geometry at different time-steps is shown in Figure 15. The results are extremely smooth: this appears to be more the exception than the rule for the ground-effect problem. Figure 16 shows the sectional lift dis-

tribution. These results are presented here more in terms of addressing the issue of the stability of the wake than for an actual comparison with existing results. It is acknowledged that considerable additional work is required. However, we feel that meaningful comparisons with exisiting data can be made only after the numerical phenomenon described above (velocities normal to the vortex sheet introduced by the concentrated vortex discretization) is eliminated by introducing a first-order formulation.

SECTION 6

CONCLUSIONS

Two integral equation methods for the free-wake analysis of helicopter rotors (for potential and rotational flows, respectively) have been presented. The rotational-flow formulation is based upon Helmholtz scalar/vector-potential decomposition. The advantages of the rotational-flow formulation over the potential-flow formulation have been discussed. The numerical equivalence of the two methods has been demonstrated. It should be noted again that, whereas in the potential-flow formulation viscosity may be introduced only as artificial viscosity, in the rotational-flow formulation the presence of viscosity (or eddy-viscosity) is consistent with the corresponding assumptions. Therefore, this formulation is applicable to the solution of time-averaged Navier-Stokes equations: in particular, a simplified thin-wake analysis with an elementary eddy-viscosity model for turbulence was used for the numerical applications.

Results obtained indicate that, for appropriate values of empirical parameters (e.g., thickness of the wake at the trailing edge, eddy-Reynolds number, intensity of the far wake sink disk), the solution reaches steady-state, with the wake converging to a smooth geometry and the sectional lift distribution in good agreement with the numerical results of Rao and Schatzle [Ref. 7] and, indirectly, with the experimental ones of Bartsch [Ref. 16]. However, a sensitivity analysis over the effects of these paramenters indicates that the results were not always as good. For some values of these parameters, the solution may reach a steady state but the sectional lift distribution does not necessarily show a marked improvement as the wake rolls up. For other values of these parameters, the solution may be completely unstable. The main reason for this sensitivity to the values of the empirical paramenter is attributed to the fact that concentrated vortices are used for the discretization

of the formulation (see Section 5.4). Ground effect results are also included, and show that stable results with the proper trend may be obtained.

Most of the computations were performed on a VAX-780 computer. Case 7, for ground effect, took 10 hours and 58 minutes to perform 72 iterations (in addition to 62 time steps with frozen wake). It takes one hour to generate 12 time steps for a single-bladed rotor. Some runs were made on an IBM 3081. The longest run (Case 5, for single-bladed rotor with two free spirals) took 2 hours and 2 minutes to perform 80 iterations. It took one hour and 18 minutes for Case 4, for single-bladed rotor with one free spiral, also for 80 iterations. The potential-flow formulation requires approximately the same amount of computer time as the rotational-flow formulation (a significantly shorter time than that encountered by Morino, Kaprielian and Sipcic, Ref. 1). In summary, we may conclude that the new formulation presented here (for rotational flows) has much broader applicability than the formulation for potential flows, while requiring approximately the same amount of computer time.

In conclusion, we believe that the investigation was completed in terms of the original goals of the project, i.e., development of a rotational-flow formulation as efficient as the potential-flow formulation, but free of the inherent limitations of the latter. However, the investigation should not be considered as completed, since it has not addressed in a fully satisfactory fashion all the issues encountered. In particular, in terms of recommendations for future work, we believe that the most important item to be addressed is the first-order formulation for the wake (as outlined in Section 4). As discussed in Section 5.4, the main problem encountered in this effort has to do with the presence of induced velocities normal to the wake sheet: this is attributable exclusively to the zeroth-order formulation. It may be noted that a first-order formulation (as outlined in Section 4) has been implemented, under a separate effort, for the problem of an airplane wing [Ref. 39]. The incorporation of this formulation into the code for free-wake analysis of helicopter rotors is not expected to present any significant difficulty, but the issue of numerical instabilities needs to be addressed again.

A second item which requires further investigation is the modelling for the intermediate and far wakes. We do not believe that we have addressed

this model are now given as input data: self-adjusting models should be incorporated into the formulation. Similar comments should be made about the turbulence modelling and the boundary layer analysis: while we believe that we have shown that actual turbulence modelling and boundary layer analysis can be incorporated in the formulation, a considerable amount of work is needed to accomplish that, even for the relatively simple problem of attached flows.

After these items have been addressed, more extensive convergence analysis and comparison of the numerical results with existing experimental results should be undertaken, especially as far as the ground effect problem is concerned.

Finally, it should be emphasized that all of the results were obtained through a time-accurate, step-by-step solution. Therefore, the formulation is applicable, at least in theory, to the solution of more general time-domain problems. The accuracy, robustness and efficiency of the algorithm should be addressed by applying it, for instance, to helicopter rotors in forward flight.

REFERENCES

1. Morino, L., Kaprielian, Z., Jr., and Sipcic, S.R., 'Free Wake Aerodynamic Analysis of Helicopter Rotors,' Boston University, College of Engineering, CCAD-TR-83-01 (1983).

2. Morino, L., Kaprielian, Z., Jr., and Sipcic, S.R. 'Free Wake Analysis of Helicopter Rotors,' to be published in Vertica.

3. Sipcic, S.R., and Morino, L., 'Wake Dynamics for Incompressible and Compressible Flows,' in *Computational Methods in Potential Aerodynamics* (Ed.: L. Morino), Computational Mechanics International, Southhampton, England (in print).

4. Landgrebe, A.J., Moffitt, R.C., and Clark, D.R. 'Aerodynamic Technology for Advanced Rotorcraft, Part I,' Journal of American Helicopter Society, Vol. 22, No. 2, April 1977, pp. 21-27.

5. Landgrebe, A.J., Moffitt, R.C., and Clark, D.R., 'Aerodynamic Technology for Advanced Rotorcraft, Part II,' Journal of American Helicopter Society, Vol. 22, No. 3, July 1977, pp. 2-9.

6. Summa, J.M., 'Potential Flow about Impulsively Started Rotors,' Journal of Aircraft, Vol. 13, No. 4, April 1976, pp. 317-319.

7. Rao, B.M., and Schatzle, P.R., 'Analysis of Unsteady Airloads of Helicopter Rotors in Hover,' AIAA Paper 77-159, AIAA 15th Aerospace Sciences Meeting, Los Angeles, California, January 1977.

8. Kandil, O.A., 'Wake Dynamics in Incompressible Flows,' *Computational Methods in Potential Aerodynamics* (Ed.: L. Morino), Computational Mechanics International, Southhampton, England, (in print).

9. Suciu, E.O., Morino, L., 'Nonlinear Steady Incompressible Lifting-Surface

Analysis with Wake Roll-Up,' AIAA Journal, Vol. 15, No. 1, January 1977, pp. 54-58.

10. Suciu, E.O., and Morino, L., 'Analysis of Interfering Lifting Surfaces in Steady, Oscillatory and Transient Incompressible Flows,' AIAA 17th Aerospace Sciences Meeting, New Orleans, LA, AIAA Paper No. 79-0347, January 15-17, 1979.

11. Morino, L., Freedman, M.I., and Tseng, K., 'An Integral Equation for Compressible Potential Flows Around Bodies Having Arbitrary Motion,' Boston University, College of Engineering, CCAD-TR-85-3, (in preparation).

12. Landgrebe, A.J., 'An Analytical Method for Predicting Rotor Wake Geometry,' Journal of the American Helicopter Society, Vol. 14, No. 4, October 1969, pp. 20-32.

13. Landgrebe, A.J., 'An Analytical and Experimental Investigation of Helicopter Rotor Hover Performance and Wake Geometry Characterictics,' USAAMRDL Technical Report 71-24, Eustis Directorate, U.S. Army Air Mobility Research and Development Laboratory, Fort Eustis, VA, June 1971, AD 728835.

14. Crews, S.T., Hohenemser, K.H., and Ormiston, R.A., 'An Unsteady Wake Model for a Hingeless Rotor,' Journal of Aircraft, Vol. 10, No. 12, December 1973, pp. 758-760.

15. Kocurek, J.D., 'A Lifting Surface Performance Analysis with Circulation Coupled Wake for Advanced Configuration Hovering Rotors,' Ph.D. Dissertation, Graduate College, Texas A&M University, May 1978.

16. Bartsch, E.A., 'In-Flight Measurement and Correlation with Theory of Blade Airloads and Responses on the XII-51A Compound Helicopter Rotor — Volume I: Measurement and Data Reduction of Airloads and Structural Loads,' USAAVLABS Technical Report 68-22A, U.S. Army Aviation Material Laboratories, Fort Eustis, VA, May 1968, AD 674193.

17. Scully, M.B., 'Computation of Helicopter Rotor Wake Geometry and its Influence on Rotor Harmonic Airloads,' MIT ASRL-TR-176-1, March 1971.

18. Pouradier J.M., and Horowitz. E.. 'Aerodynamic Study of a Hovering Rotor.' Sixth European Rotorcraft and Powered Lift Aircraft Forum, Paper No. 26, Bristol, England. September 1980.

19. Summa. J.M.. and Clark, D.R., 'A Lifting-Surface Method for Hover/Climb Airloads.' 35th Annual Forum of American Helicpoter Society, Washington. D.C.. May 1979.

20. Summa, J.M., 'Advanced Rotor Analysis Method for the Aerodynamics of Vortex/Blade Interactions in Hover.' Eighth European Rotorcraft and Powered Lift Aircraft Forum, Paper No. 2.8, Aix-en-Province. France, August 31-September 3, 1982.

21. Miller, R.H., 'Application of Fast Free Wake Analysis Techniques to Rotors,' Eighth European Rotorcraft and Powered Lift Aircraft Forum, Aix-en-Province, France, August 31-September 3, 1982.

22. Morino, L., 'Unsteady Compressible Potential Flow Around Lifting Bodies Having Arbitrary Shapes and Motions,' Boston University, College of Engineering, TR-72-01, NASA CR-132127, June 1972.

23. Morino. L., 'Unsteady Compressible Flow Around Lifting Bodies: General Theory,' AIAA 11th Aerospace Sciences Meeting, Washington, D.C.. AIAA Paper No. 73-196, January 1973.

24. Morino. L.. 'A General Theory of Unsteady Compressible Potential Aerodynamics,' NASA CR-2464, December 1974.

25. Morino, L., and Kuo, C.C., 'Subsonic Potential Aerodynamics for Complex Configurations: A General Theory.' AIAA J.. Vol. 12. No. 2. February 1974, pp. 191-197.

26. Morino, L., Chen, L.T., and Suciu, E.O.. 'Steady and Oscillatory Subsonic and Supersonic Aerodynamics Around Complex Configurations,' AIAA J., Vol. 13, No. 3, March 1975, pp. 368-374.

27. Morino, L., and Tseng, D., 'Nonlinear Green's Function Method for Unsteady Transonic Flows.' in *Transonic Aerodynamics*, Ed.: D. Nixon. Vol. 81 of Progress in Astronomics and Aeronautics, 1882.

28. Suciu, E.O., Preuss, R.D., and Morino, L., 'Potential Aerodynamic Analyses of Horizontal-Axis Windmills,' AIAA Paper No. 77-132, January 24-26, 1977.

29. Soohoo, P., Noll, R.B., Morino, L., and Ham, N.D., 'Green's Function Method for the Computational Aerodynamic Analysis of Complex Helicopter Configurations,' AIAA 17th Aerospace Sciences Meeting, New Orleans, LA, AIAA Paper No. 79-0347, January 15-17, 1979.

30. Serrin, F., 'Mathematical Principle of Classical Fluid Mechanics,' in *Encyclopedia of Physics*, Ed.: S. Fluegge, Vol. VII/1, Fluid Dynamics I, Springer Verlag, 1959.

31. Batchelor, G.K., *An Introduction to Fluid Dynamics*, Cambridge University Press, 1967.

32. Lamb, H., *Hydrodynamics*, 6th ed., Cambridge University Press, 1932.

33. Kutta, J., 'Auftriebskraefte in stroemenden Fluessigkeiten,' Illustrierte Aeronautische Mitteilungen, 6 (1902), 133-135. See also 'Ueber eine mit den Grundlagen des Flugproblems in Beziehung stehende zweidimensionale Stroemung,' Sitzungsberichte der Bayerischen Akademie der Wissenschaften, mathematisch-physikalische Klasse (1910), 1-58, and 'Ueber ebene Zirkulationsstroemungen nebst Flugtechnischen Anwendungen,' ibid. (1911), 65-125.

34. Joukowski, N., 'On the Adjunct Vortices,' (in Russian), Obshchestvo liubitelei estestvoznaniia, antropologii i etnografee, Moskva, Izaviestiia, 112, Transactions of the Physical Section, 13 (1907), 12-25. See also 'De la chute dans l'air de corps legers de forme allongee, animes d'un mouvement rotatoire,' Bulletin de l'Institut Aerodynamique de Koutchino, 1 (1912), 51-65; 'Ueber die Kontouren der Tragflaechen der Drachenflieger,' Zeitschrift fuer Flugtechnik und Motorluftschiffahrt, 1 (1910), 281-284, 3 (1912), 81-86, and Aerodynamique (Paris, 1916 and 1931).

35. Morino, L., 'a Finite-Element Method for Rotational Incompressible Aerodynamics,' Boston University, College of Engineering, TN-74-04, December 1974.

36. Morino, L., 'Material Contravariant Components, Vorticity Transport and Vortex Theorems,' to be published in AIAA Journal.

37. Lighthill, M.J., 'On Displacement Thickness,' Journal of Fluid Mechanics, Vol. 4, 1958, pp. 383-392.

38. Bharadvaj, B., and Morino,L.,'Integral Equations in Rotor Aerodynamics - Numerical Results,' Boston University, College of Engineering, CCAD-TR-85-5, in preparation.

39. Morino, L. and Downey, M.J., 'A First Order Formulation for Green's Function Method in Potential Aerodynamics,' Boston University, College of Engineering, CCAD-TR-85-4, 1985.

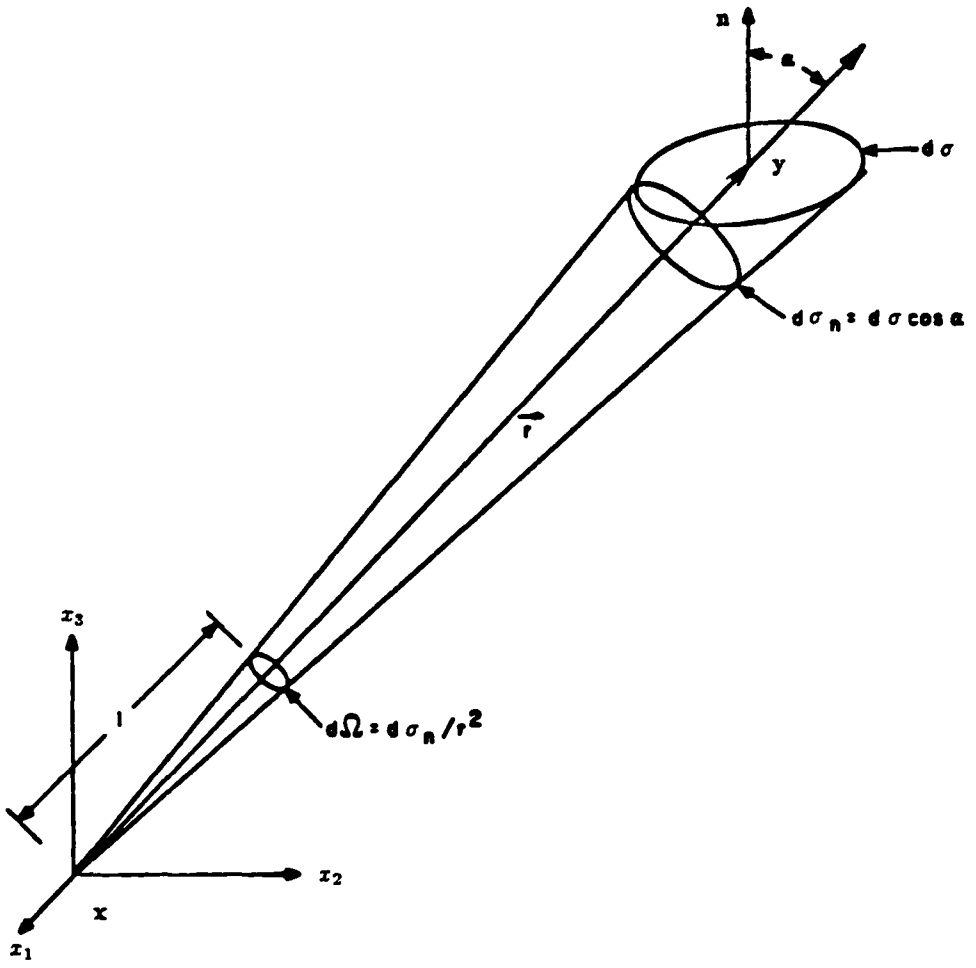

Figure 1. Geometry for Definition of Solid Angles

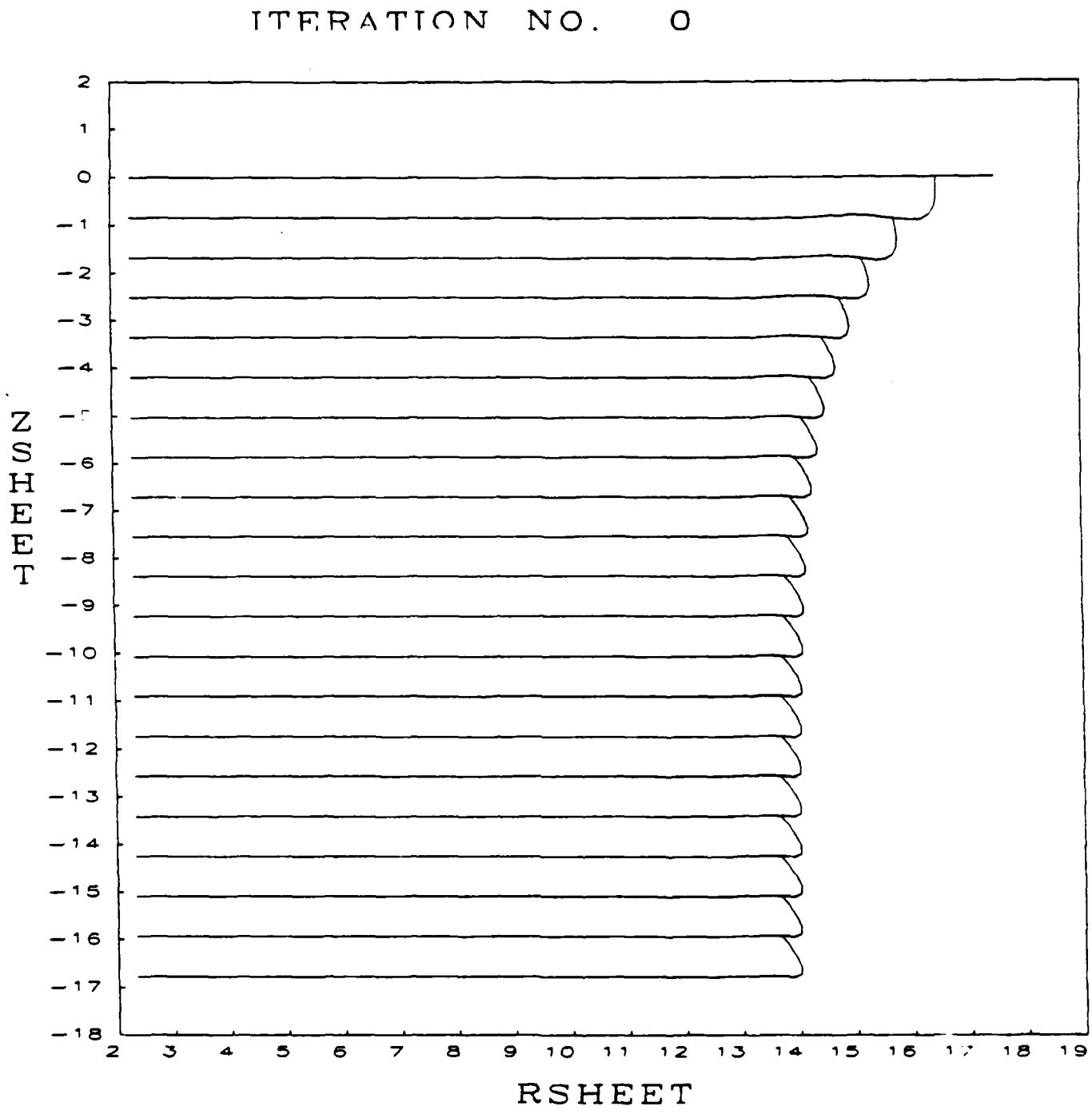

Figure 2A. Wake Geometry for Case 1

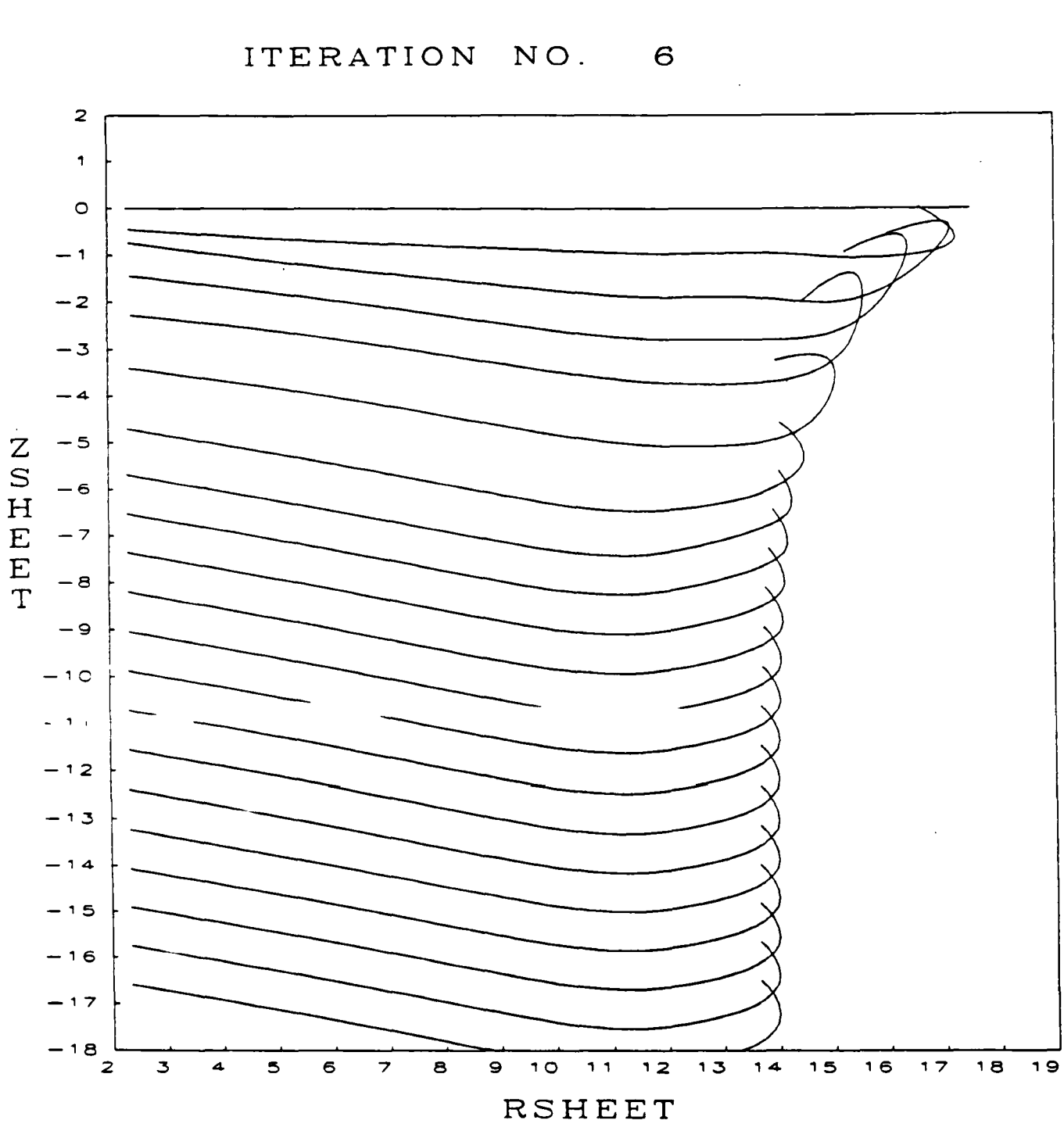

Figure 2B. Wake Geometry for Case 1

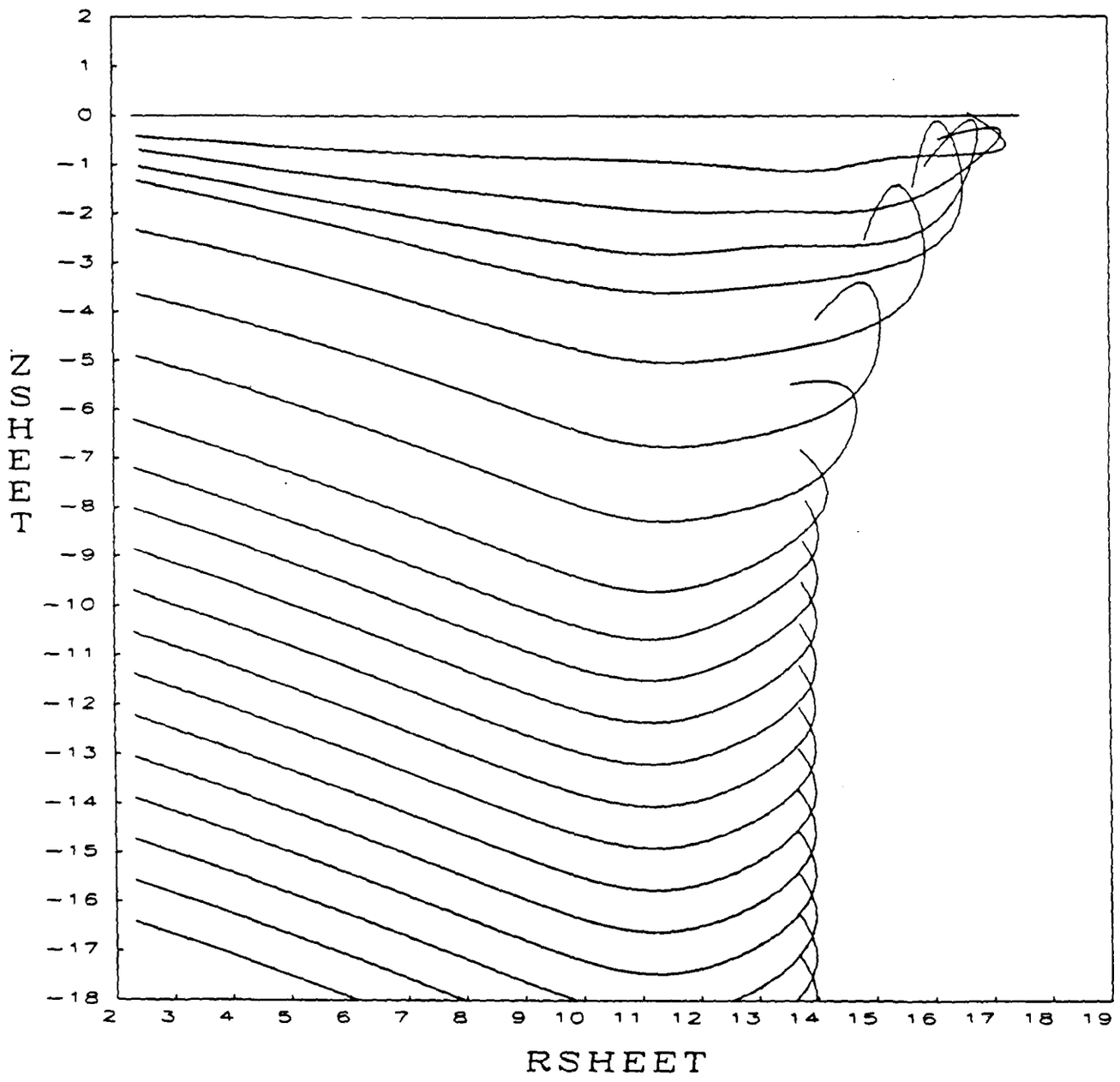

Figure 2C. Wake Geometry for Case 1

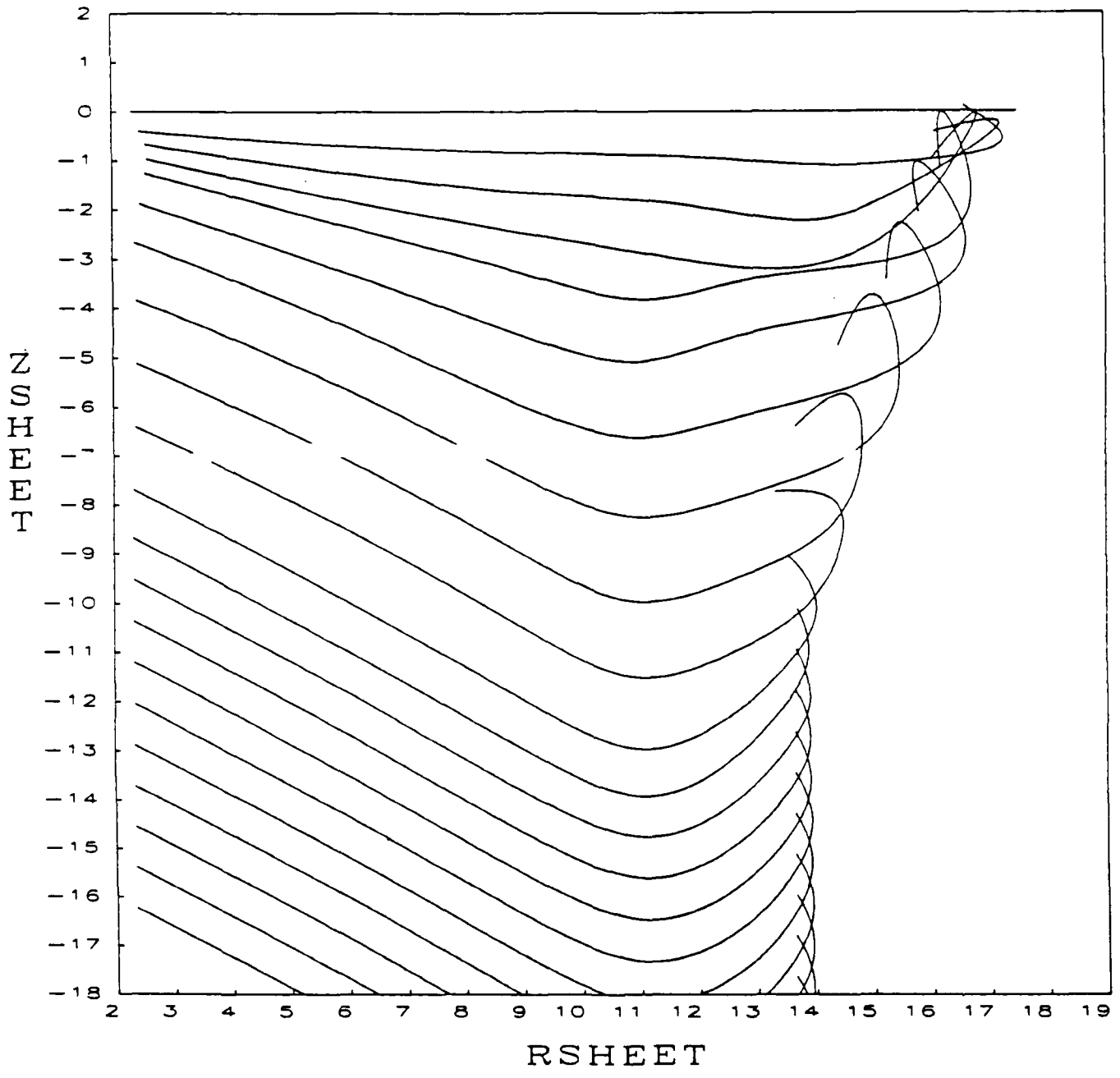

Figure 2D. Wake Geometry for Case 1

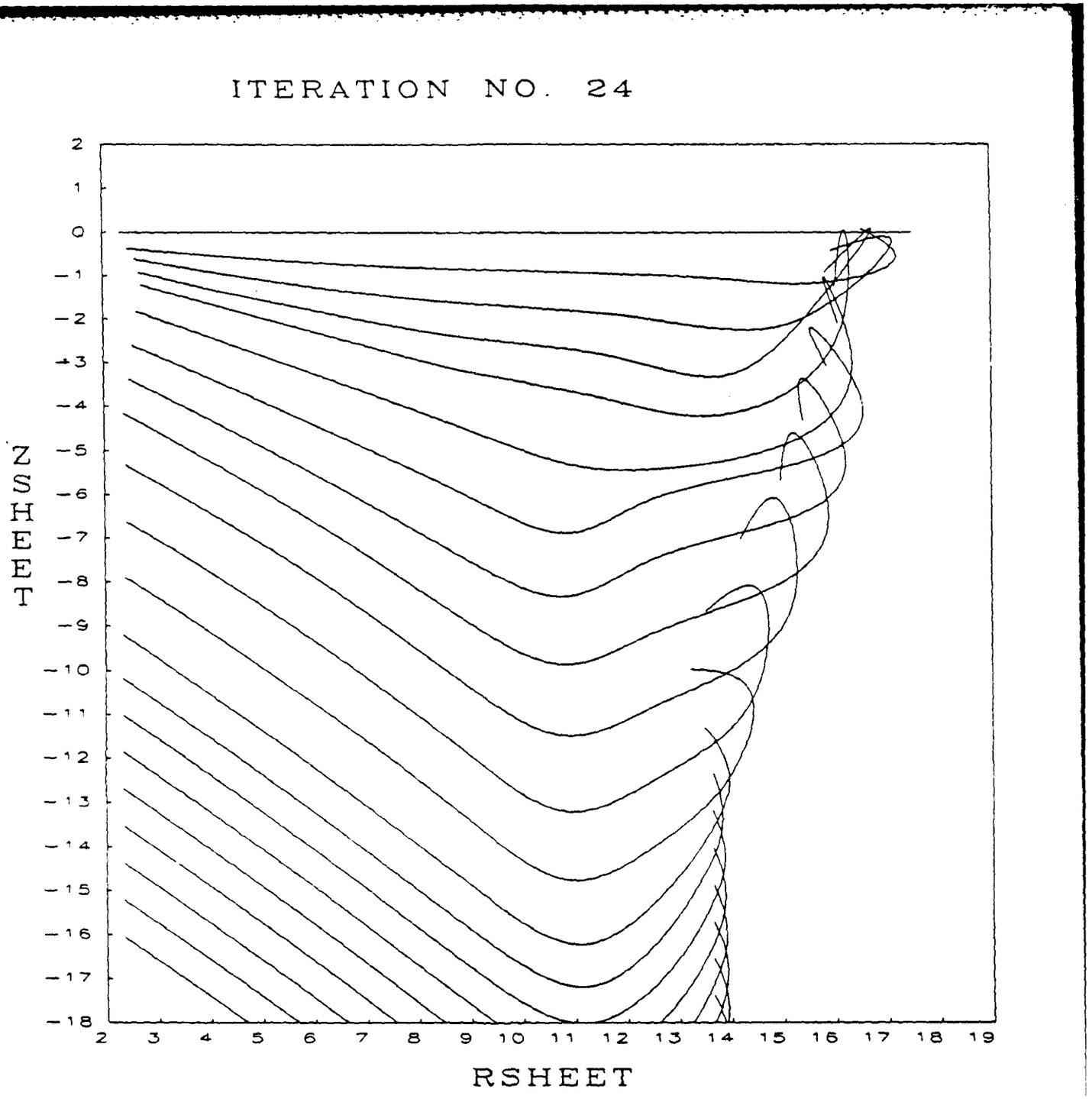

Figure 2E. Wake Geometry for Case 1

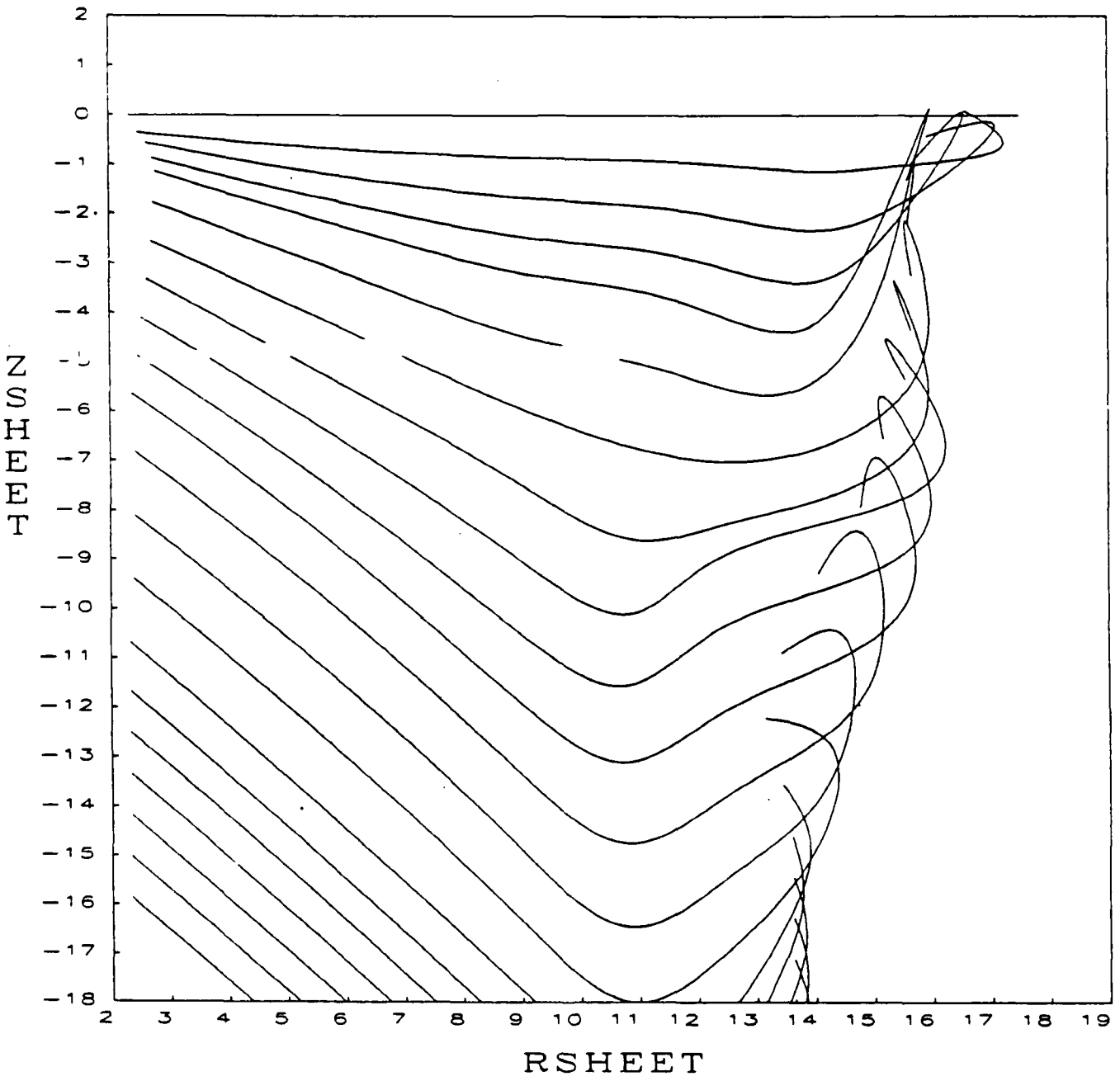

Figure 2F. Wake Geometry for Case 1

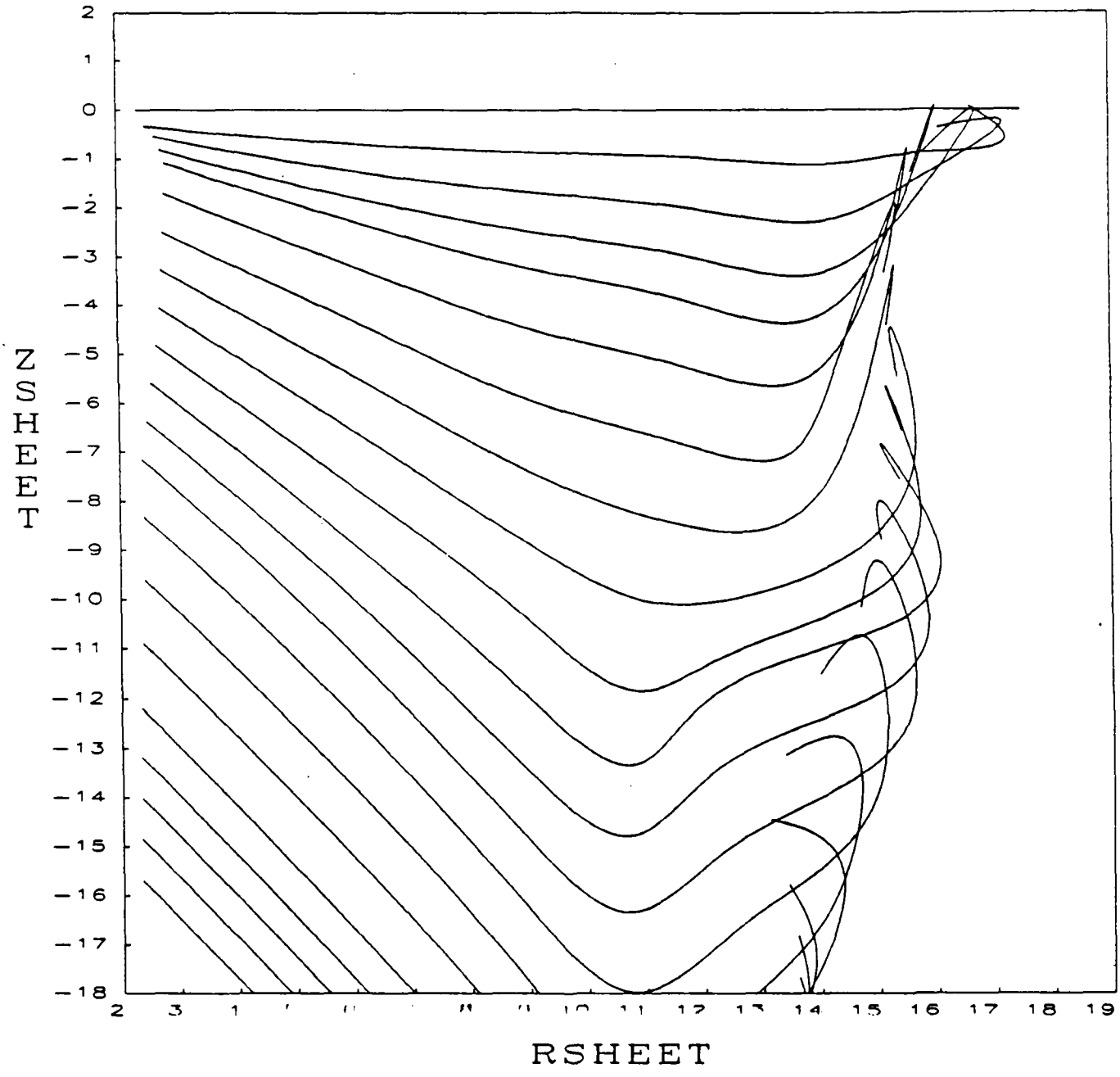

Figure 2G. Wake Geometry for Case 1

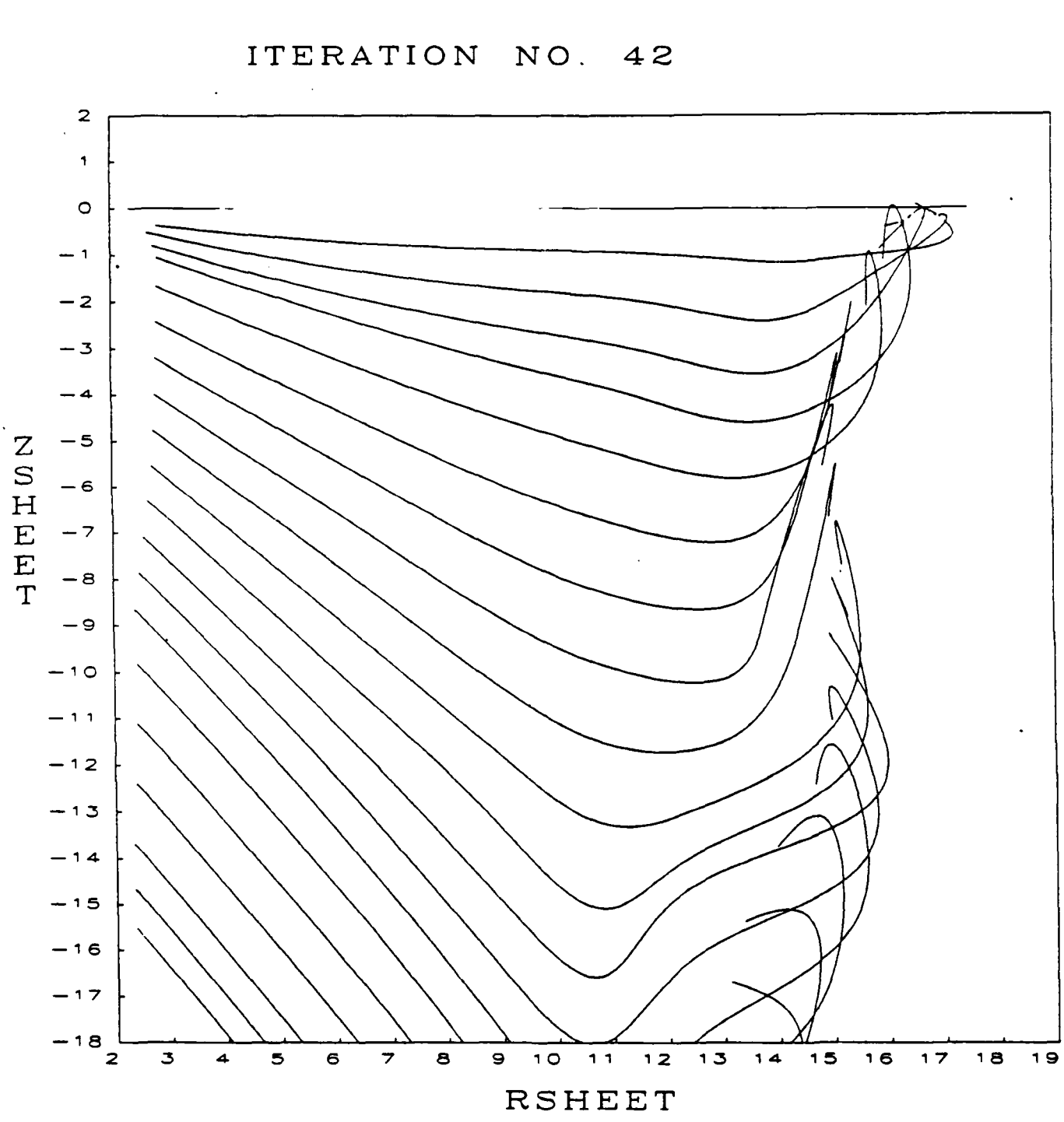

Figure 2H. Wake Geometry for Case 1

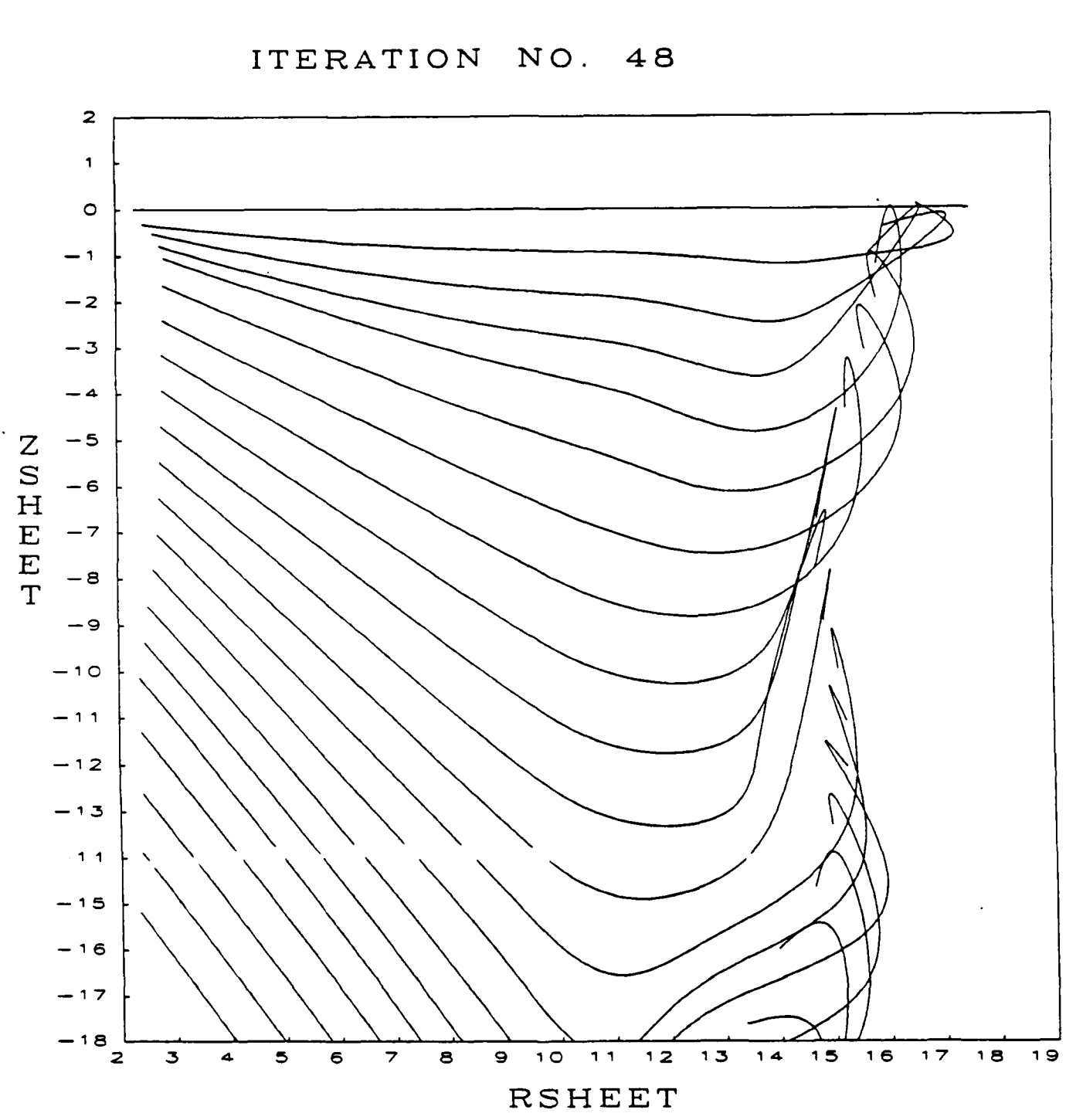

Figure 2I. Wake Geometry for Case 1

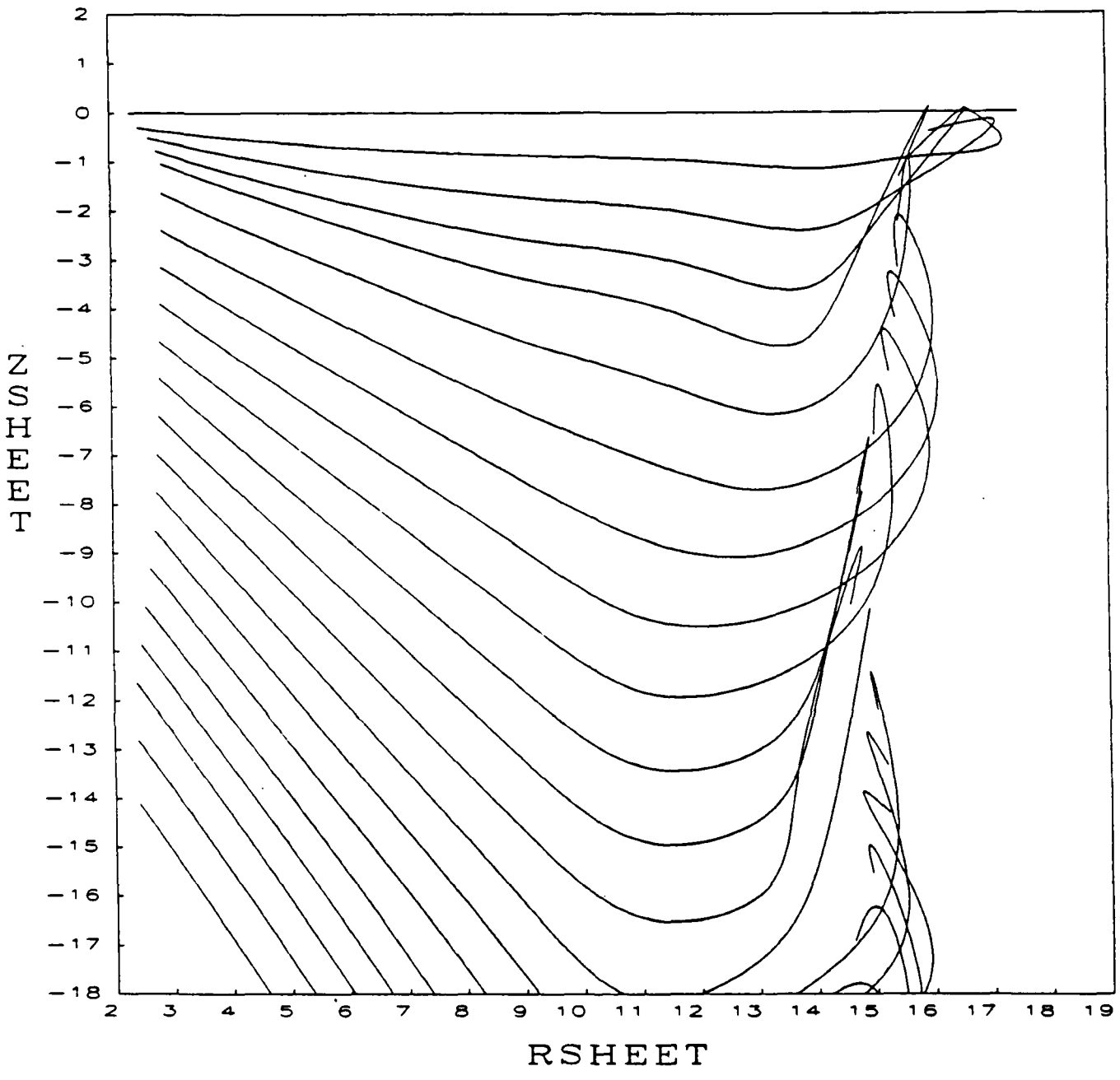

Figure 2J. Wake Geometry for Case 1

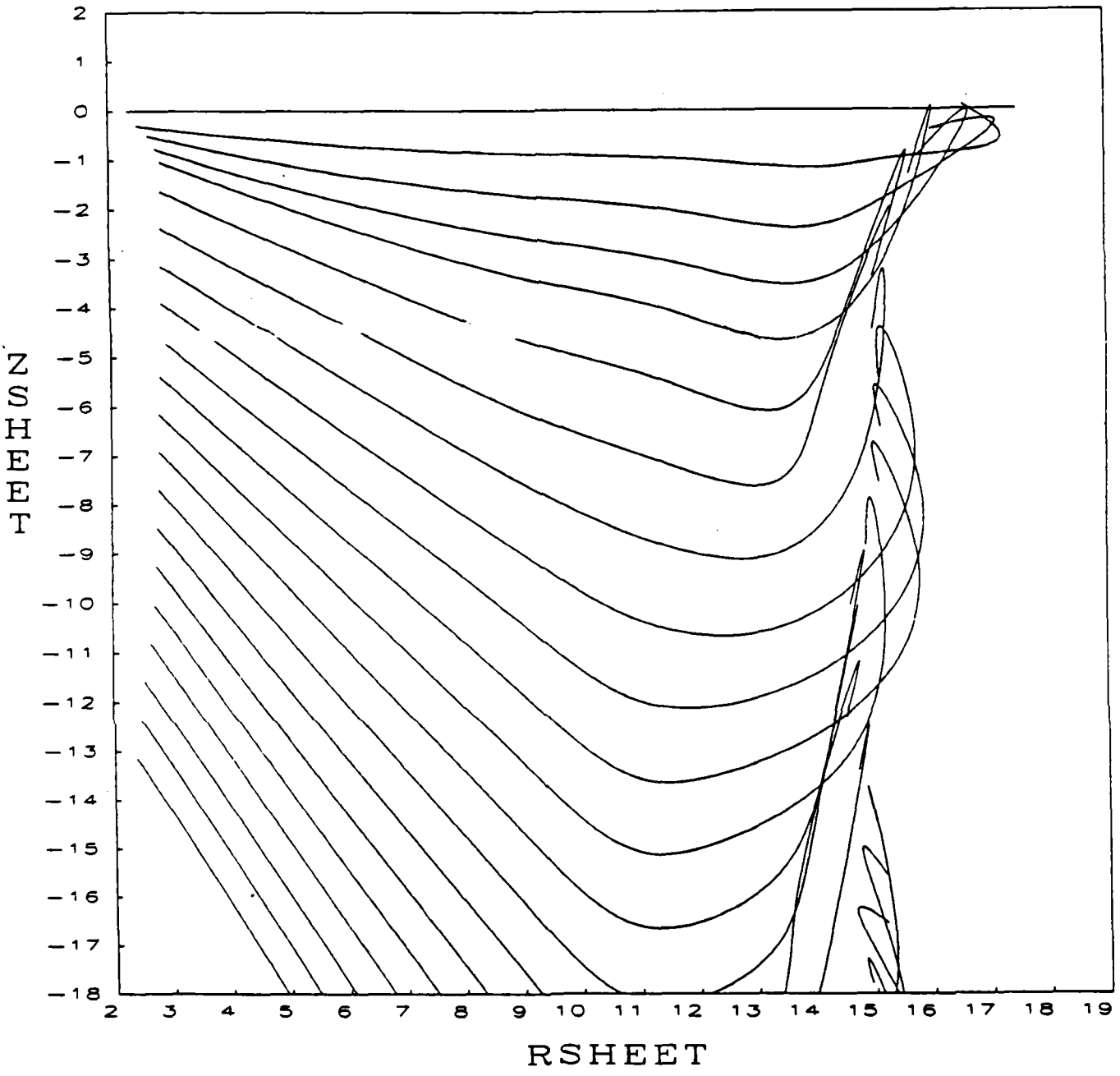

Figure 2K. Wake Geometry for Case 1

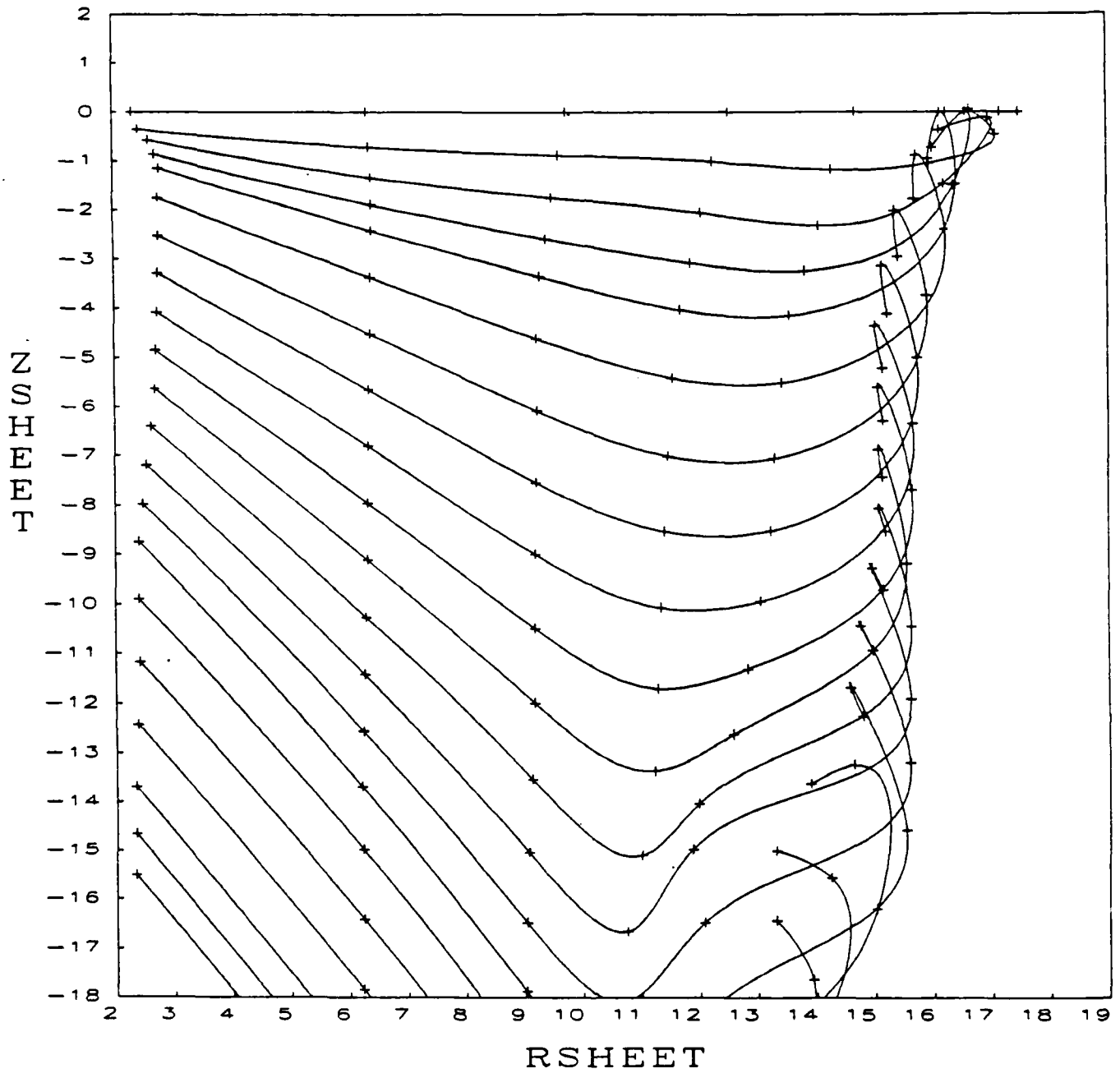

Figure 3A. Wake Geometry for Case 2

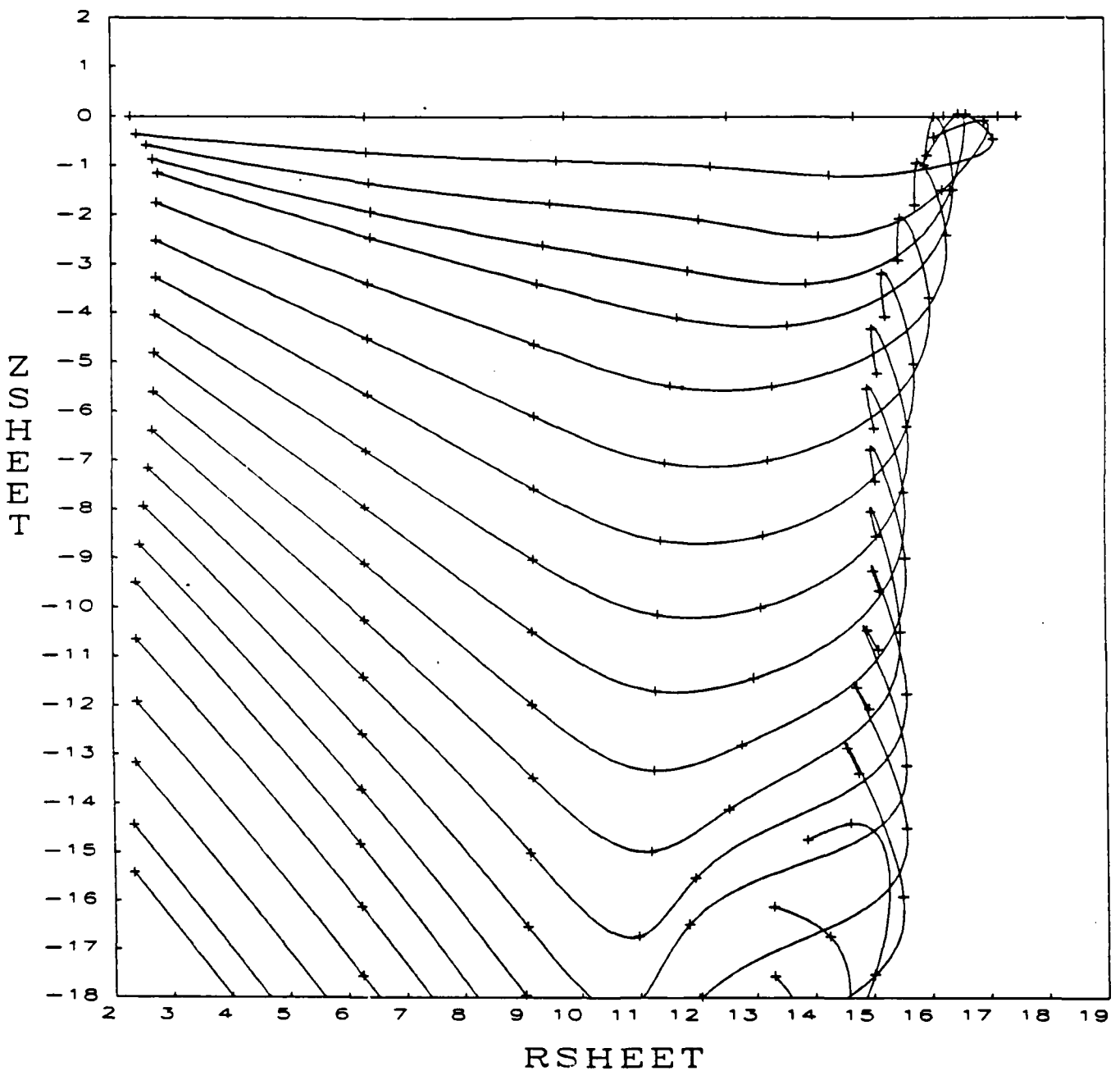

Figure 3B. Wake Geometry for Case 2

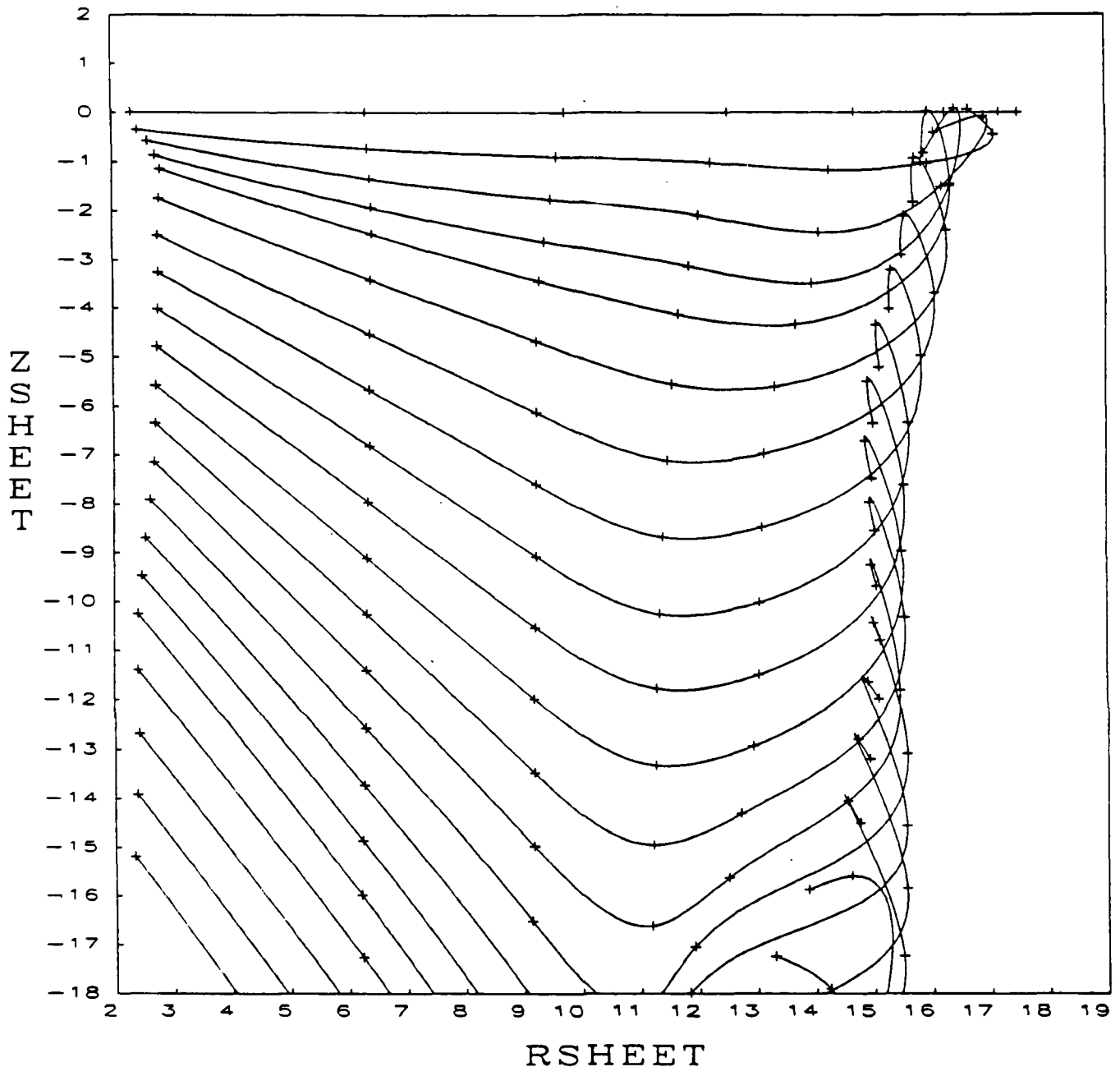

Figure 3C. Wake Geometry for Case 2

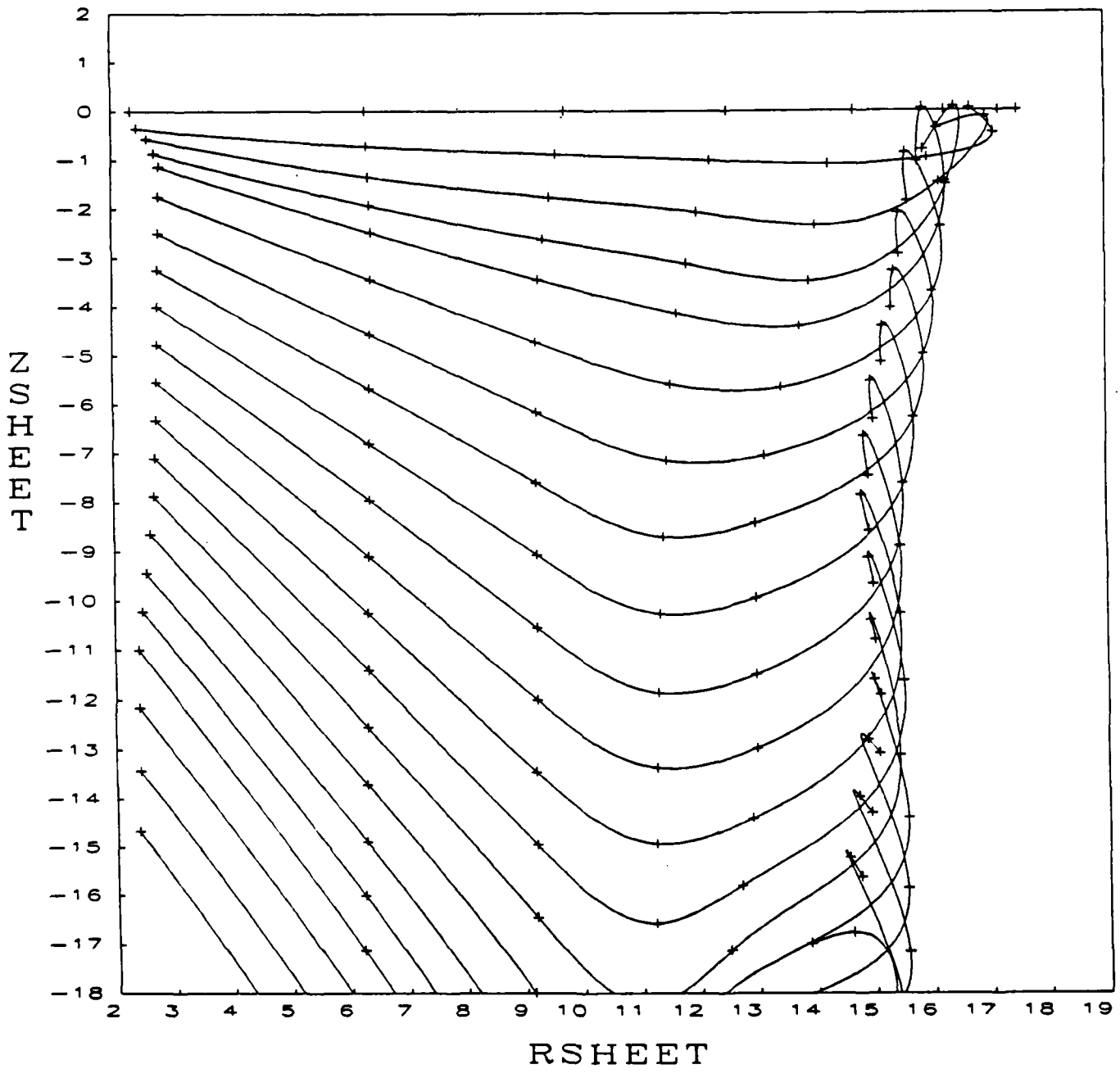

Figure 3D. Wake Geometry for Case 2

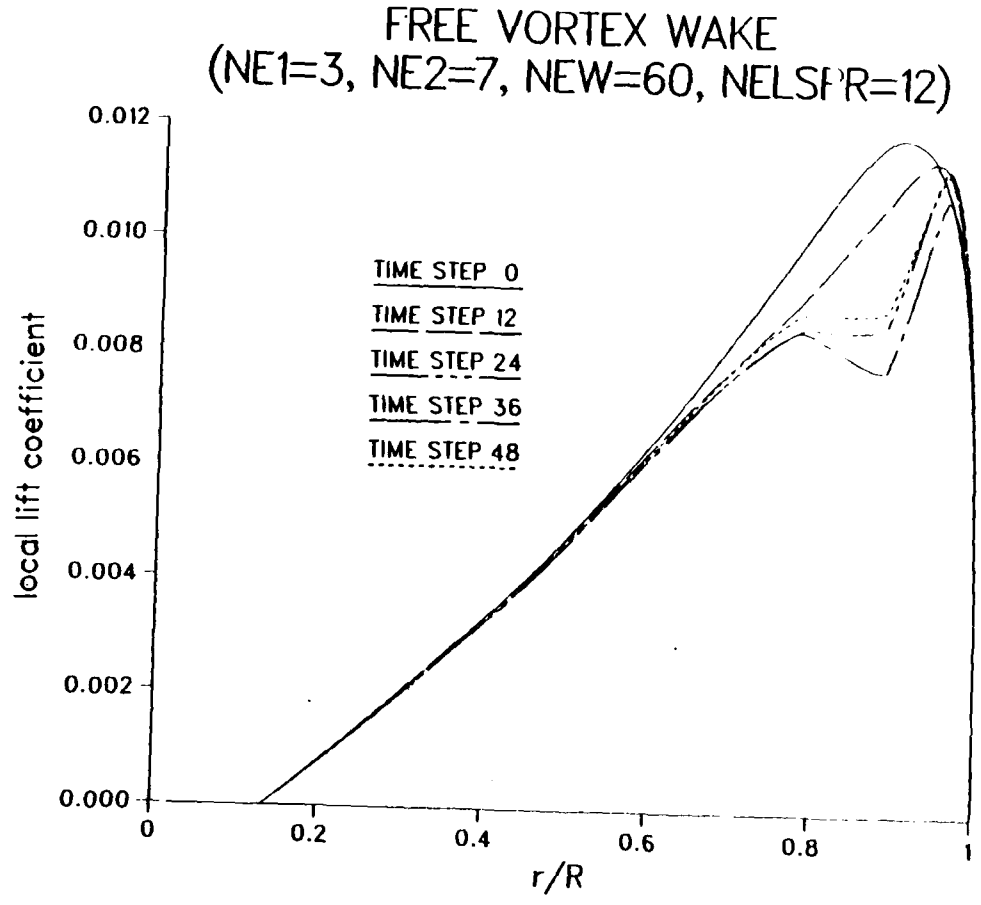

Figure 4. Sectional Lift Distribution for Case 2

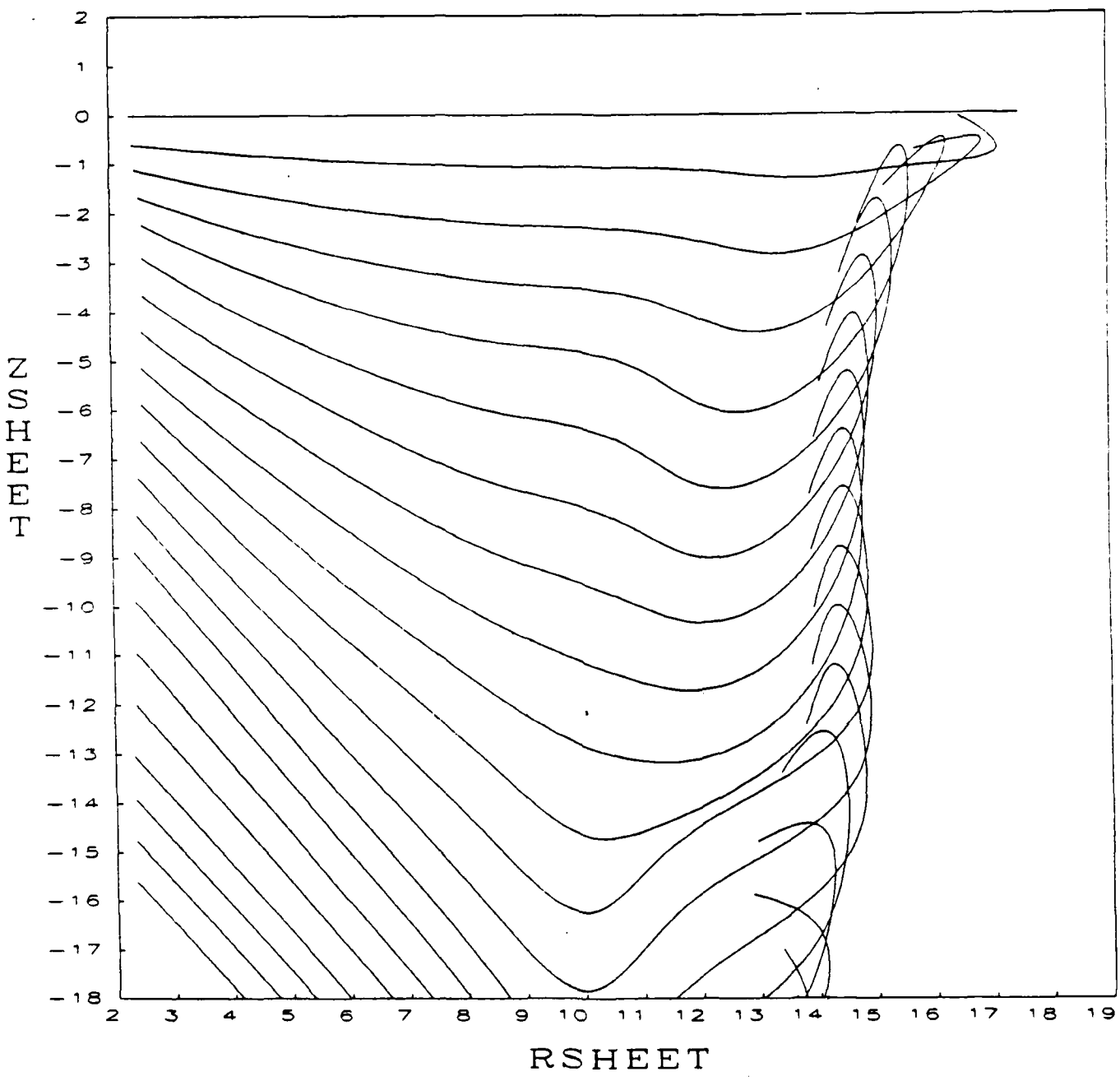

Figure 5A. Wake Geometry for Case 3

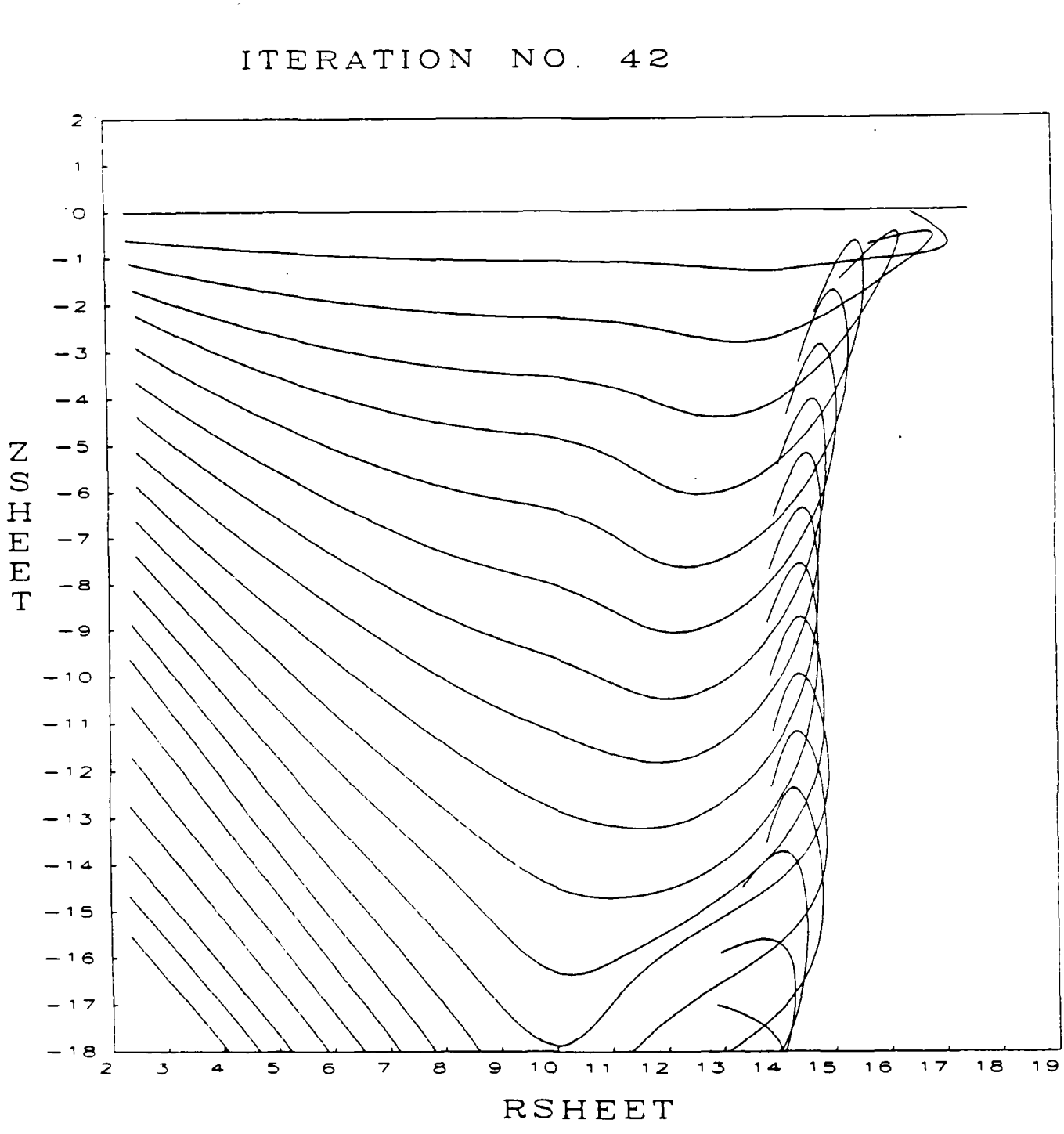

Figure 5B. Wake Geometry for Case 3

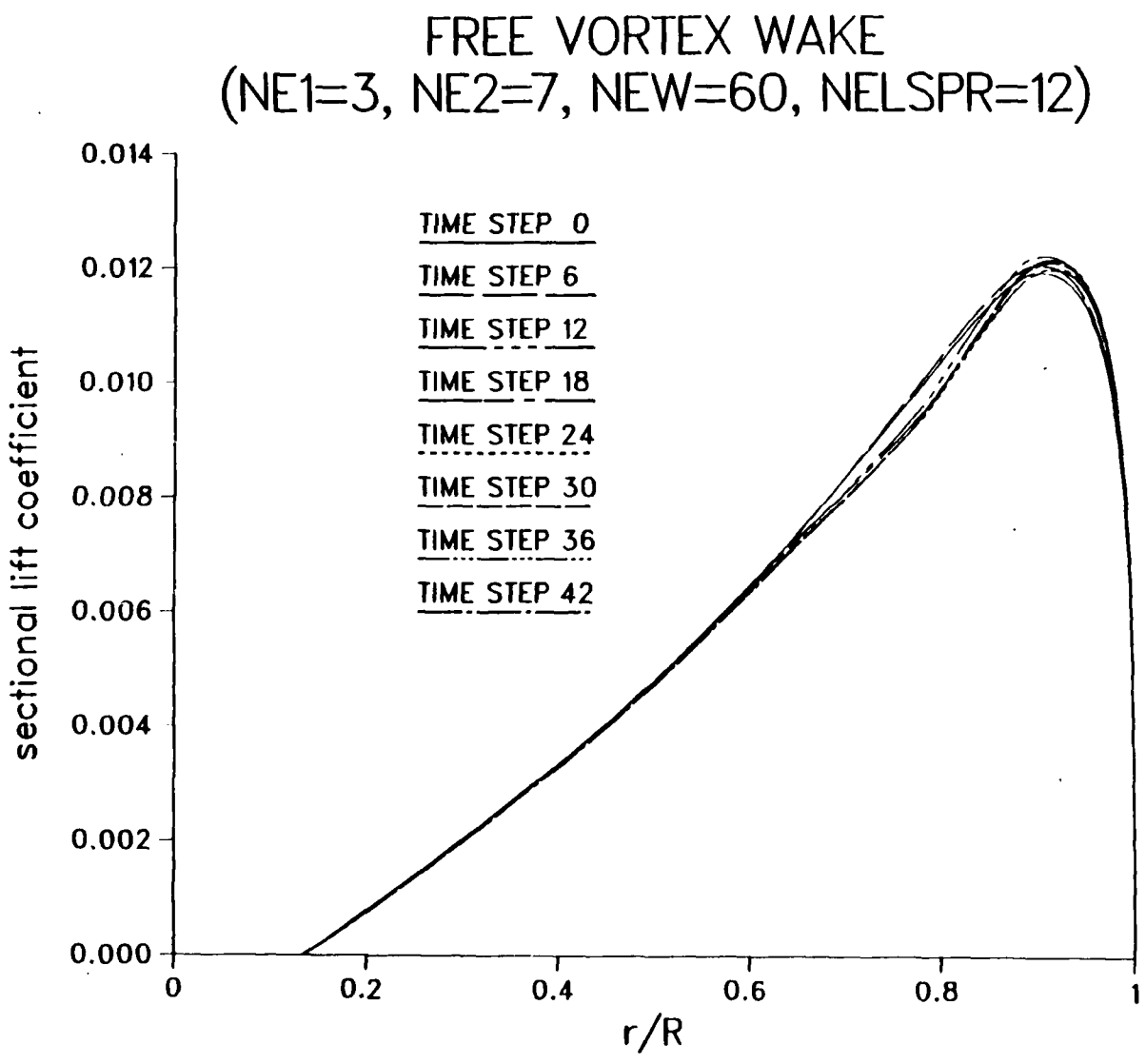

Figure 6. Sectional Lift Distribution for Case 3

AD-A161 513 TWO METHODS FOR VISCOUS AND INVISCID FREE-WAKE ANALYSIS OF HELICOPTER ROT..(U) BOSTON UNIV MA CENTER FOR COMPUTATIONAL AND APPLIED DYNAMICS.. L MORINO ET AL. 2/2

UNCLASSIFIED AUG 85 CCAD-TR-85-2 ARO-19797.3-EG F/G 20/4 NL

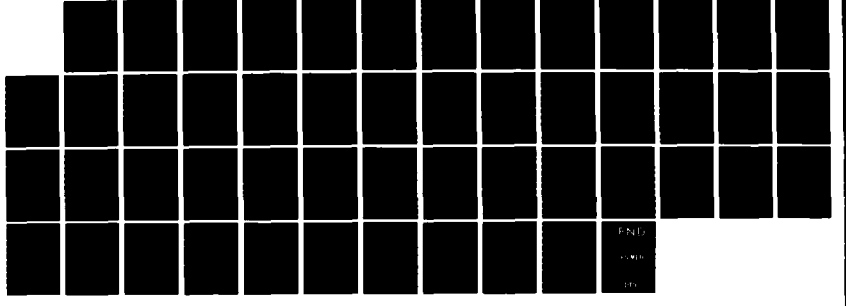

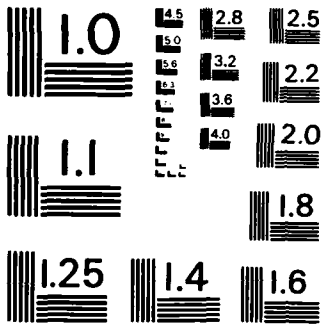

MICROCOPY RESOLUTION TEST CHART
NATIONAL BUREAU OF STANDARDS-1963-A

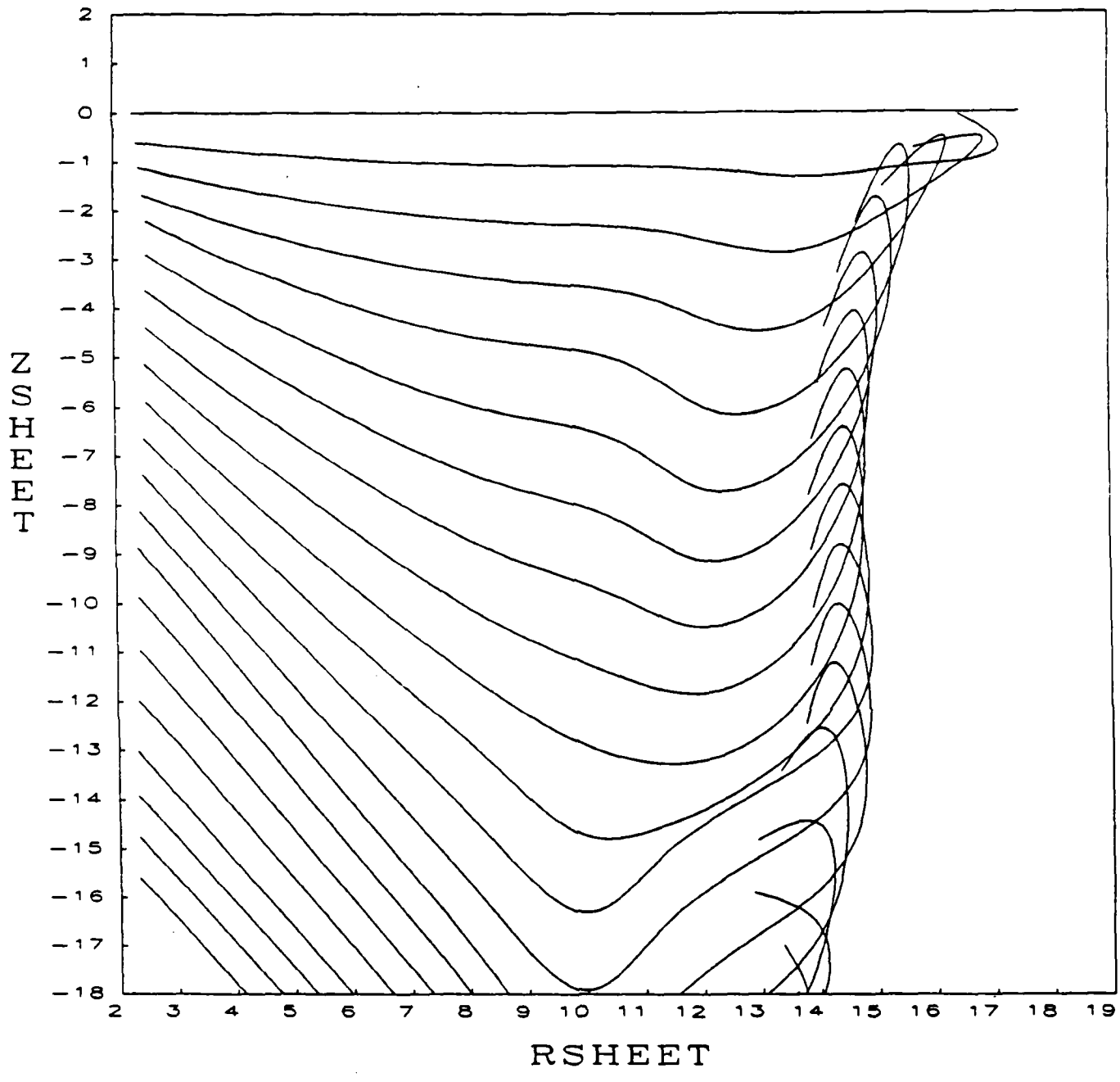

Figure 7A. Wake Geometry for Case 3A

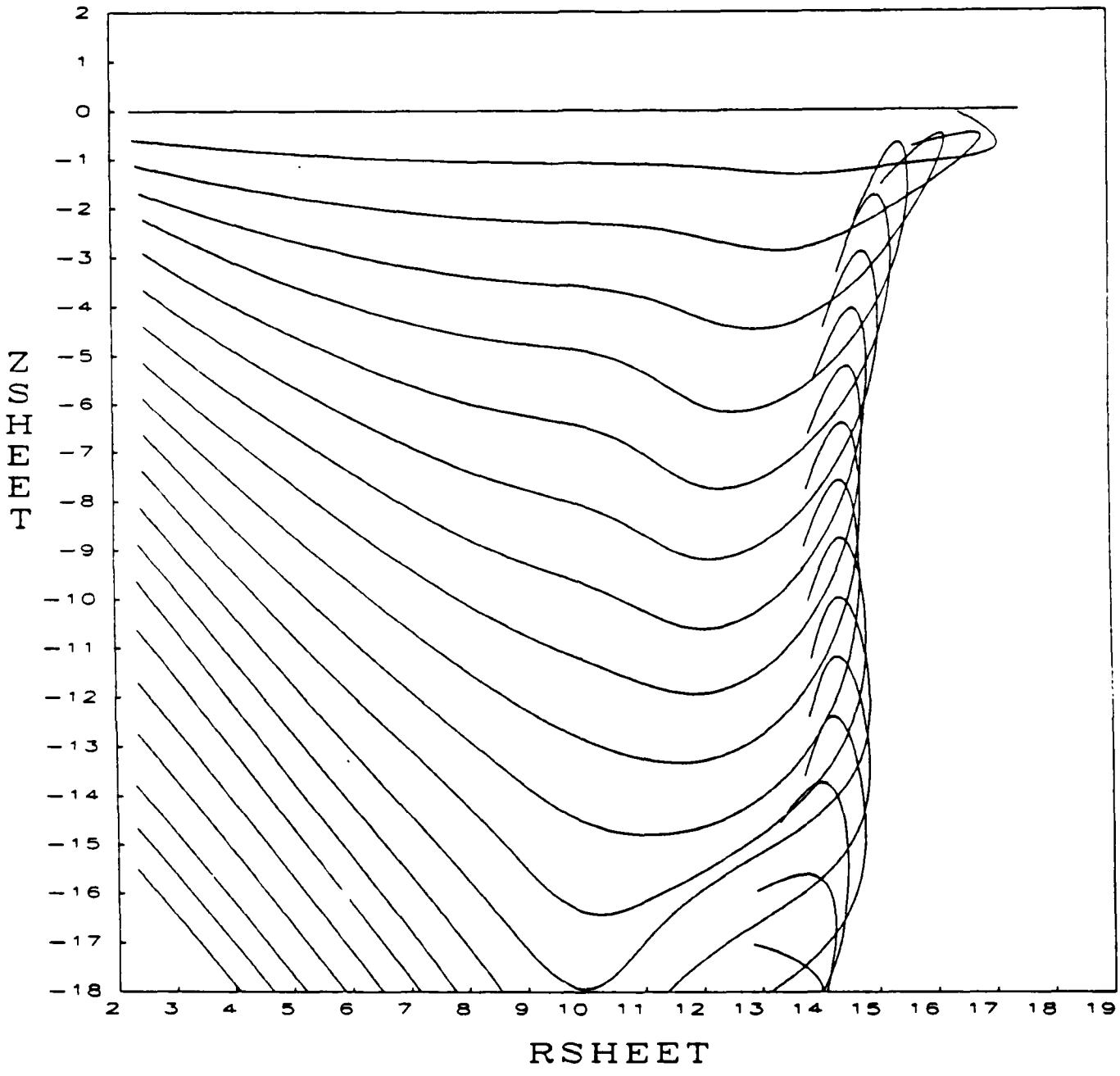

Figure 7B. Wake Geometry for Case 3A

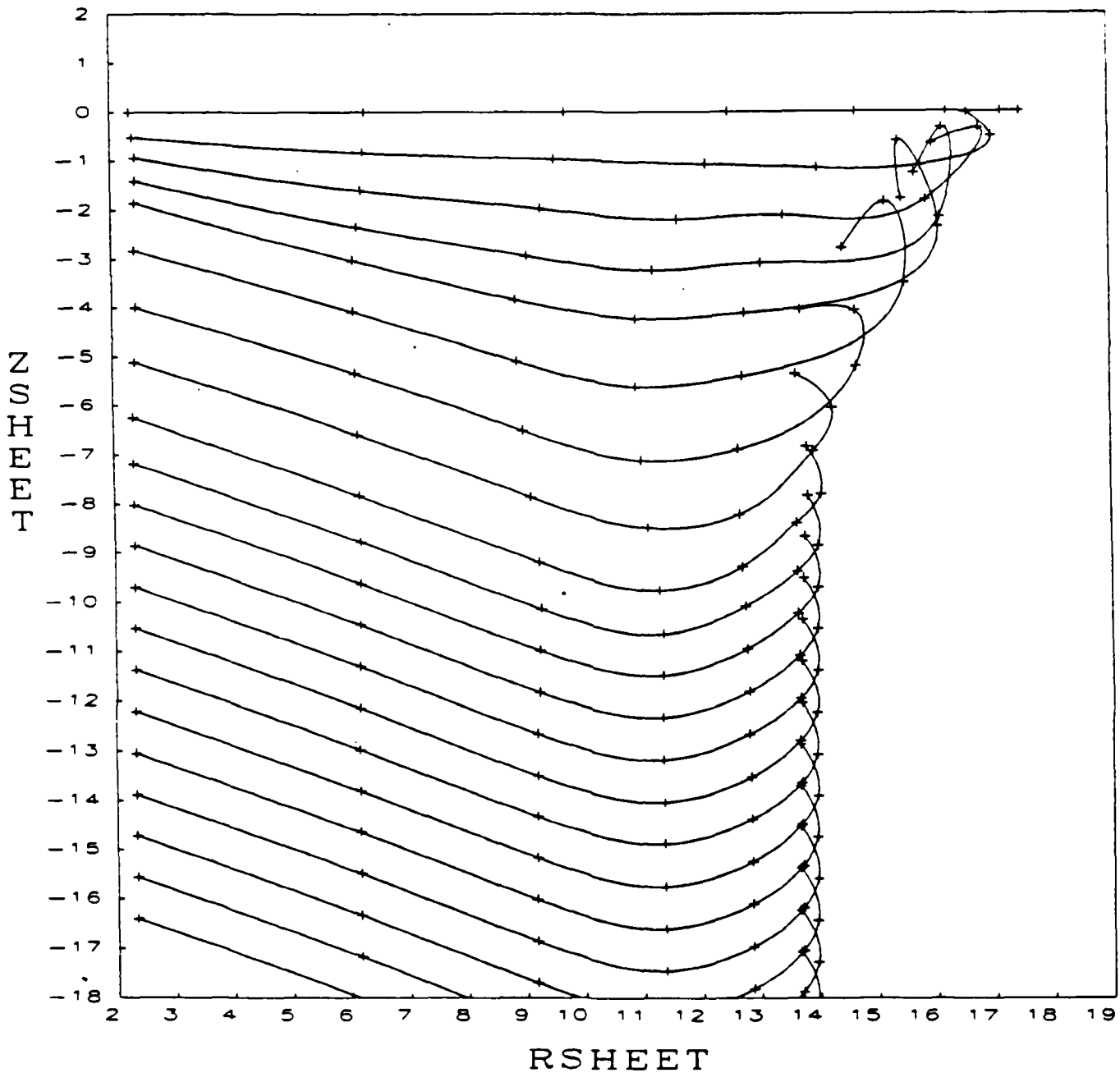

Figure 8A. Wake Geometry for Case 4

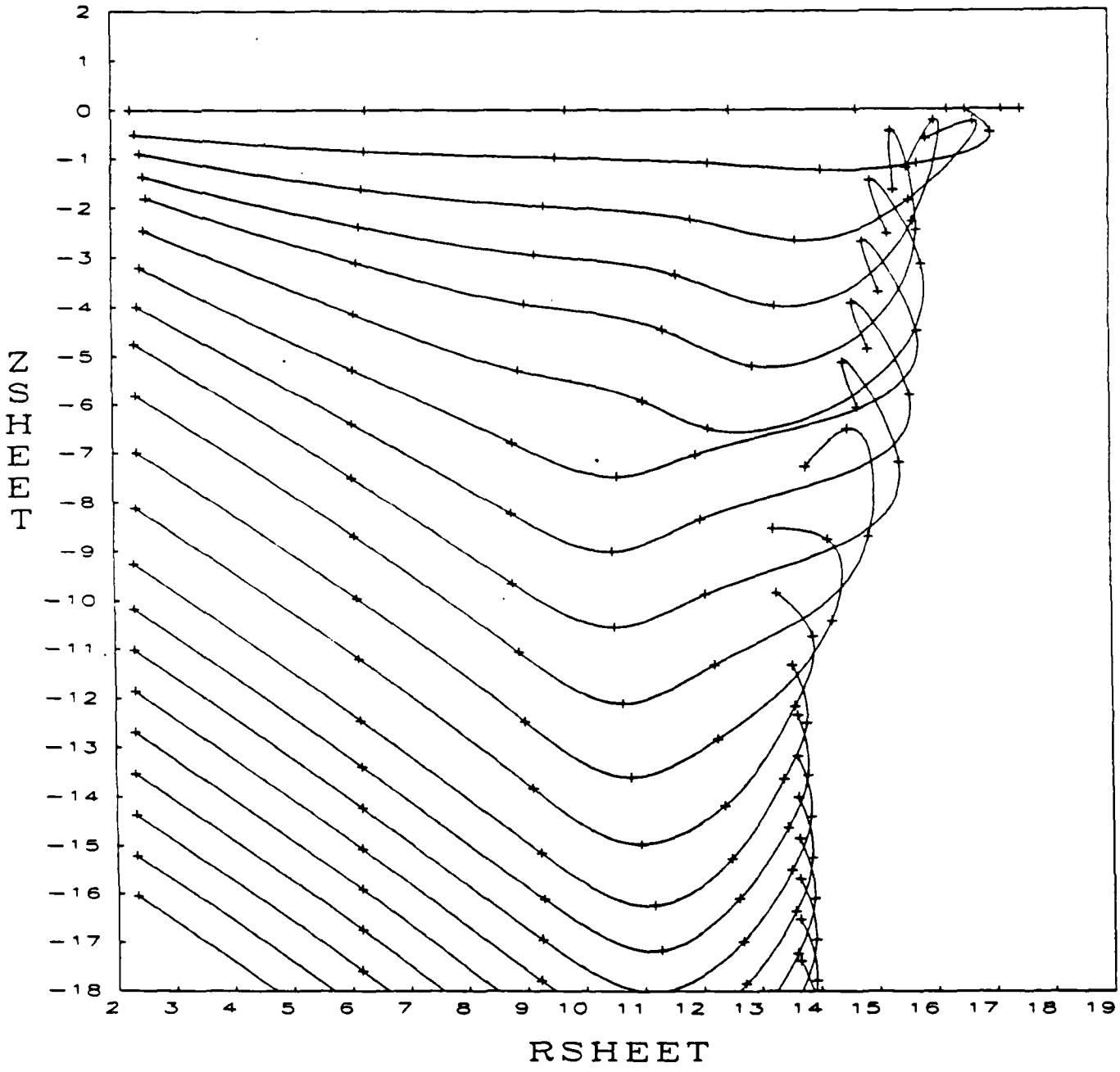

Figure 8B. Wake Geometry for Case 4

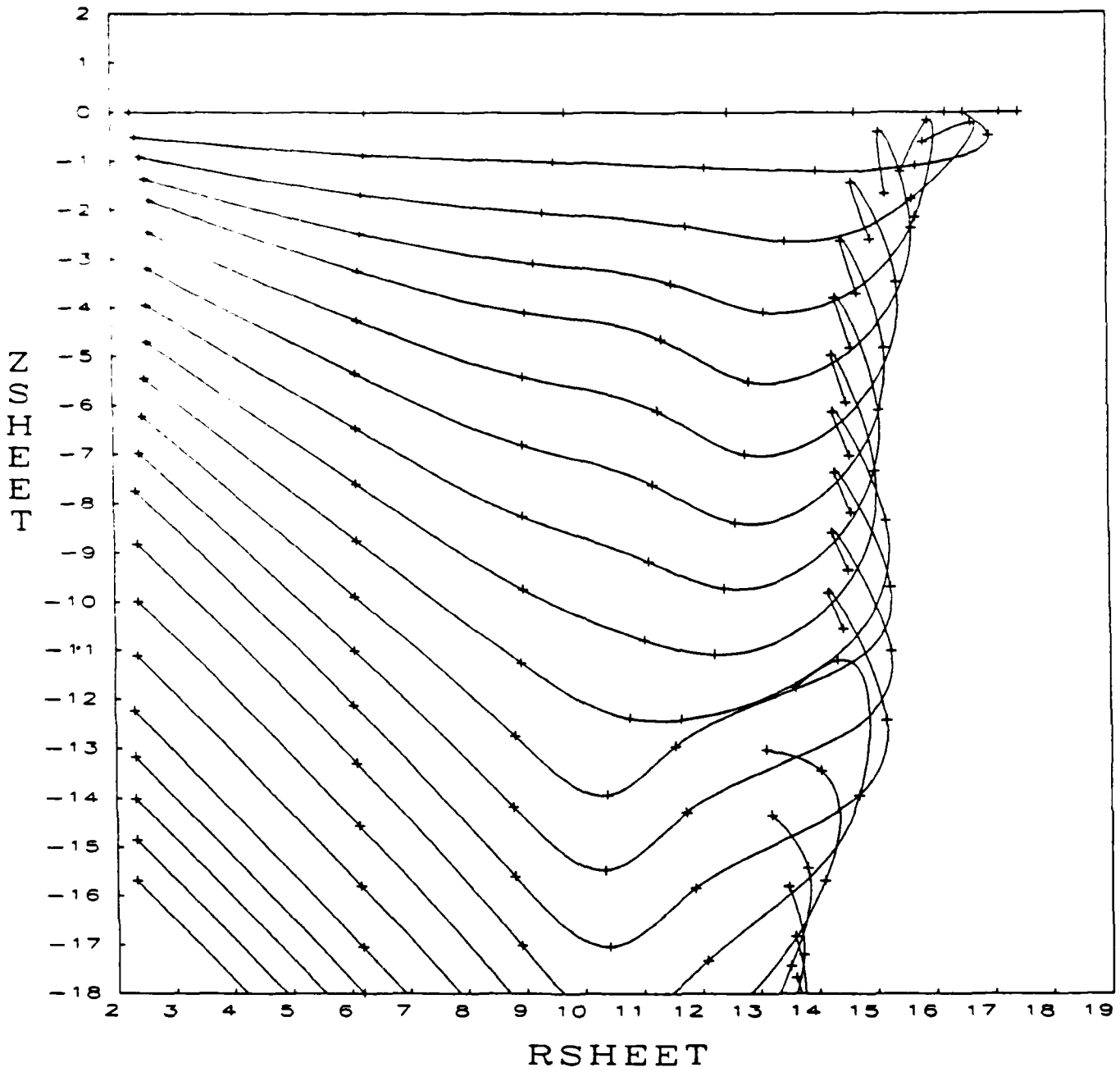

Figure 8C. Wake Geometry for Case 4

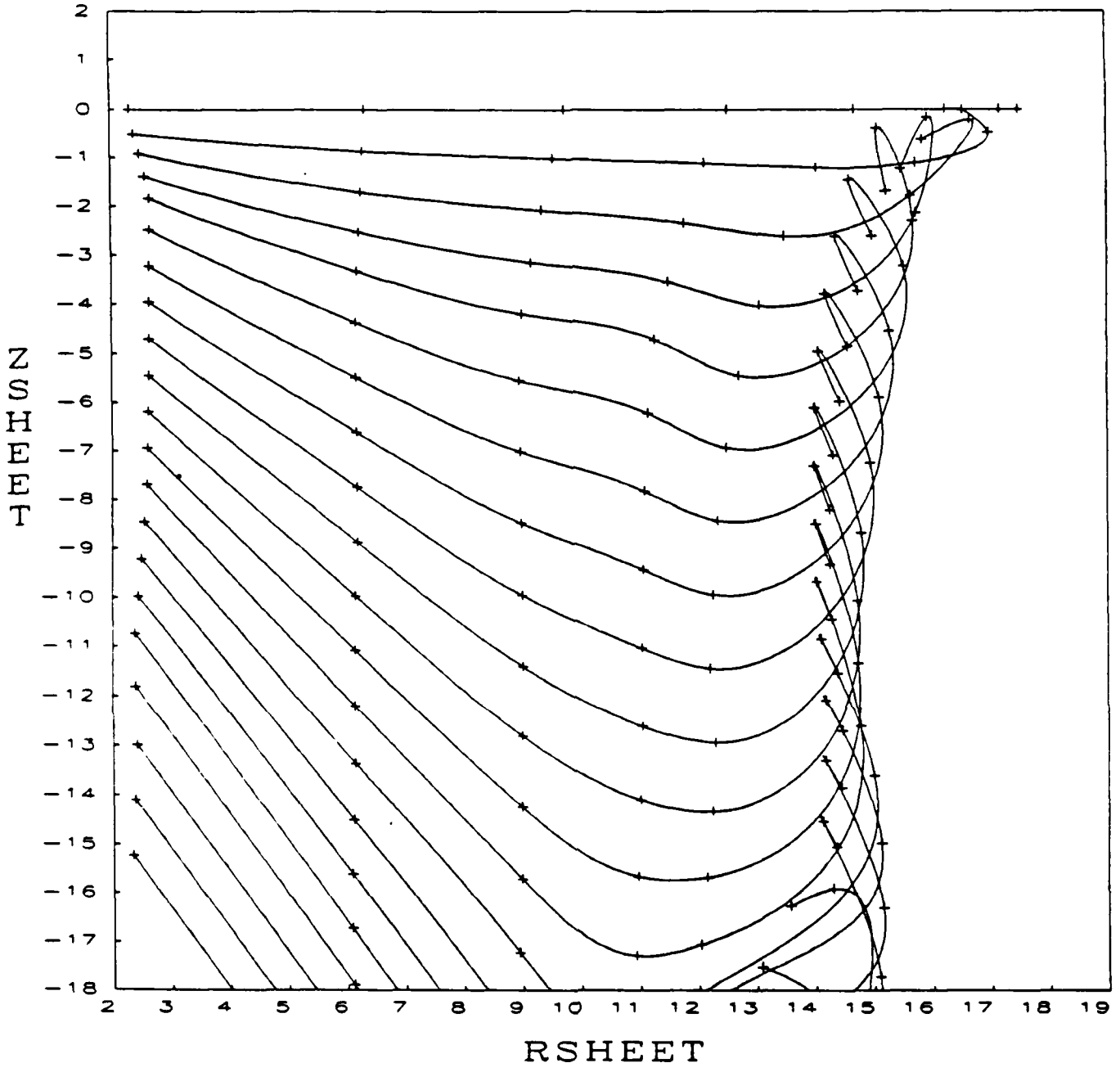

Figure 8D. Wake Geometry for Case 4

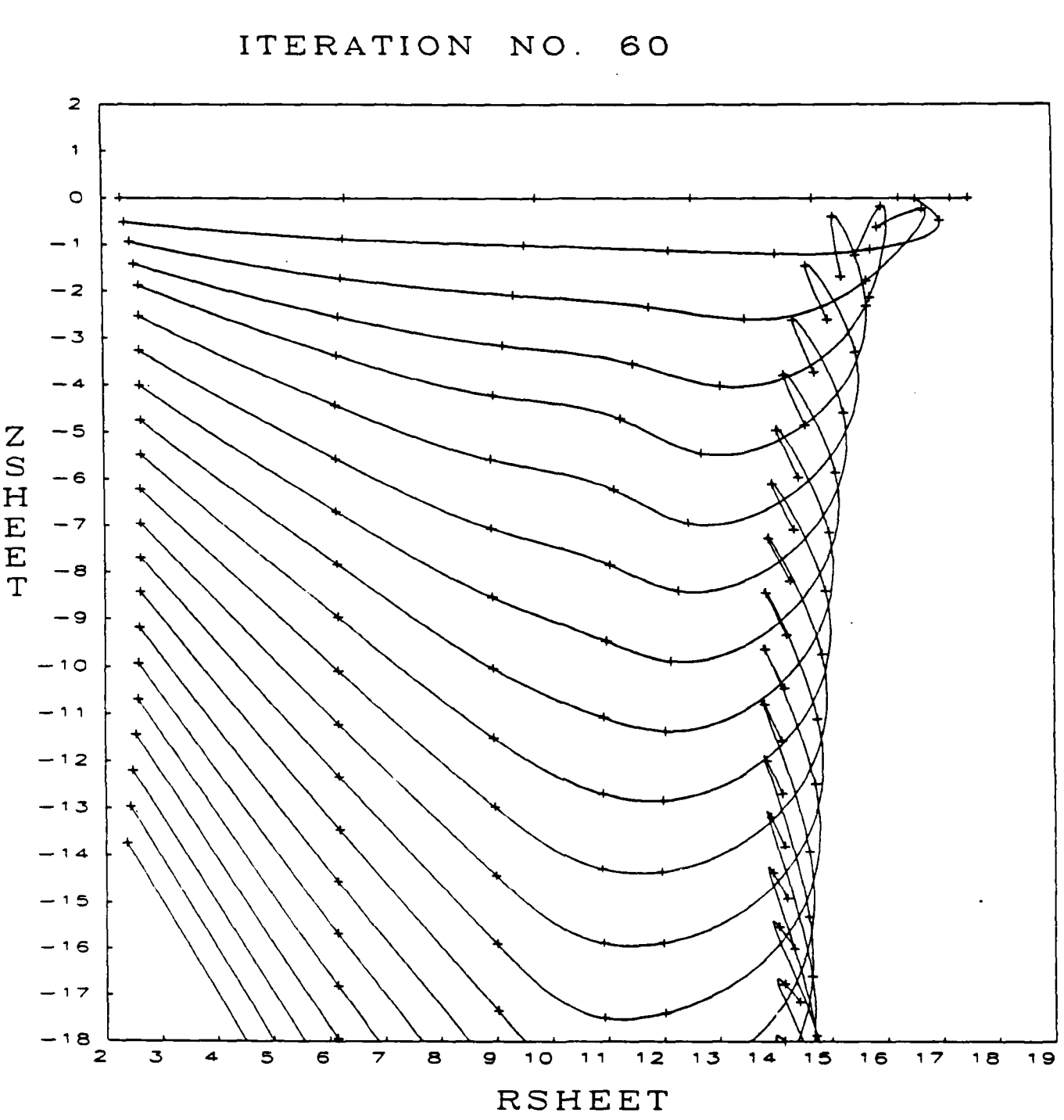

Figure 8E. Wake Geometry for Case 4

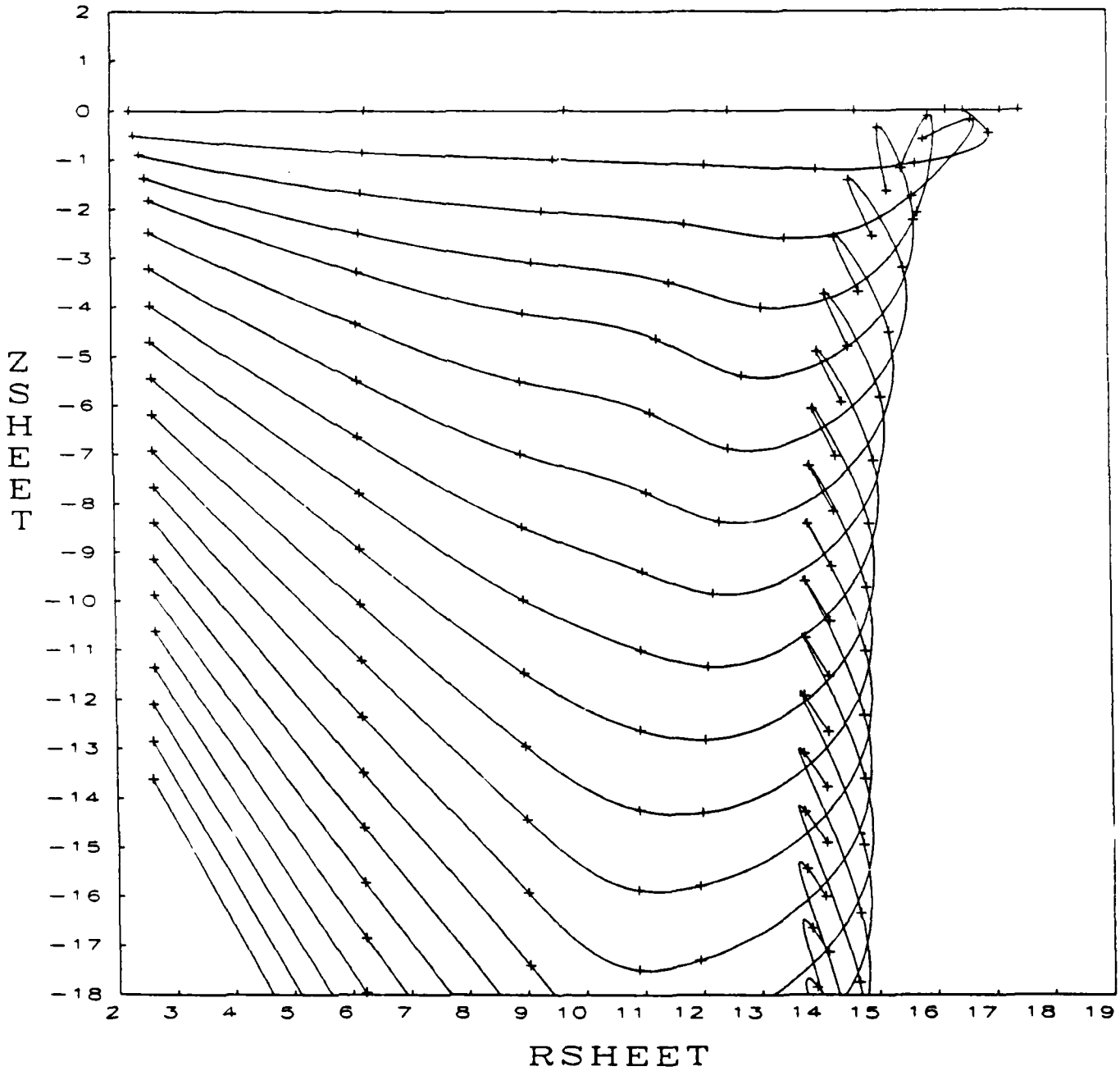

Figure 8F. Wake Geometry for Case 4

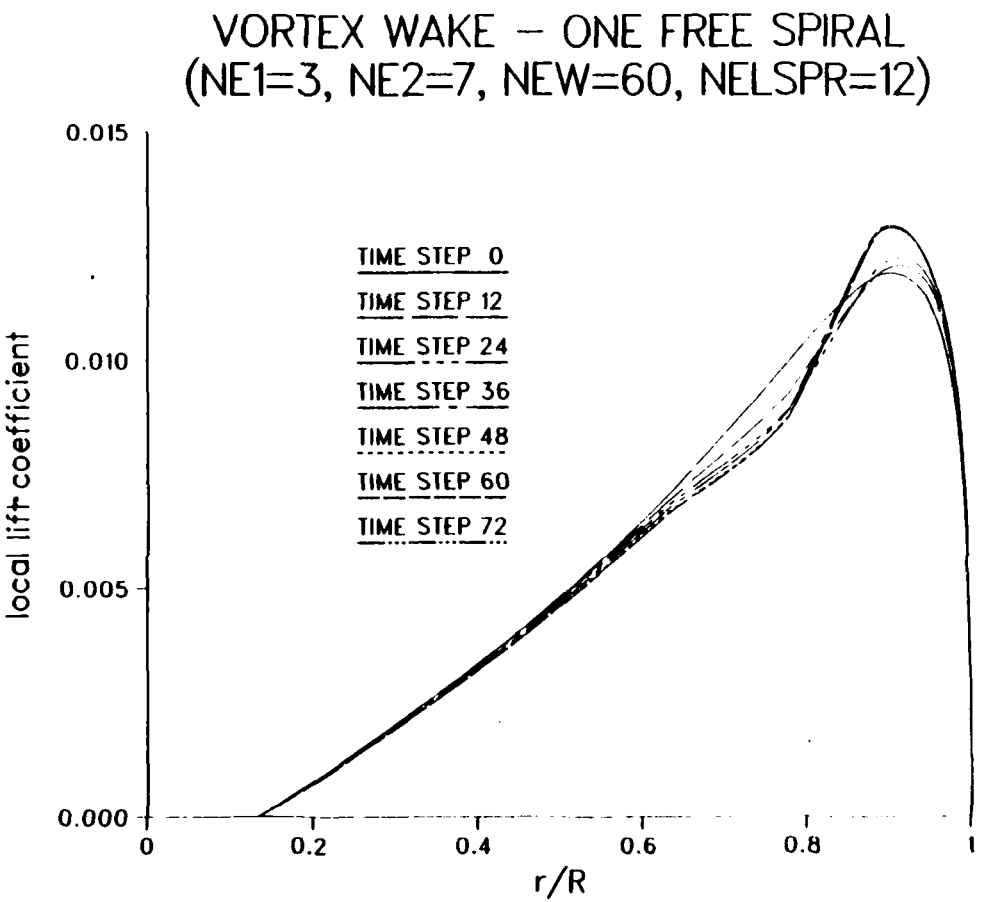

Figure 9. Sectional Lift Distribution for Case

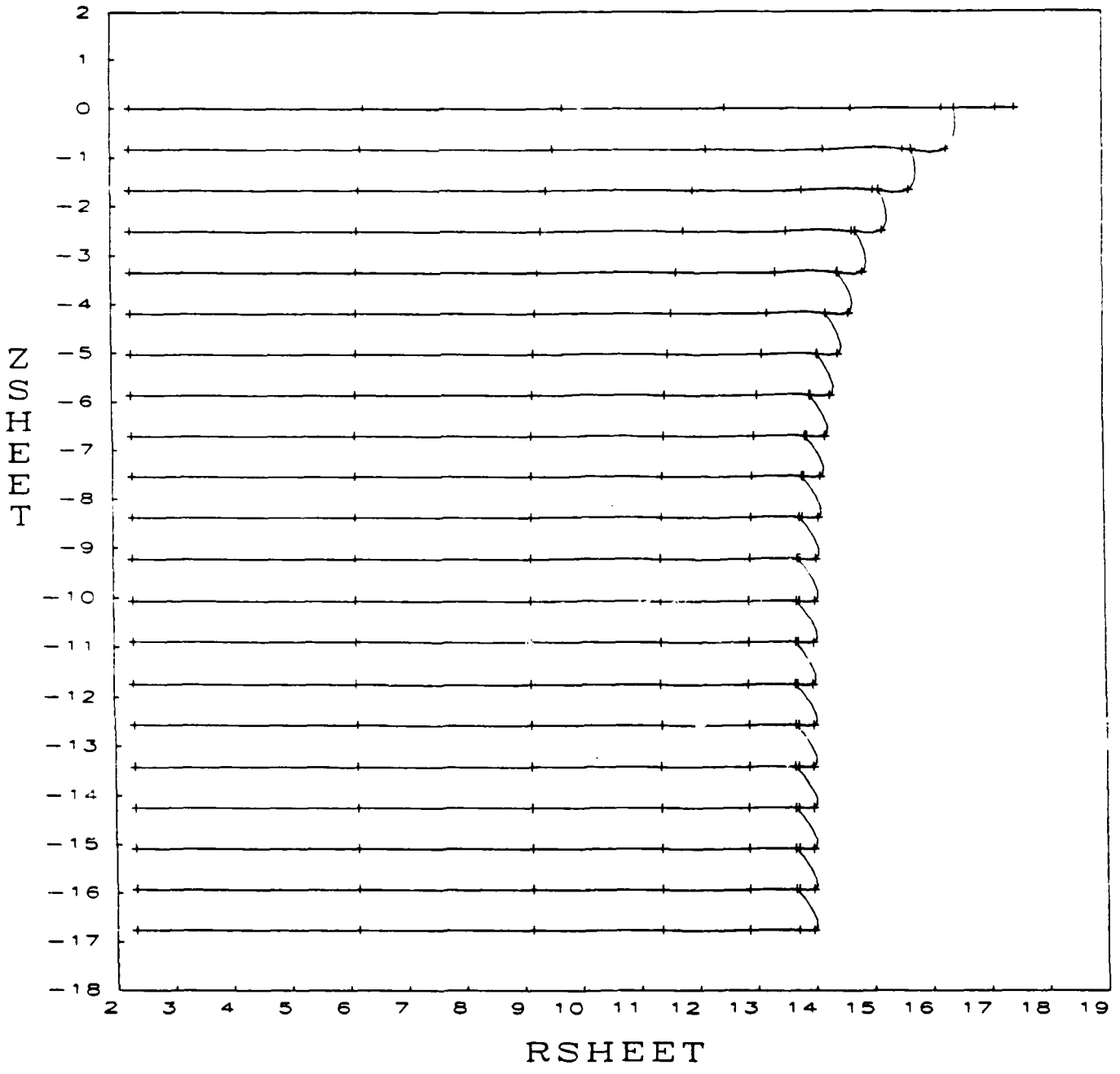

Figure 10A. Wake Geometry for Case 5

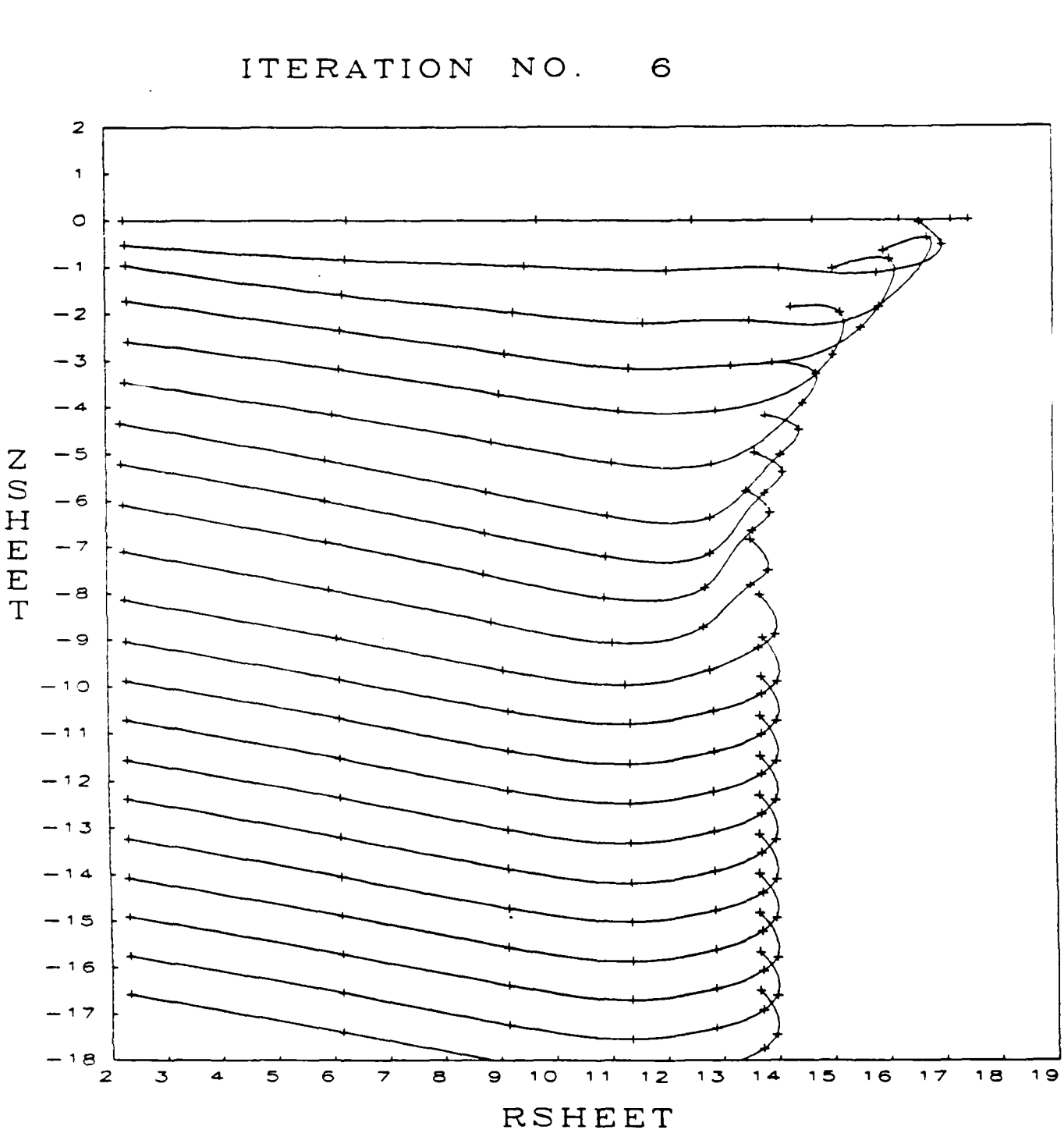

Figure 10B. Wake Geometry for Case 5

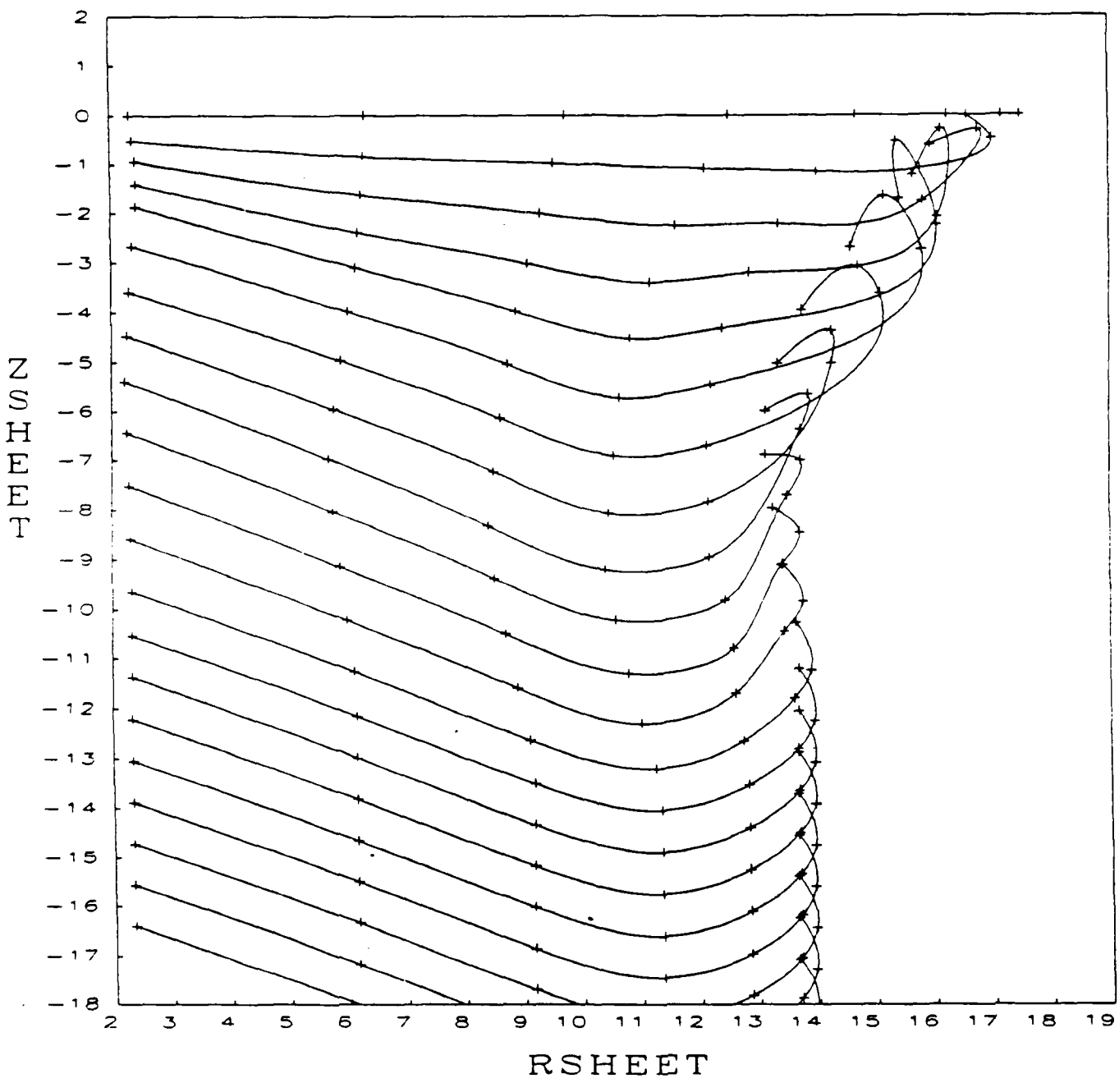

Figure 10C. Wake Geometry for Case 5

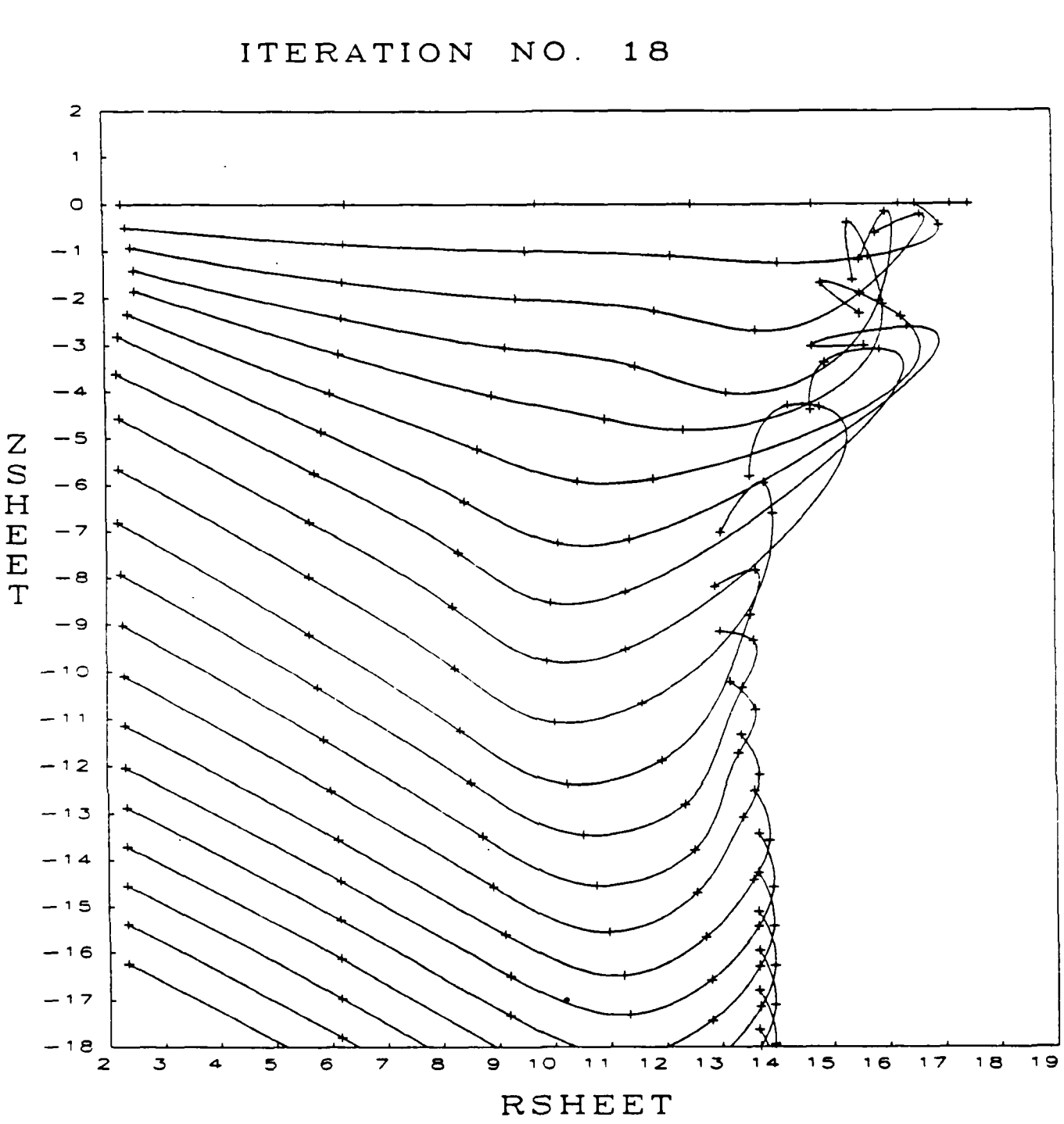

Figure 10D. Wake Geometry for Case 5

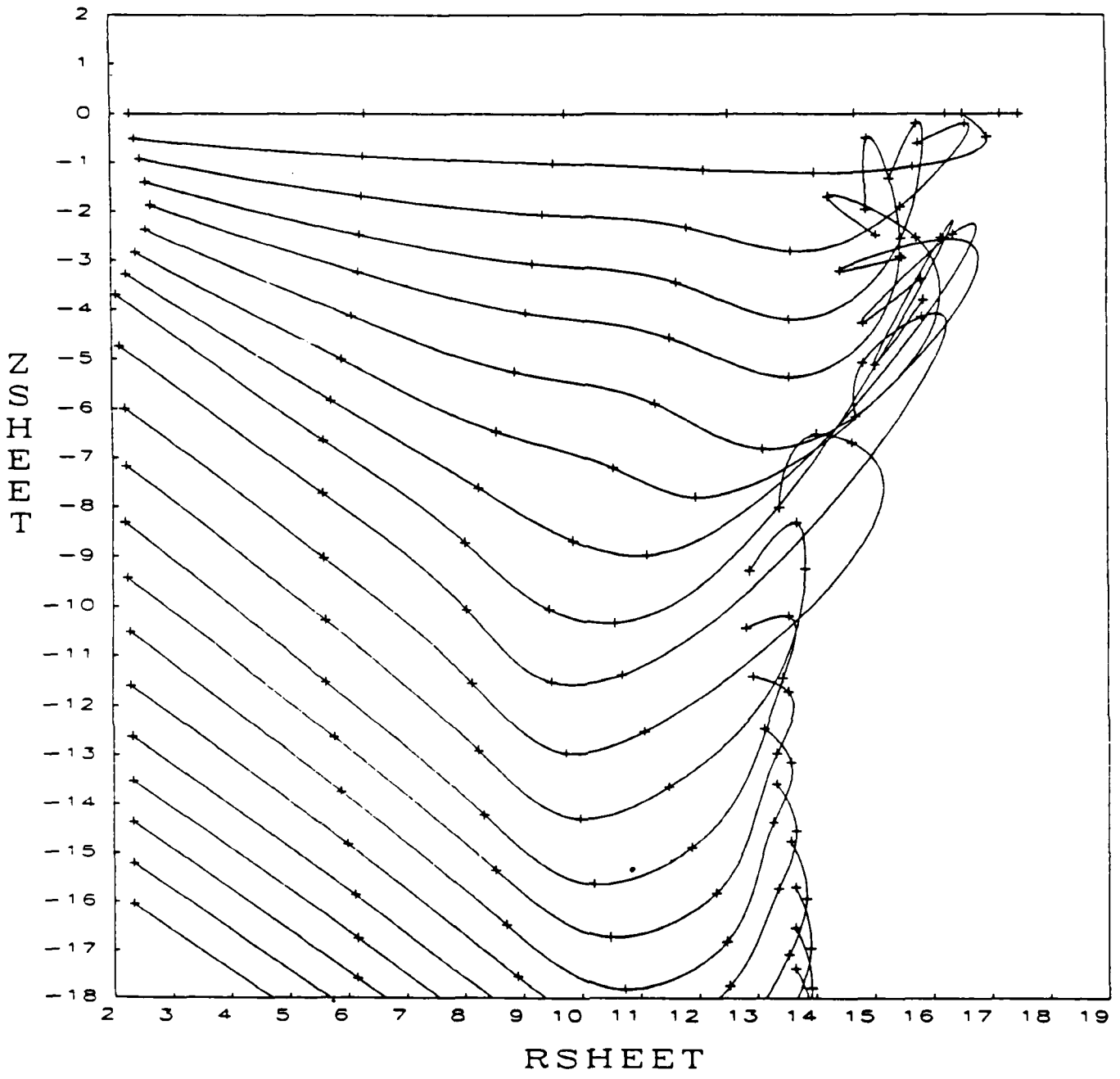

Figure 10E. Wake Geometry for Case 5

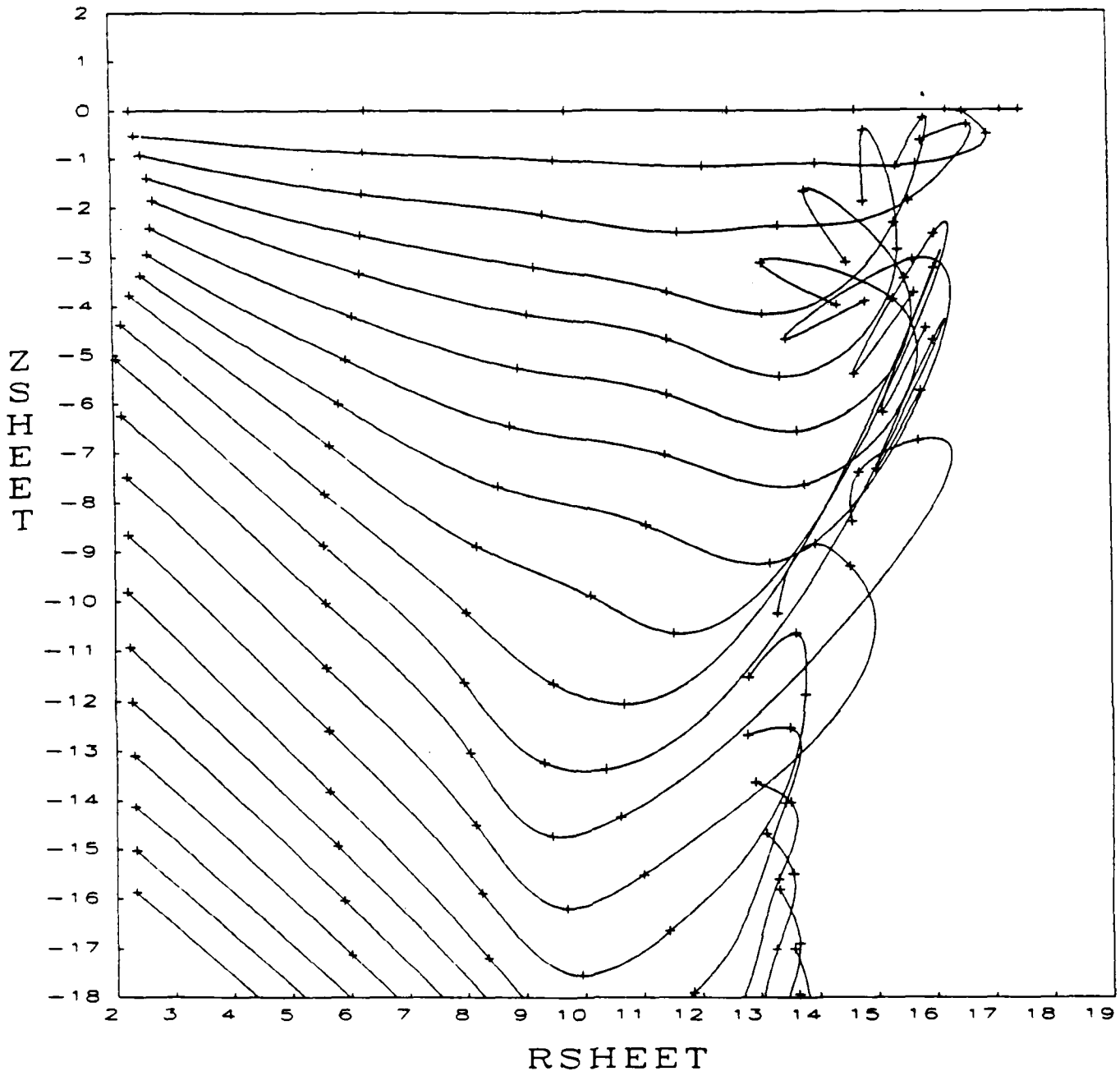

Figure 10F. Wake Geometry for Case 5

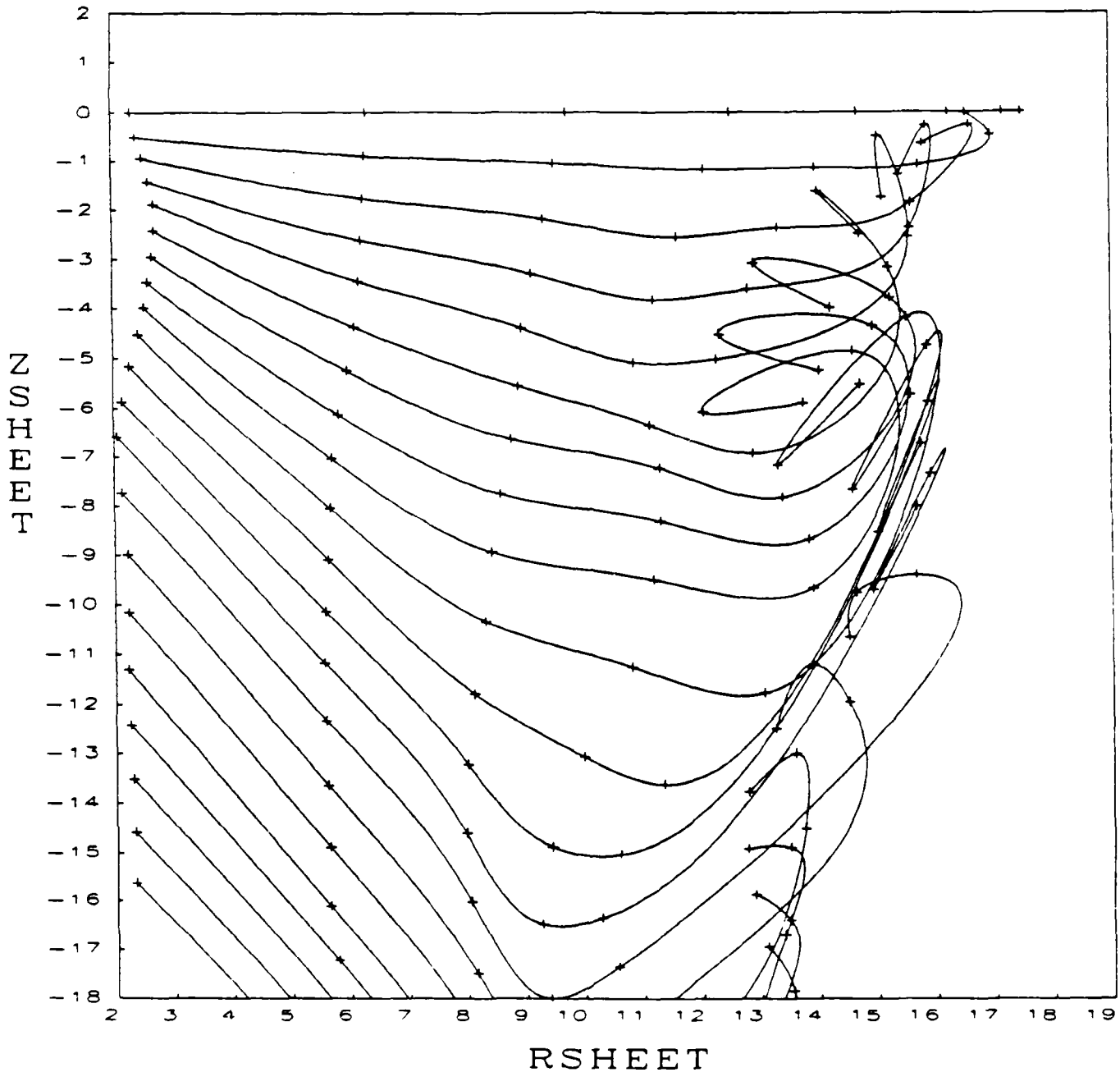

Figure 10G. Wake Geometry for Case 5

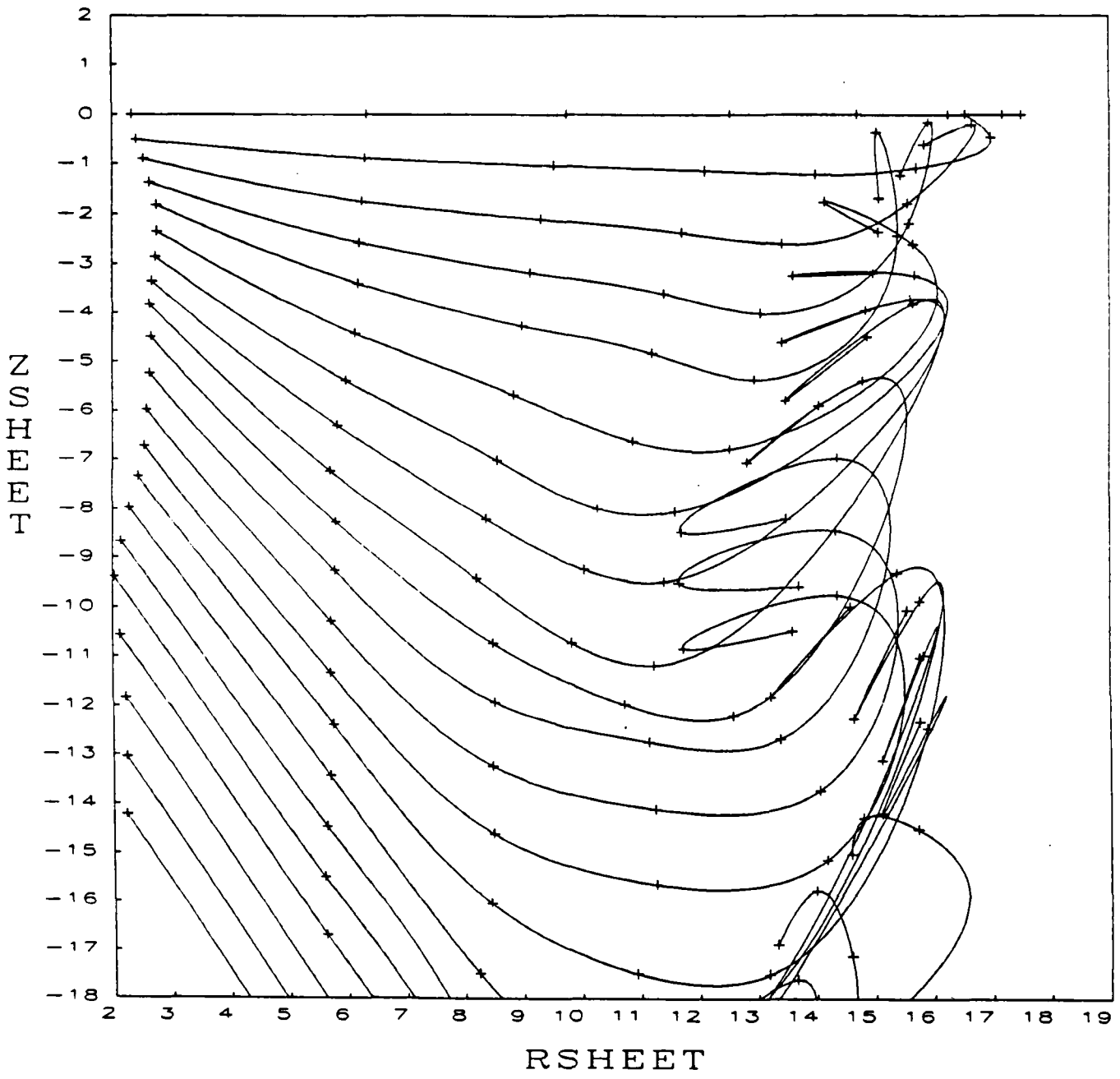

Figure 10H. Wake Geometry for Case 5

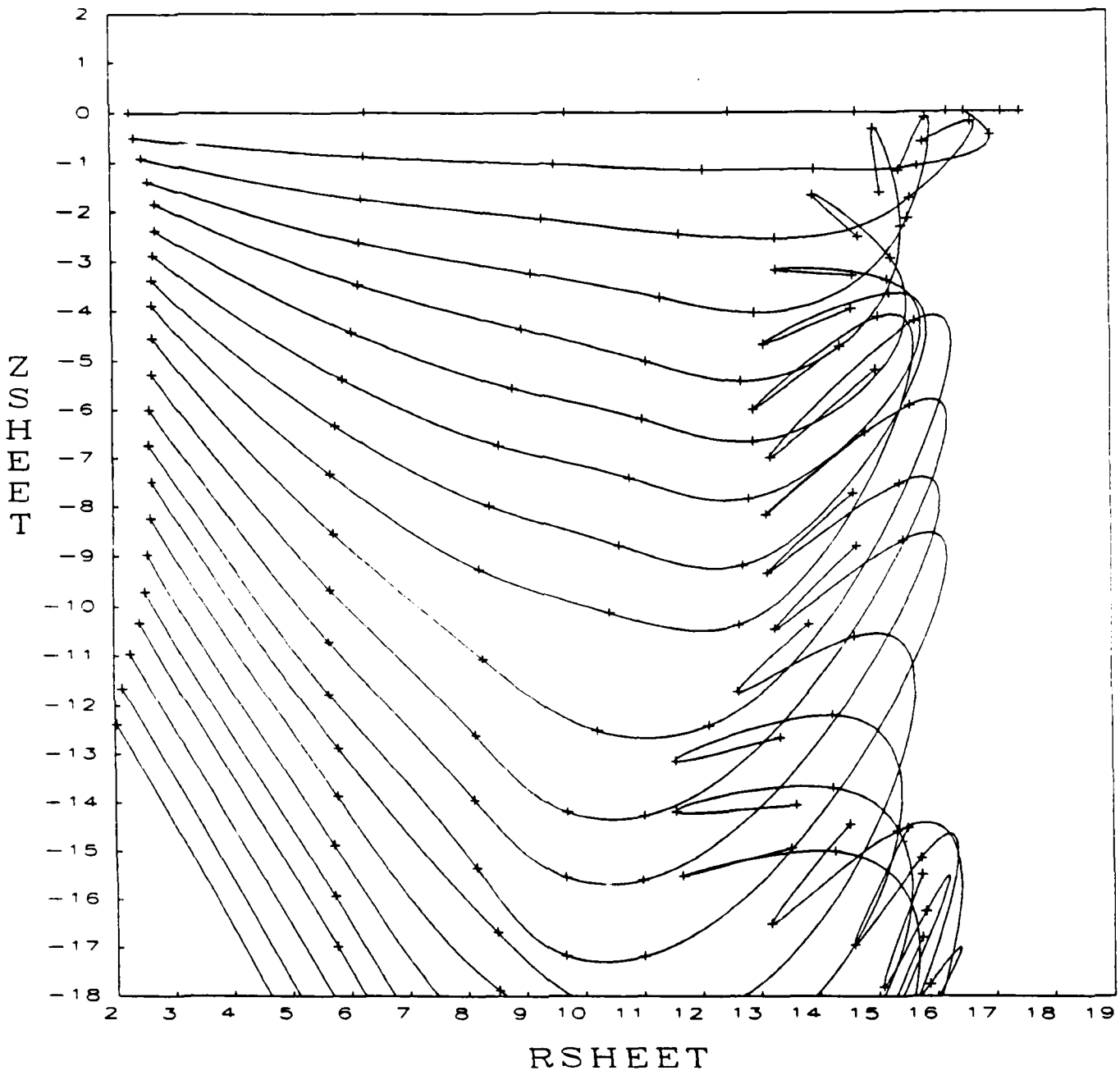

Figure 10I. Wake Geometry for Case 5

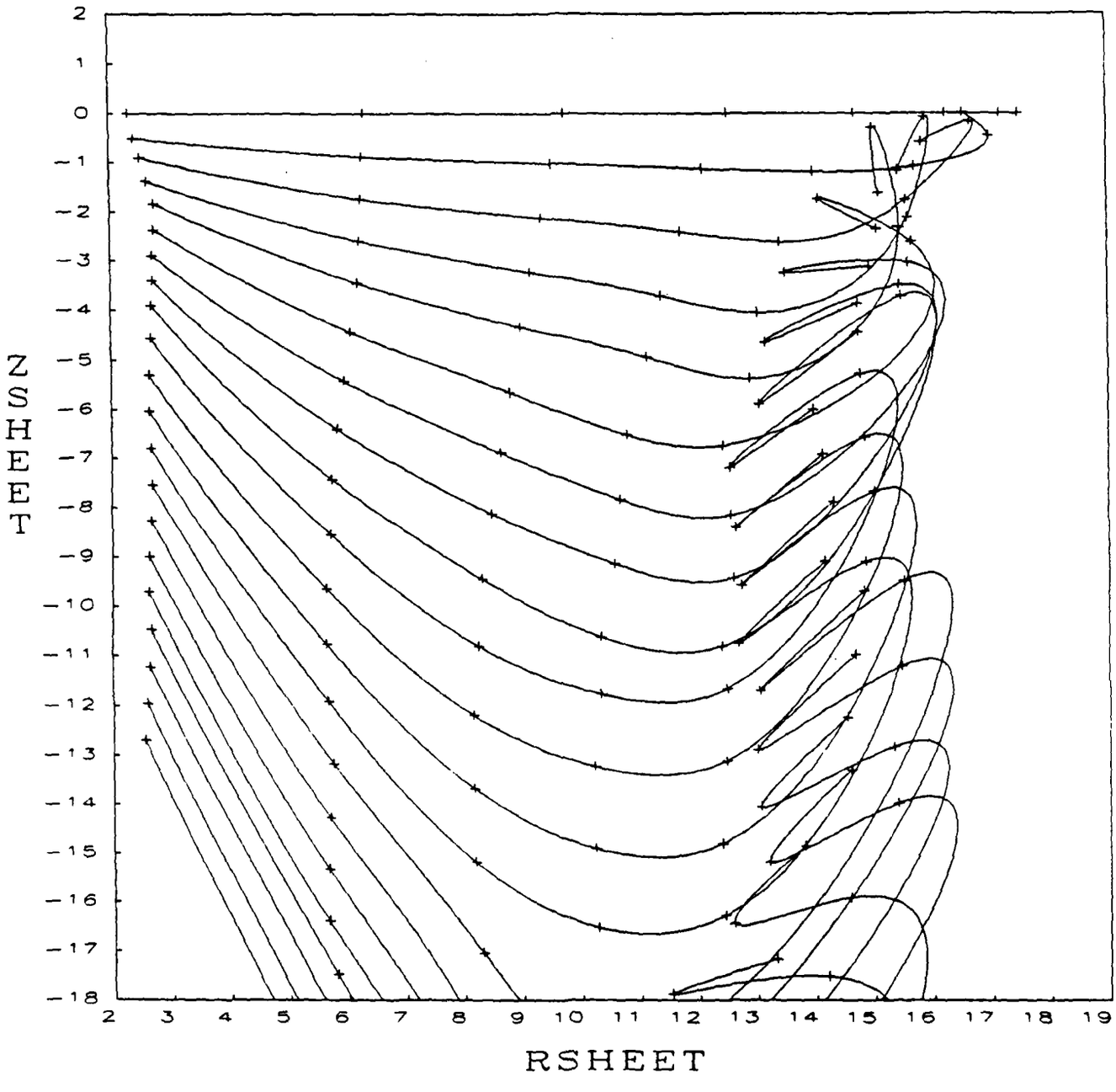

Figure 10J. Wake Geometry for Case 5

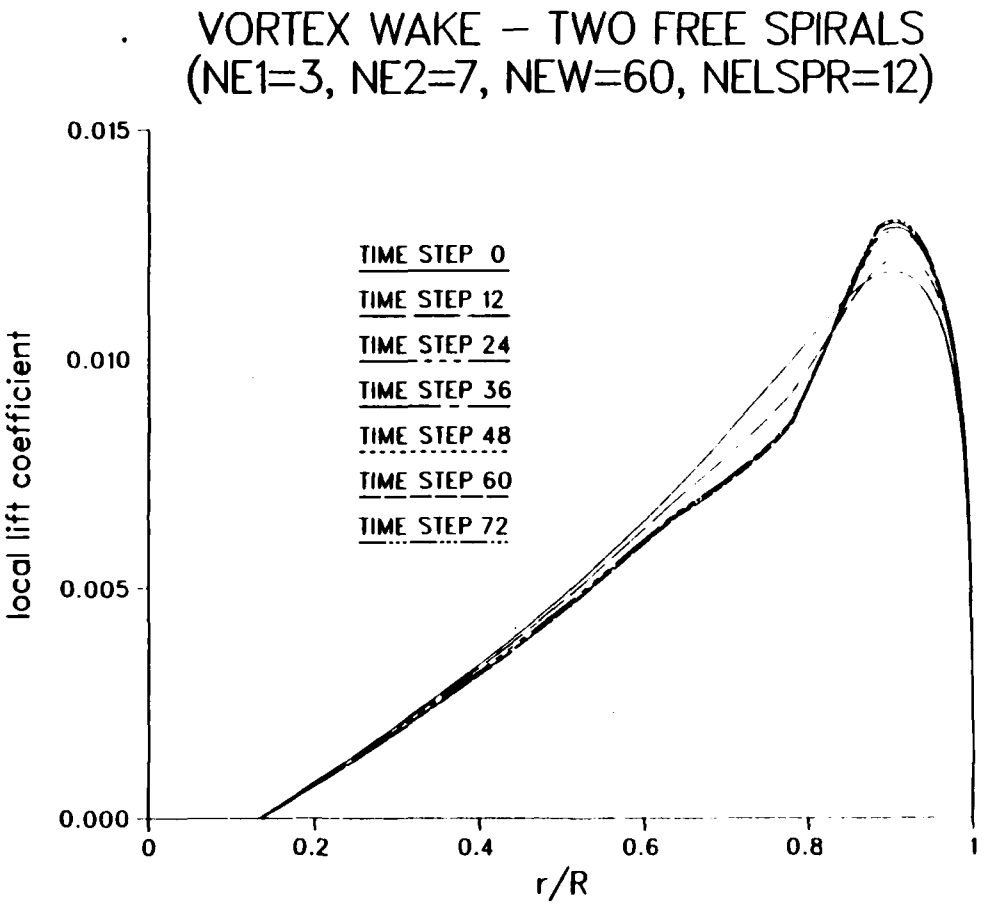

Figure 11. Sectional Lift Distribution for Case 5

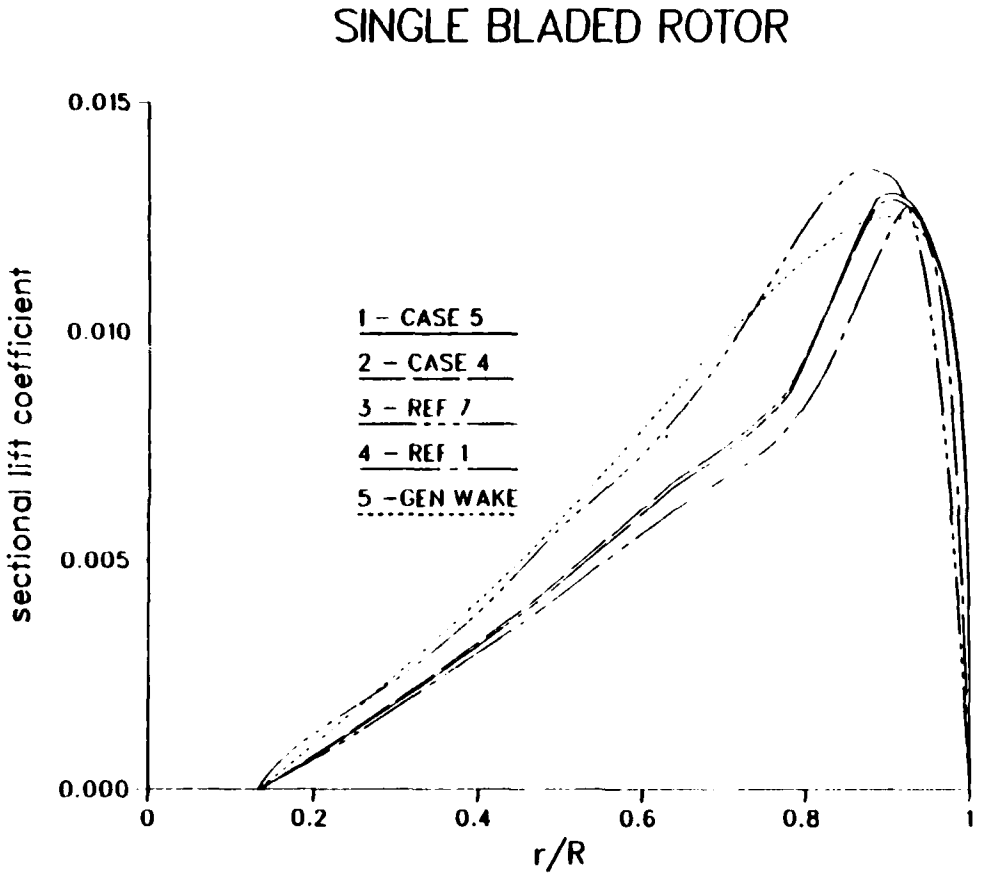

Figure 12. Comparison of present results for one-bladed rotor (free wake analysis of cases 4 and 5 and generalized wake analysis) with those of Rao and Schatzle (Ref. 7) and Morino, Kaprielian, and Sipic (Ref.1).

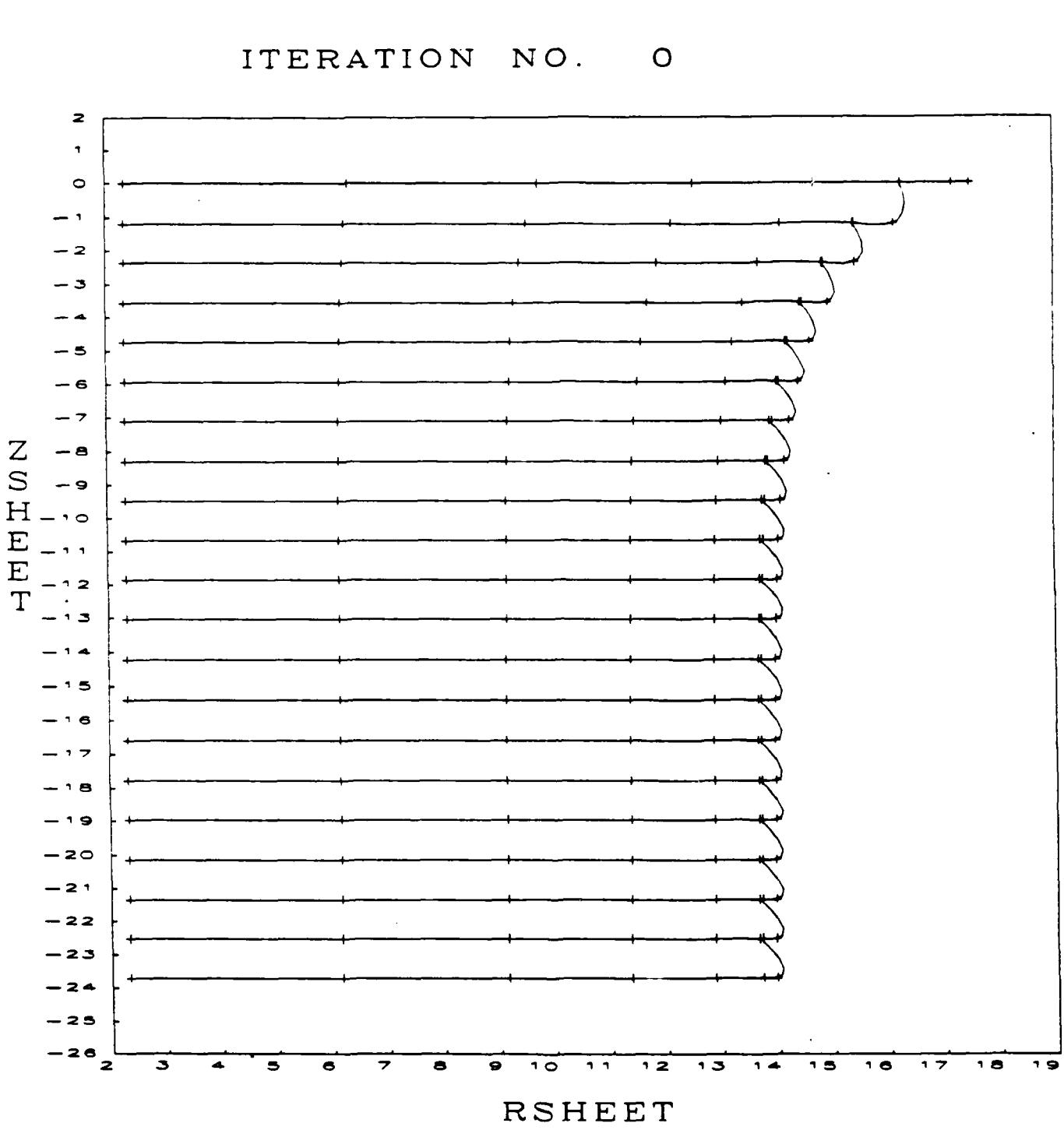

Figure 13A. Wake Geometry for Case 6

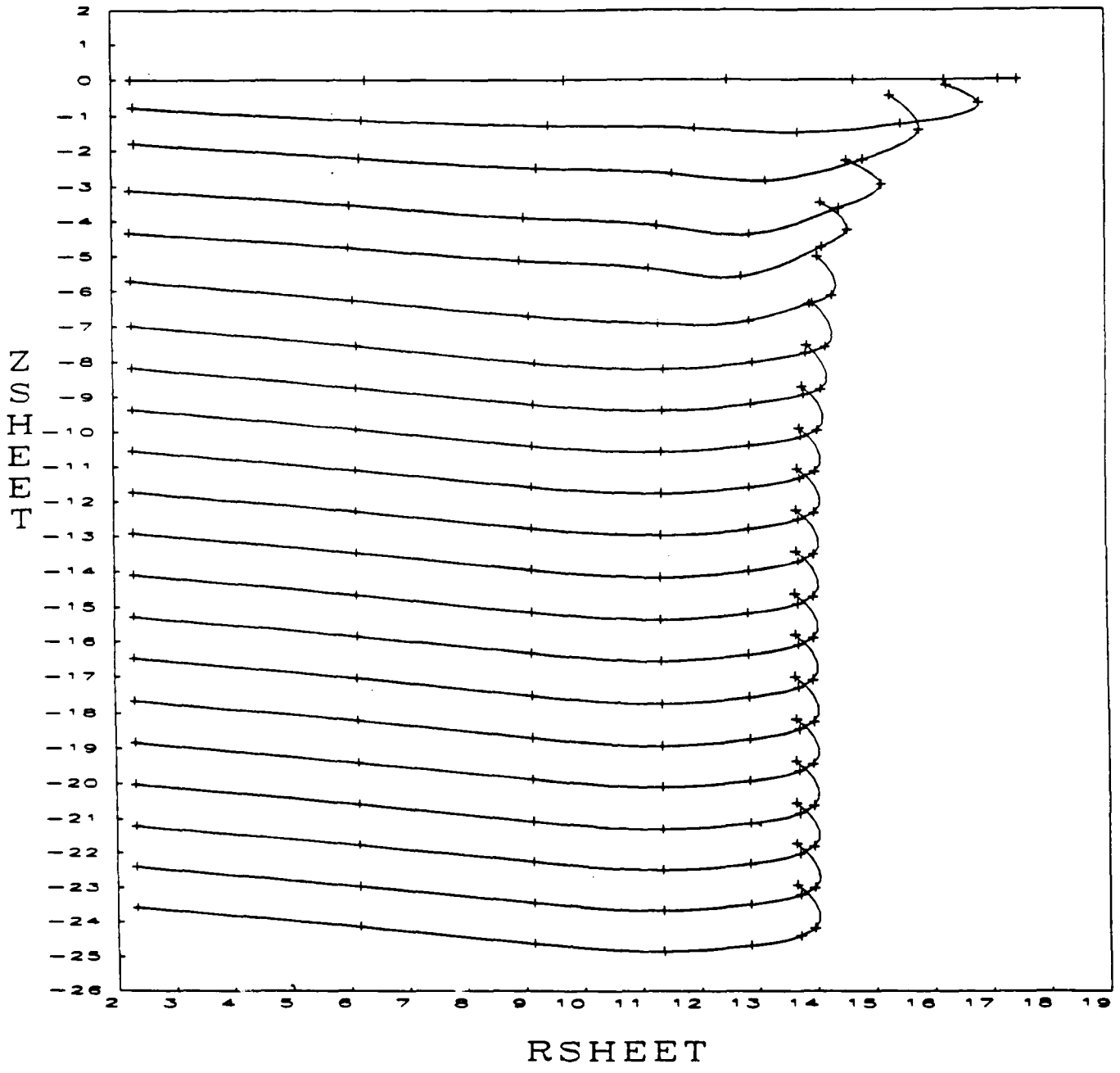

Figure 13B. Wake Geometry for Case 6

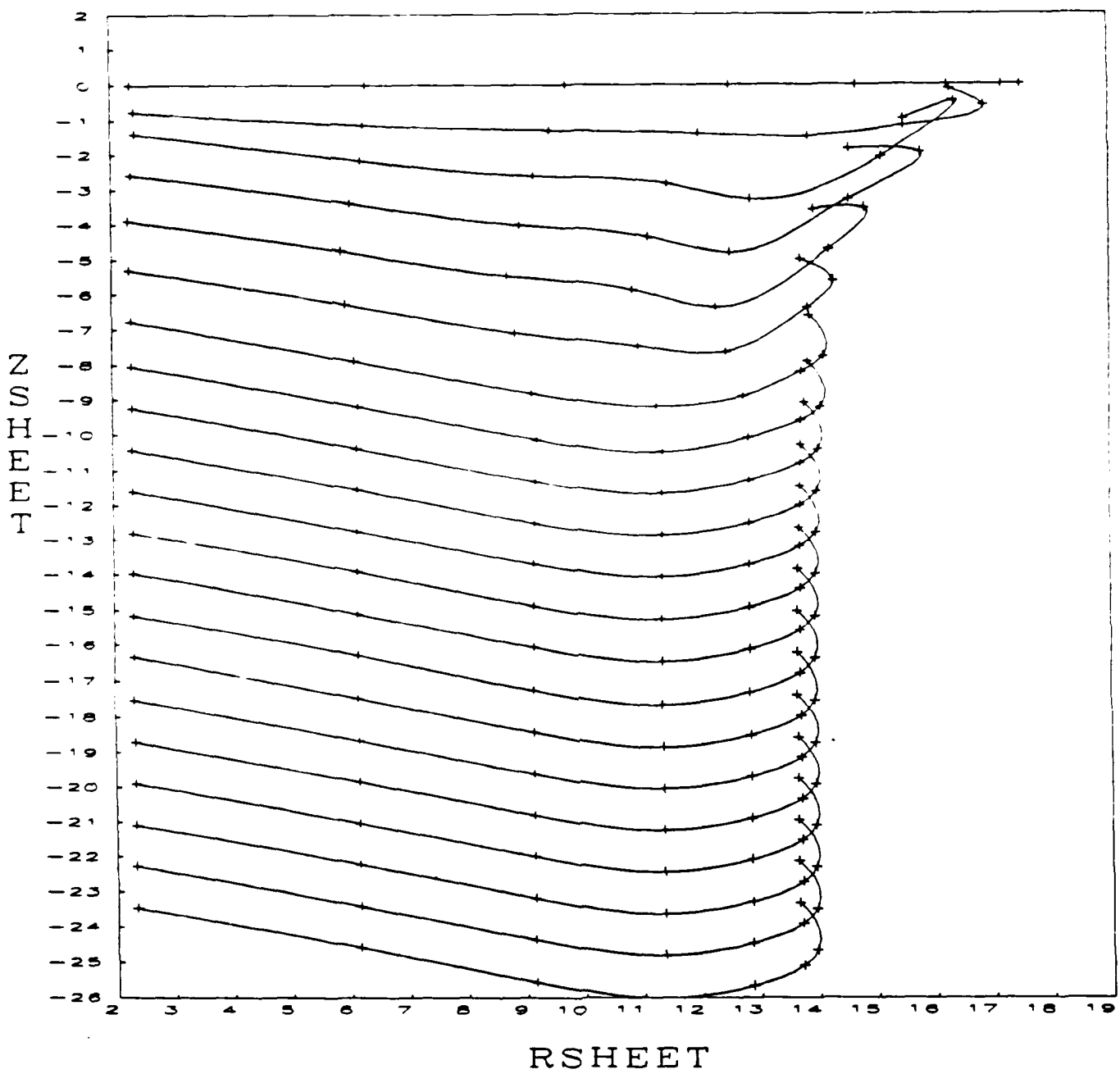

Figure 13C. Wake Geometry for Case 6

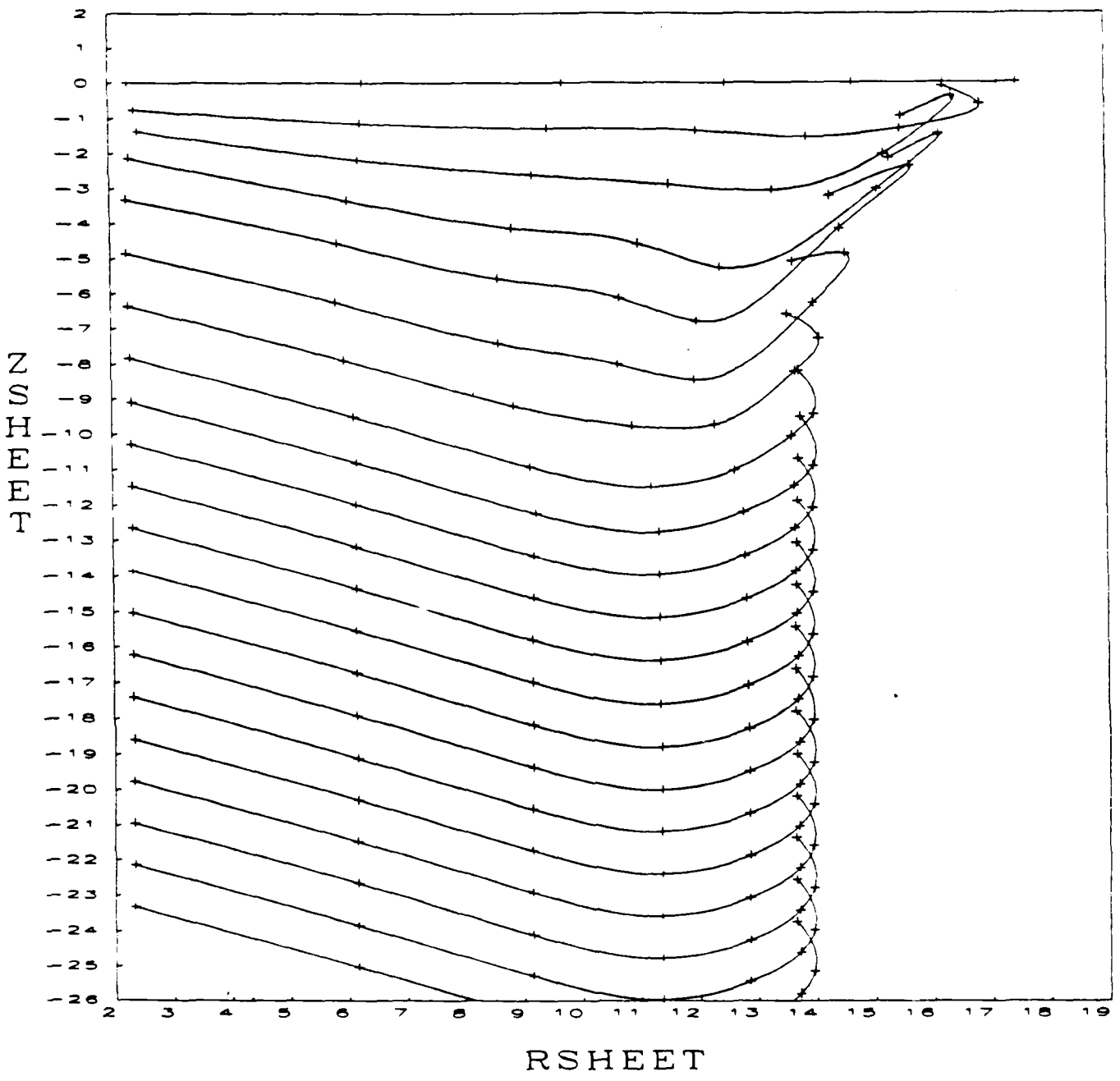

Figure 13D. Wake Geometry for Case 6

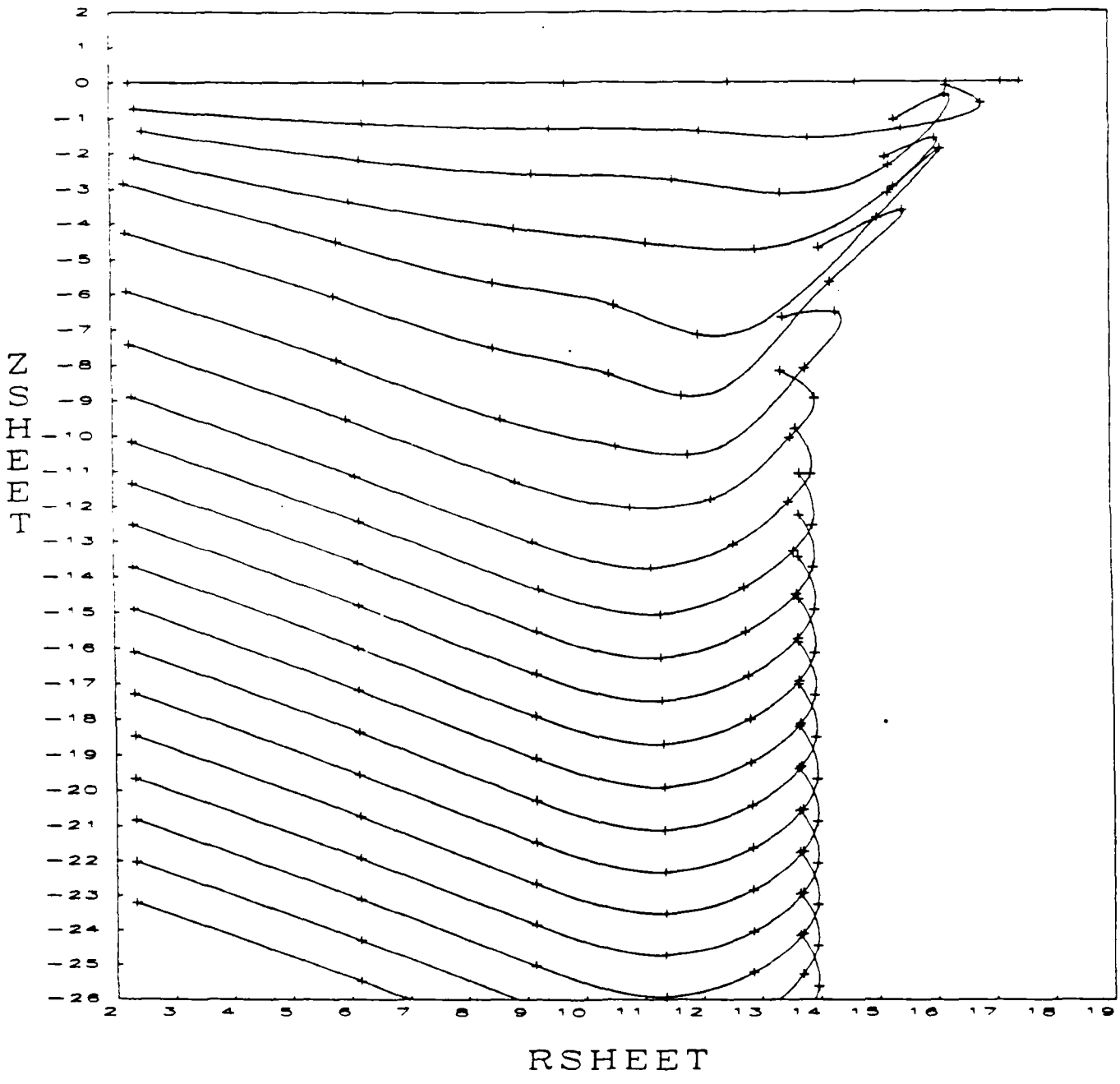

Figure 13E. Wake Geometry for Case 6

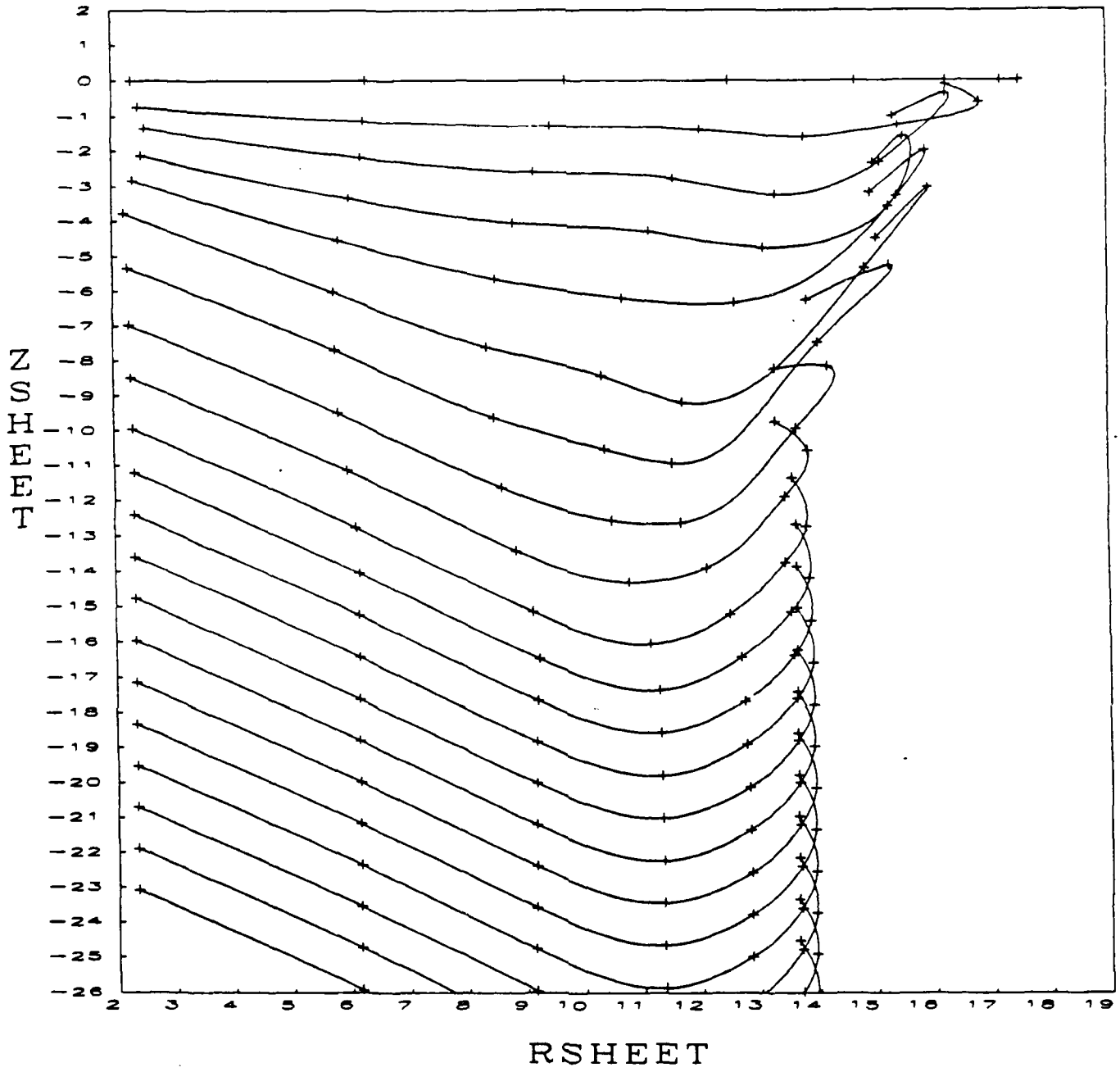

Figure 13F. Wake Geometry for Case 6

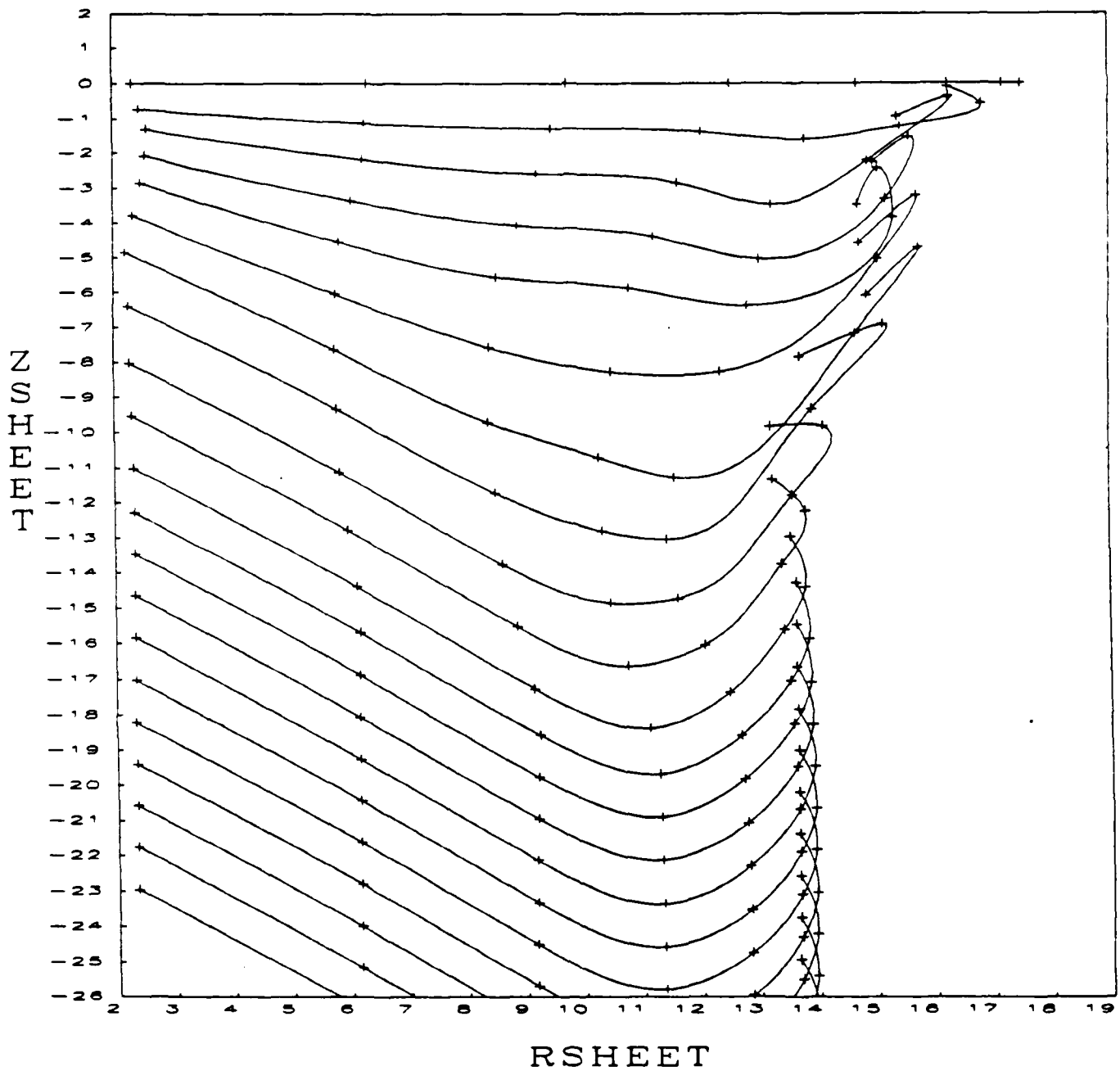

Figure 13G. Wake Geometry for Case 6

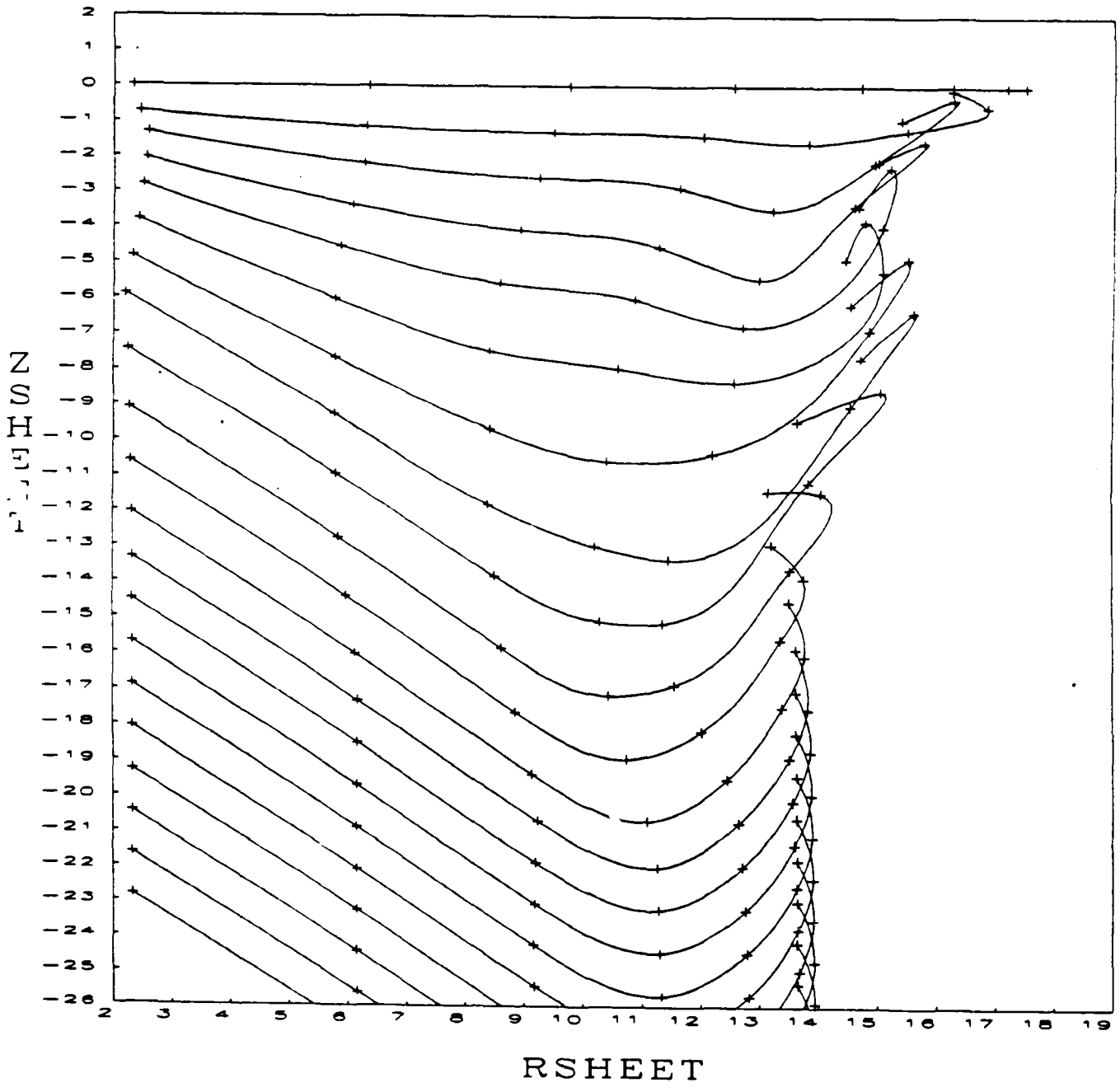

Figure 13H. Wake Geometry for Case 6

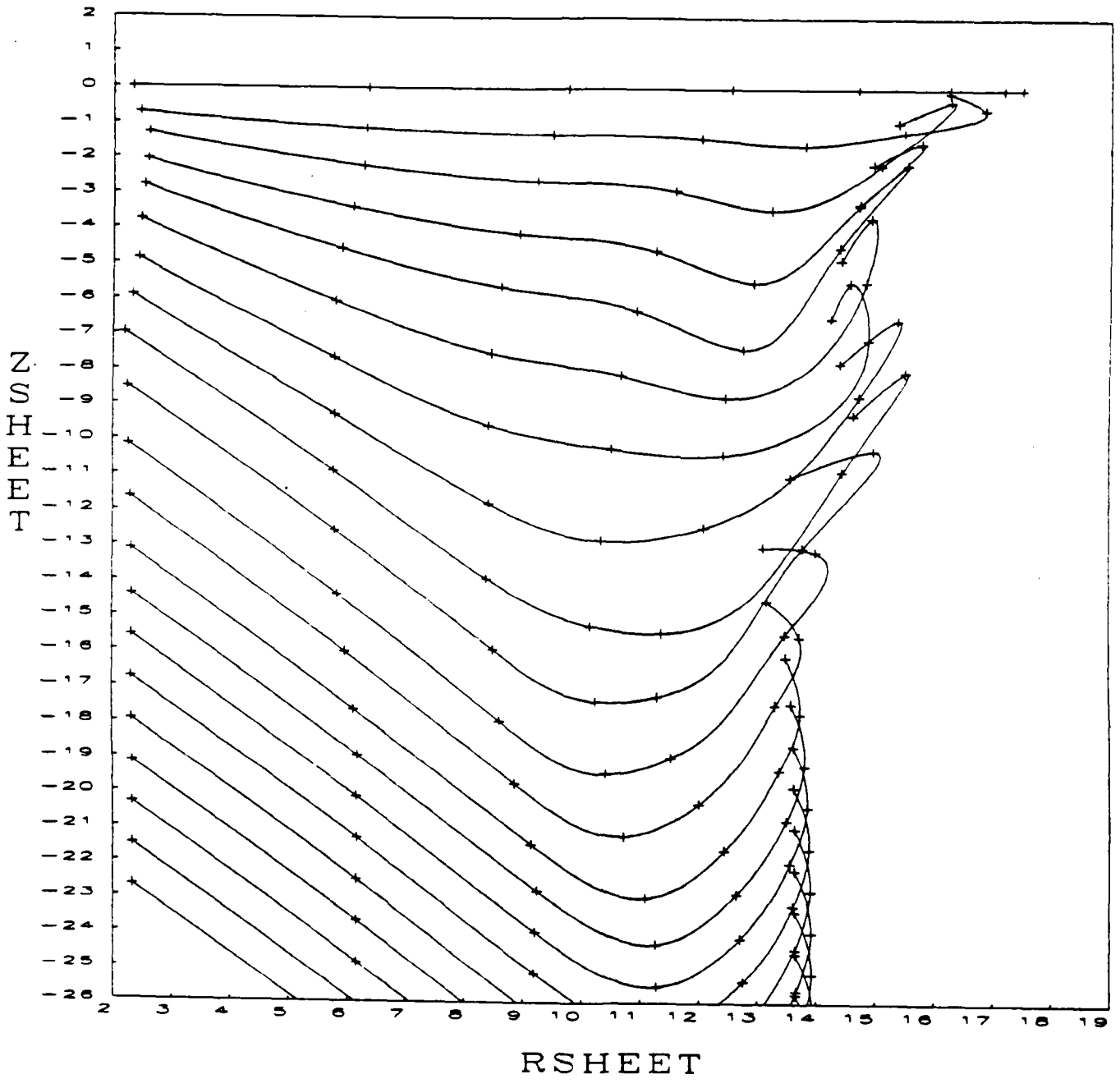

Figure 13I. Wake Geometry for Case 6

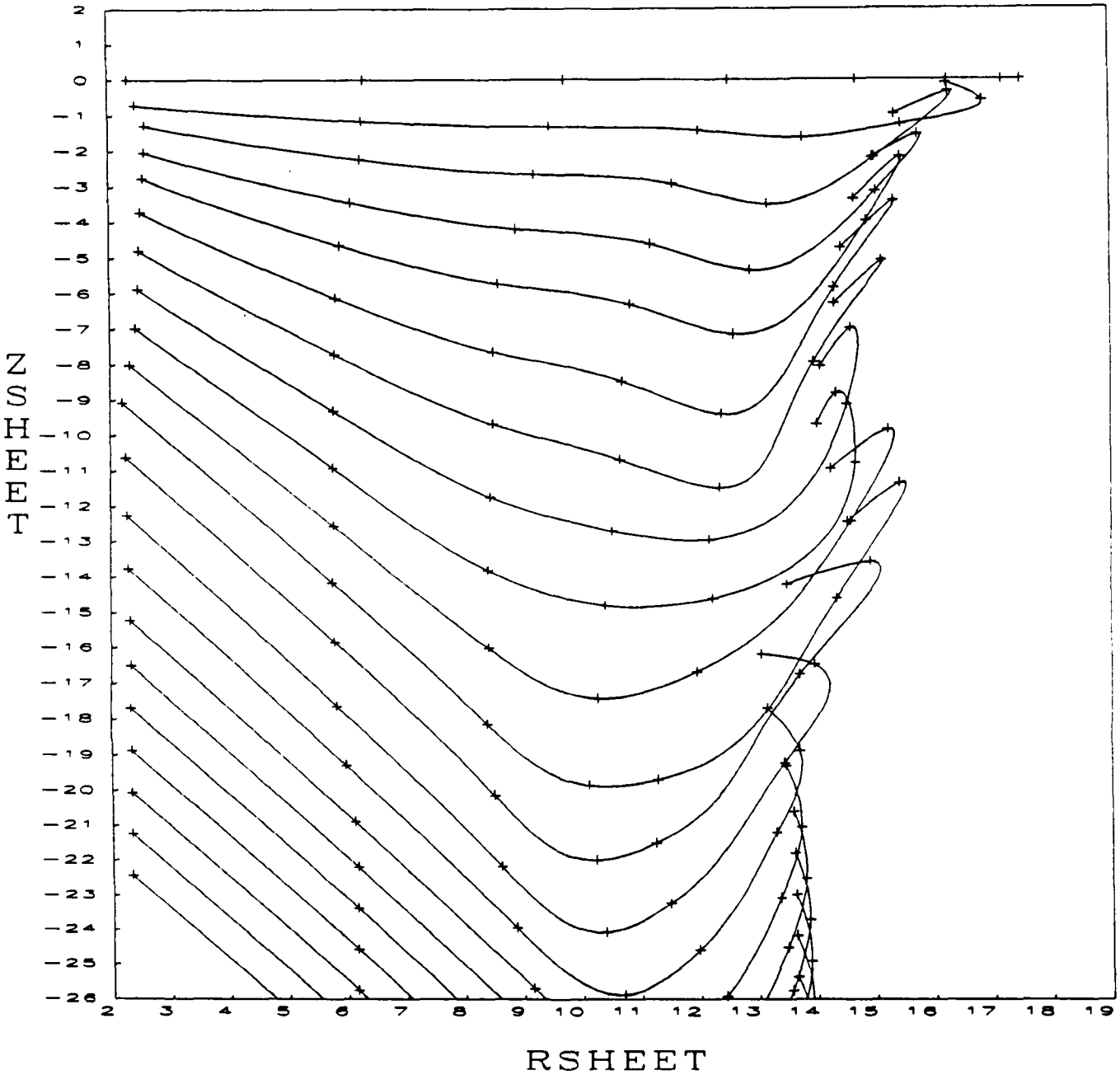

Figure 13J. Wake Geometry for Case 6

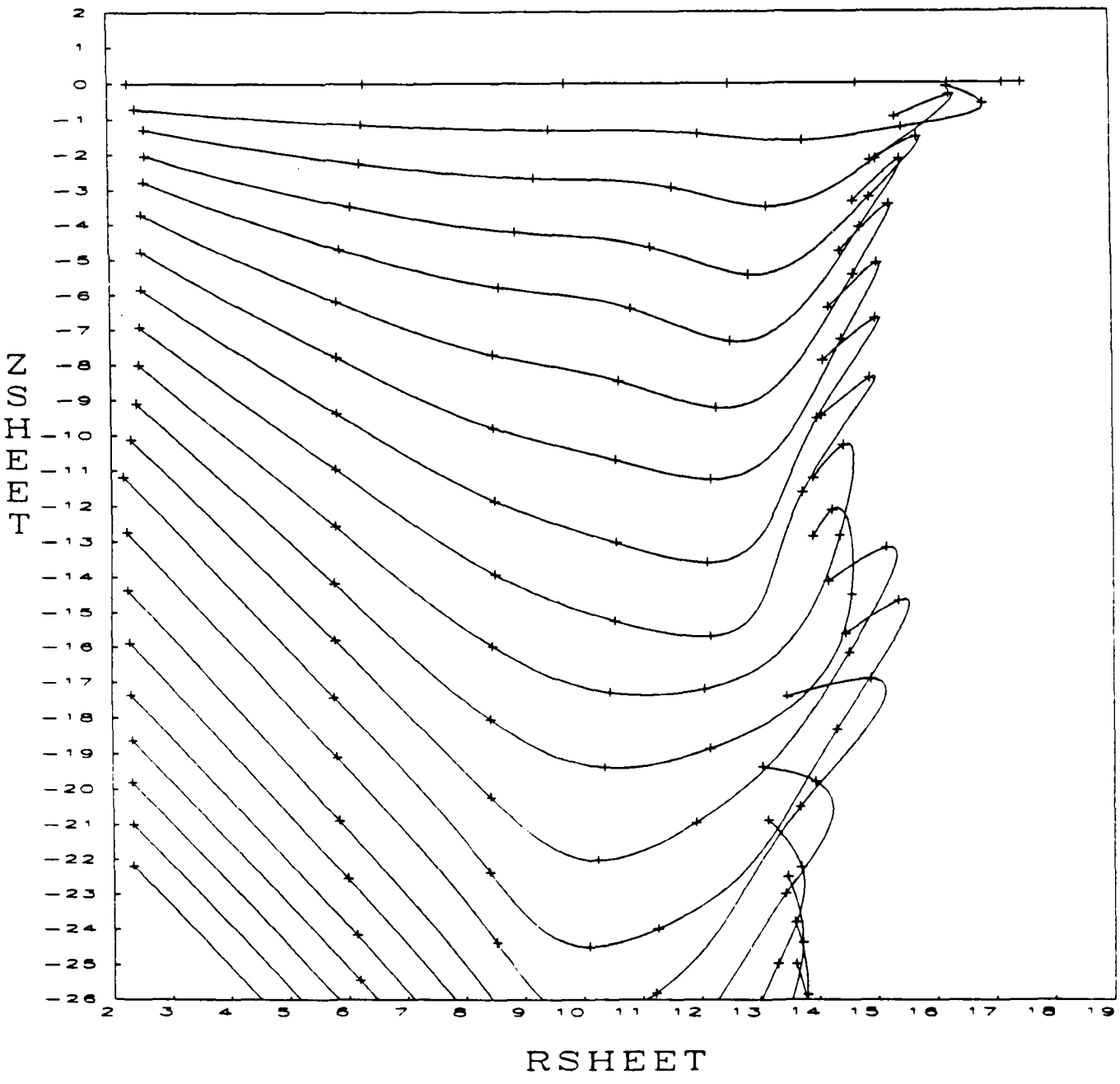

Figure 13K. Wake Geometry for Case 6

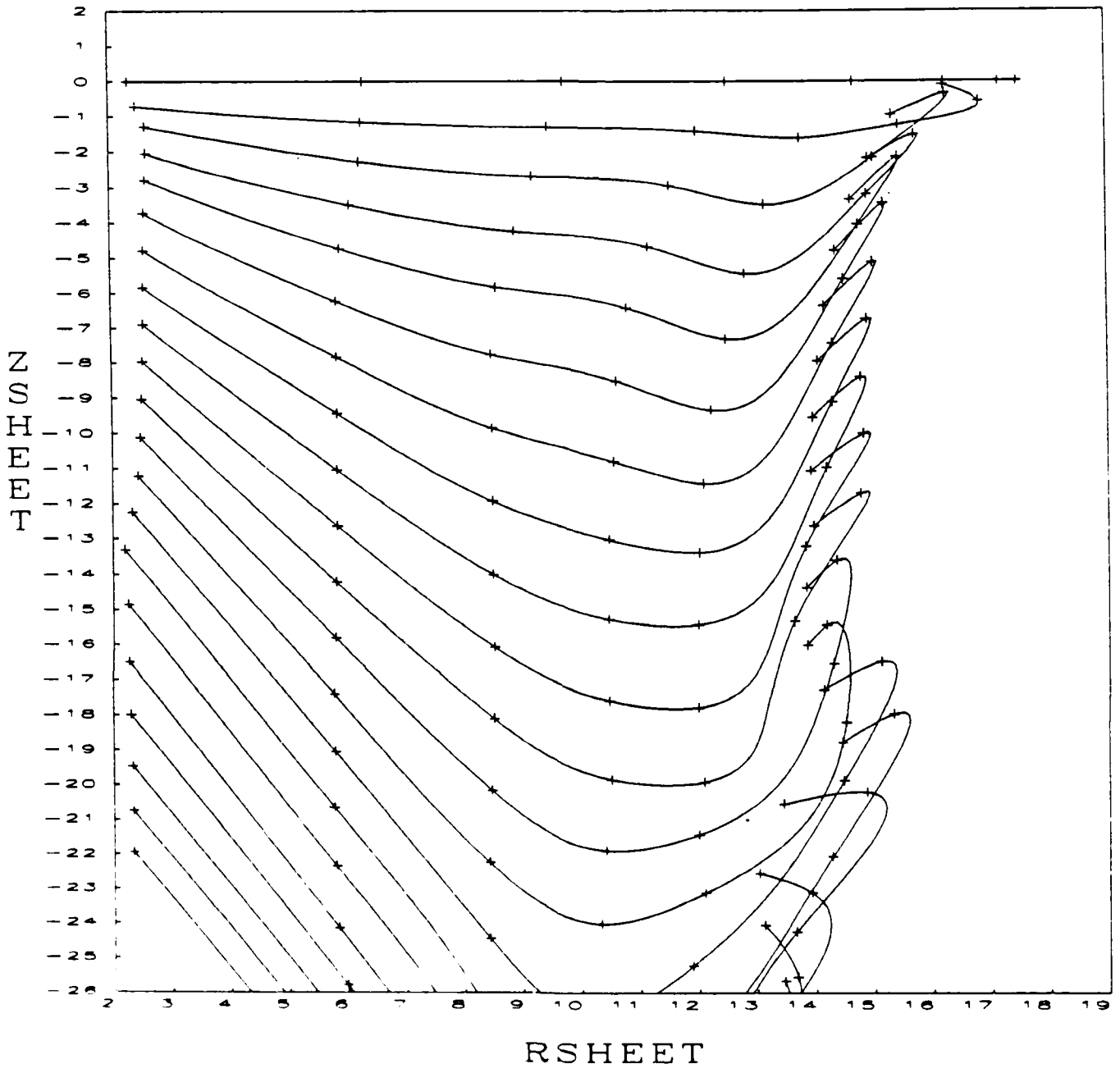

Figure 13L. Wake Geometry for Case 6

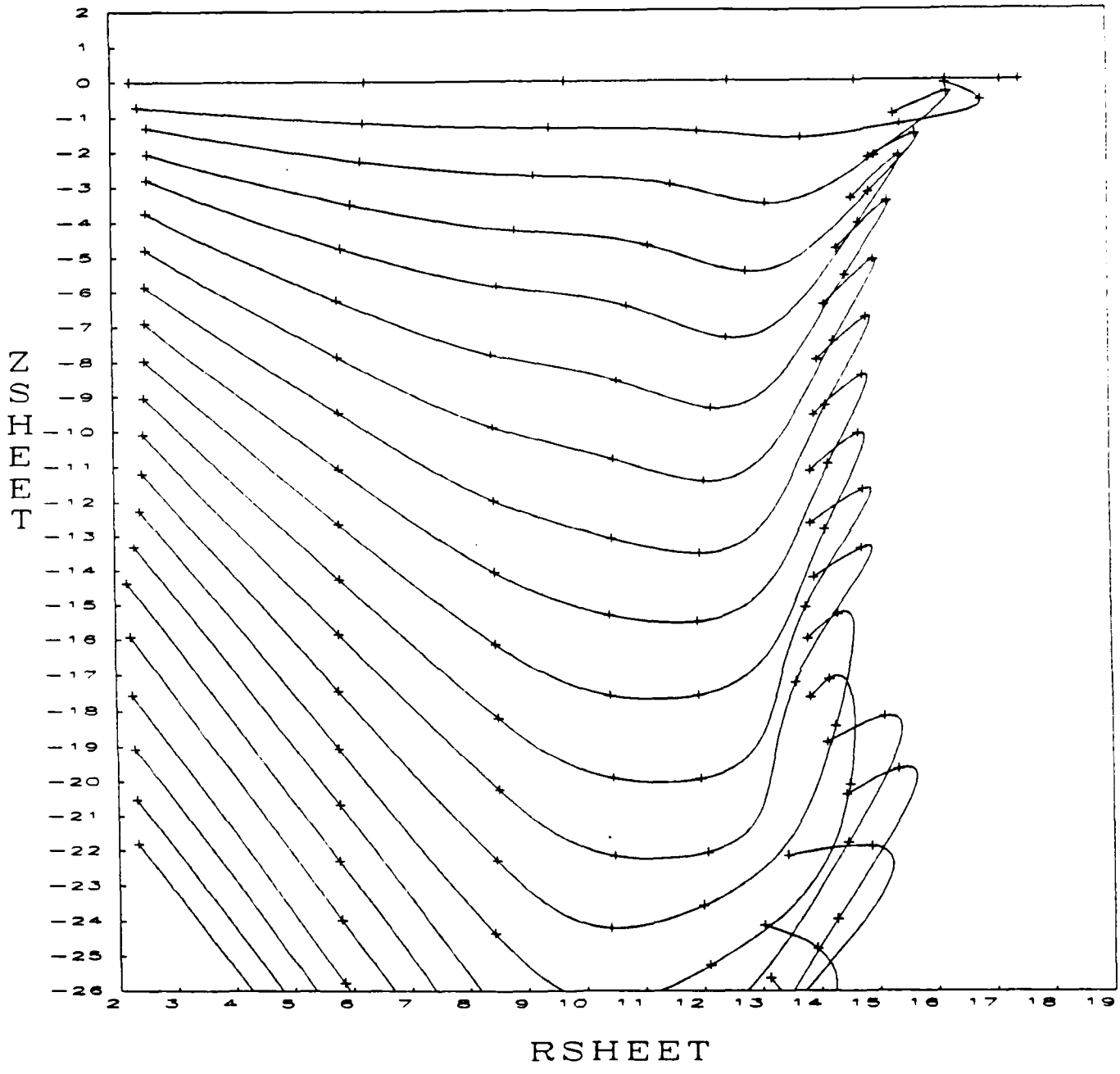

Figure 13M. Wake Geometry for Case 6

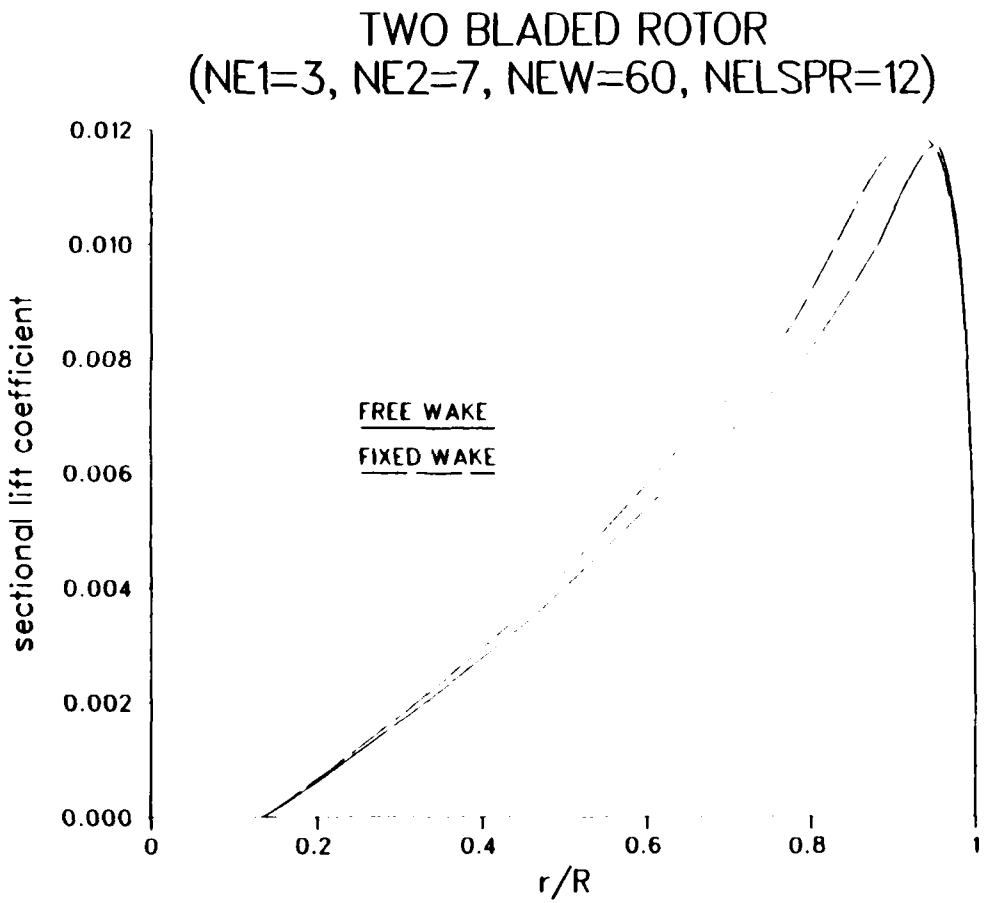

Figure 14. Current results for two-bladed rotor (free-wake and generalized-wake analysis).

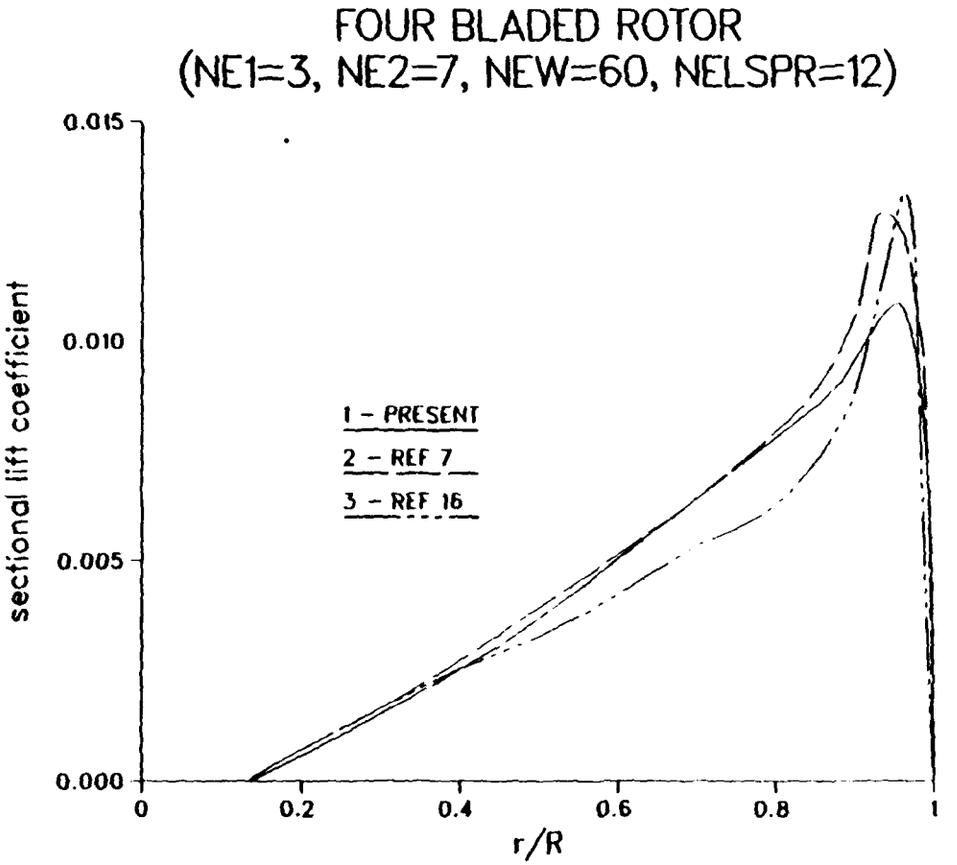

Figure 14A. Comparison of present results for four-bladed rotor (generalized wake analysis) with those of Rao and Schatzle (Ref. 7) and the experiments of Bartsch (Ref. 16).

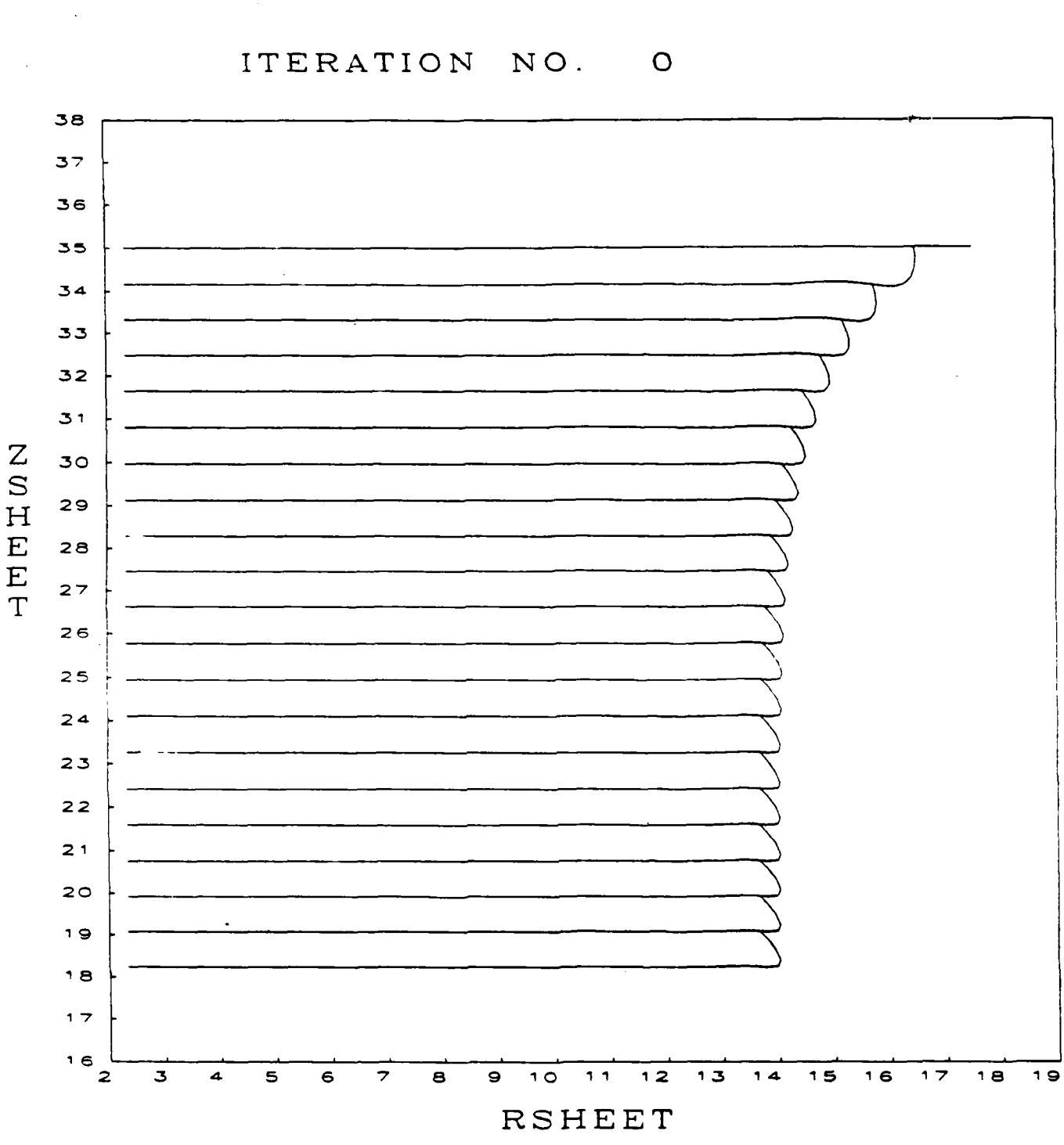

Figure 15A. Wake Geometry for Case 7

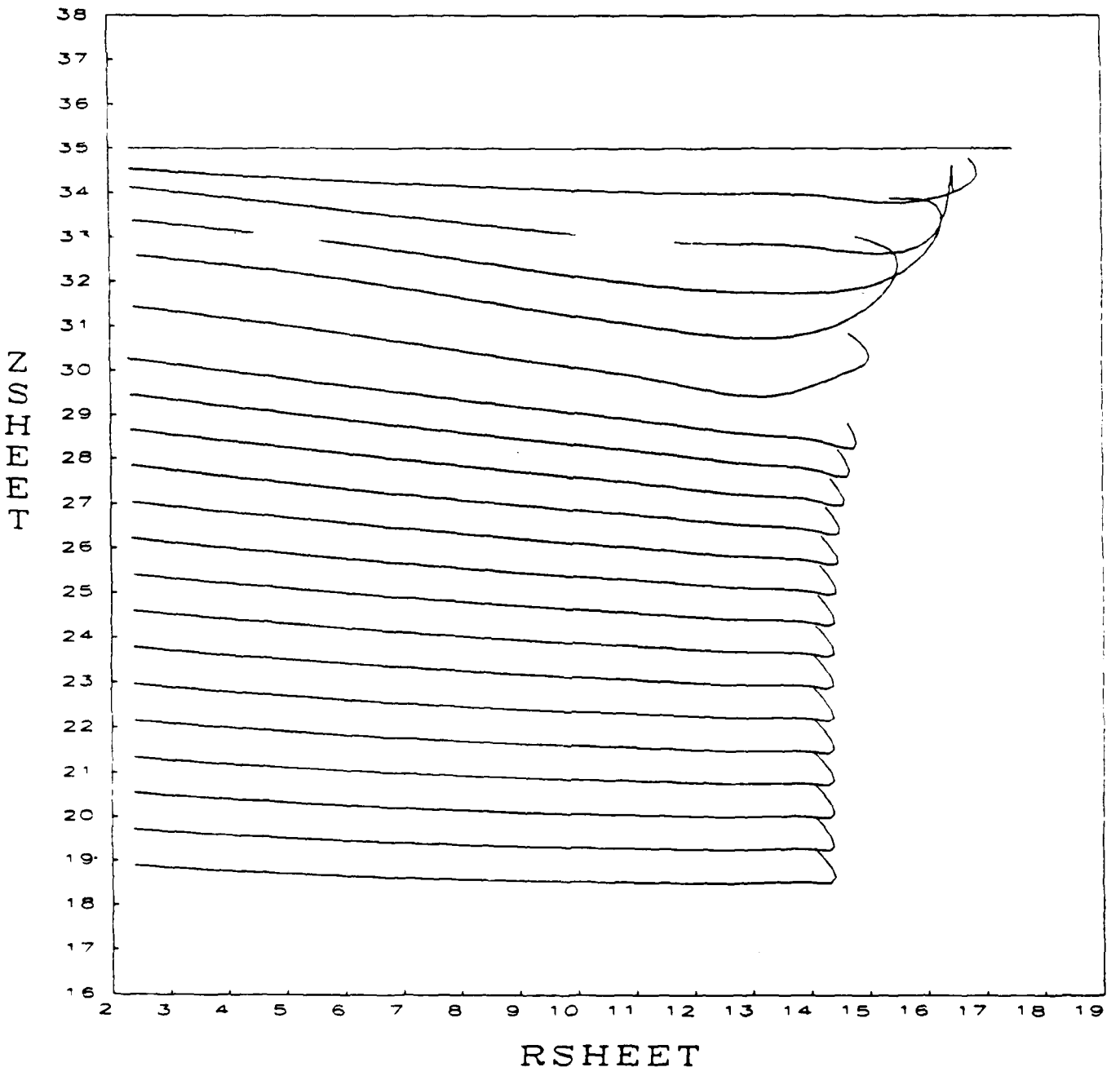

Figure 15B. Wake Geometry for Case 7

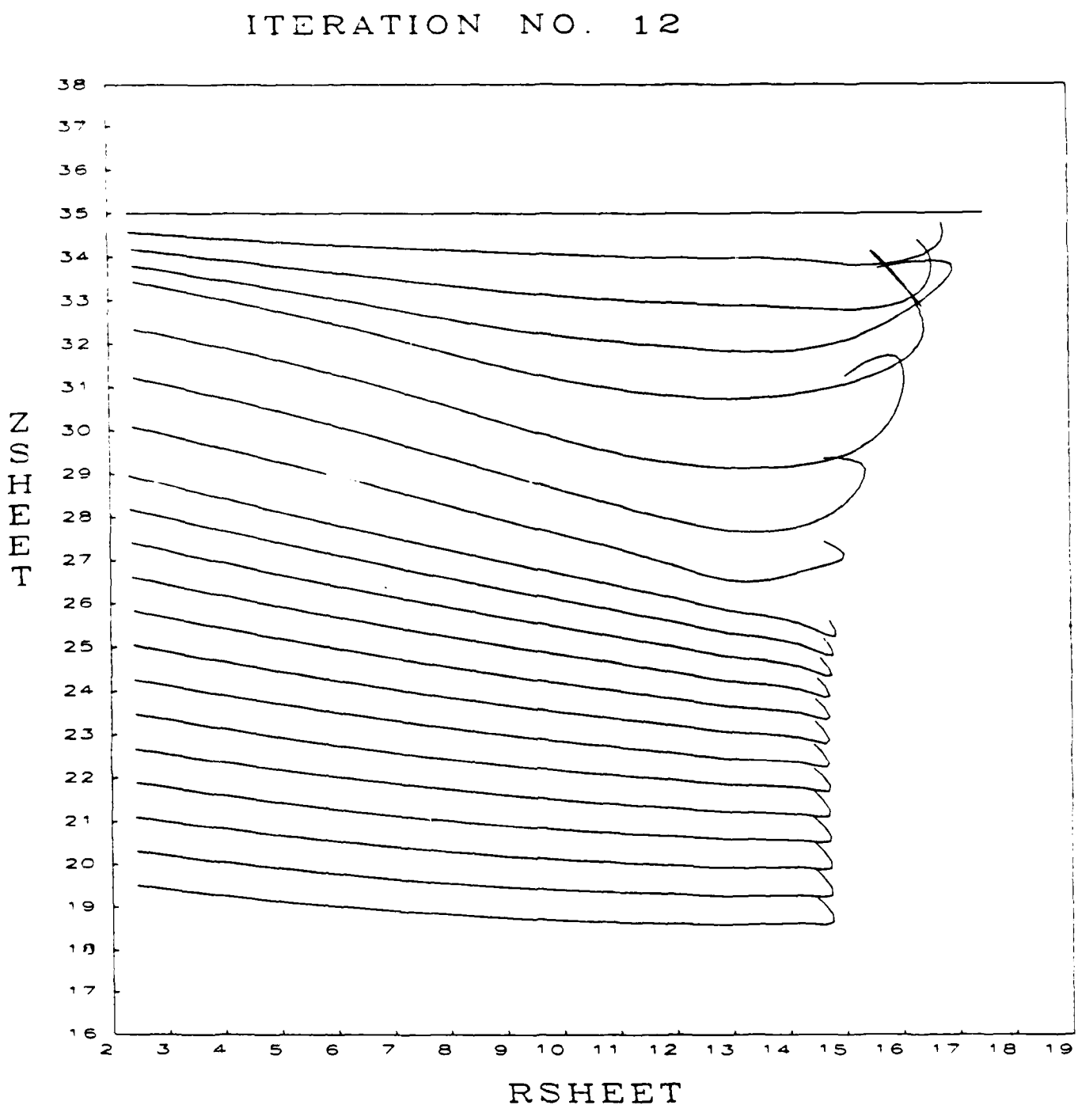

Figure 15C. Wake Geometry for Case 7

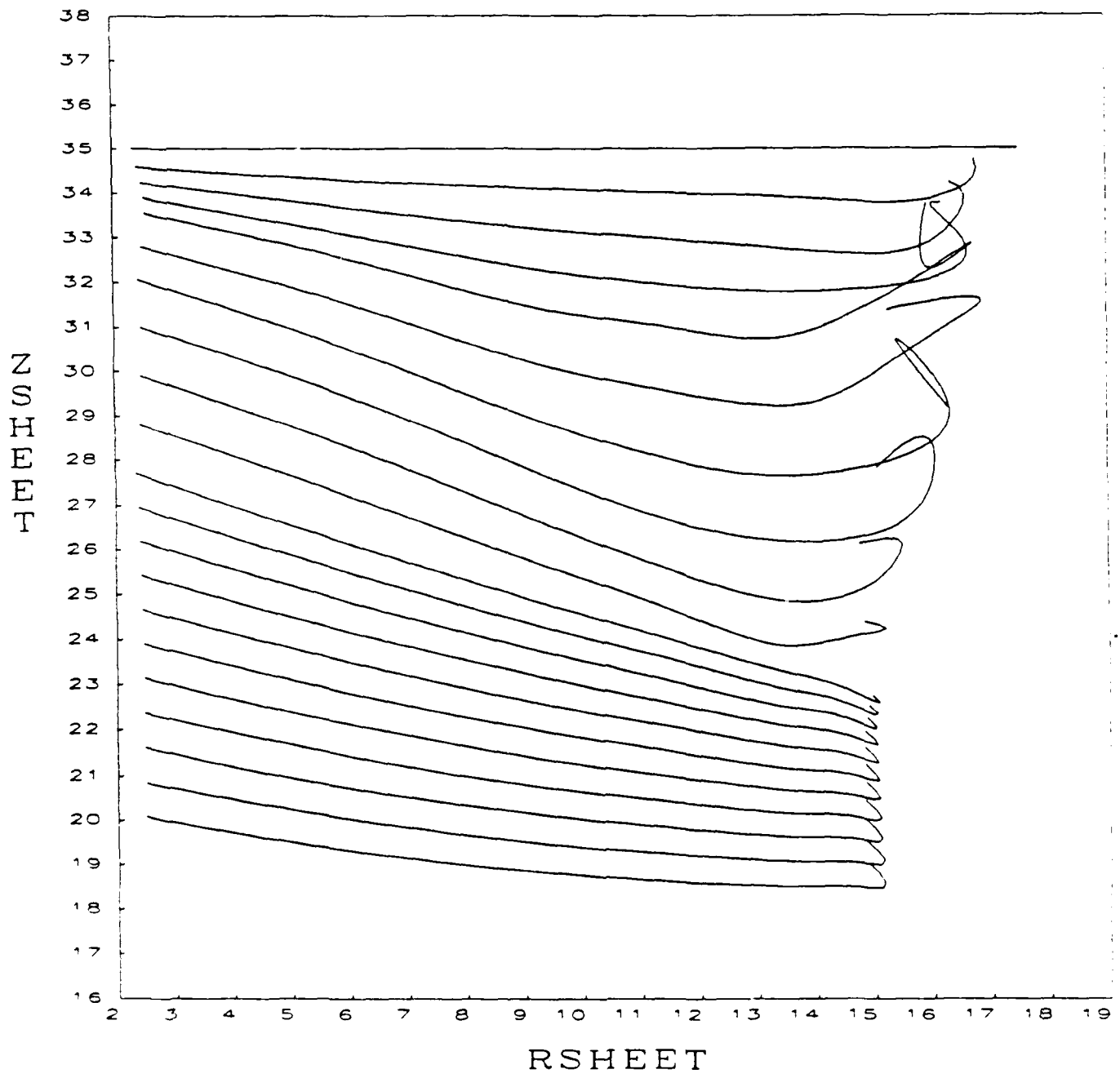

Figure 15D. Wake Geometry for Case 7

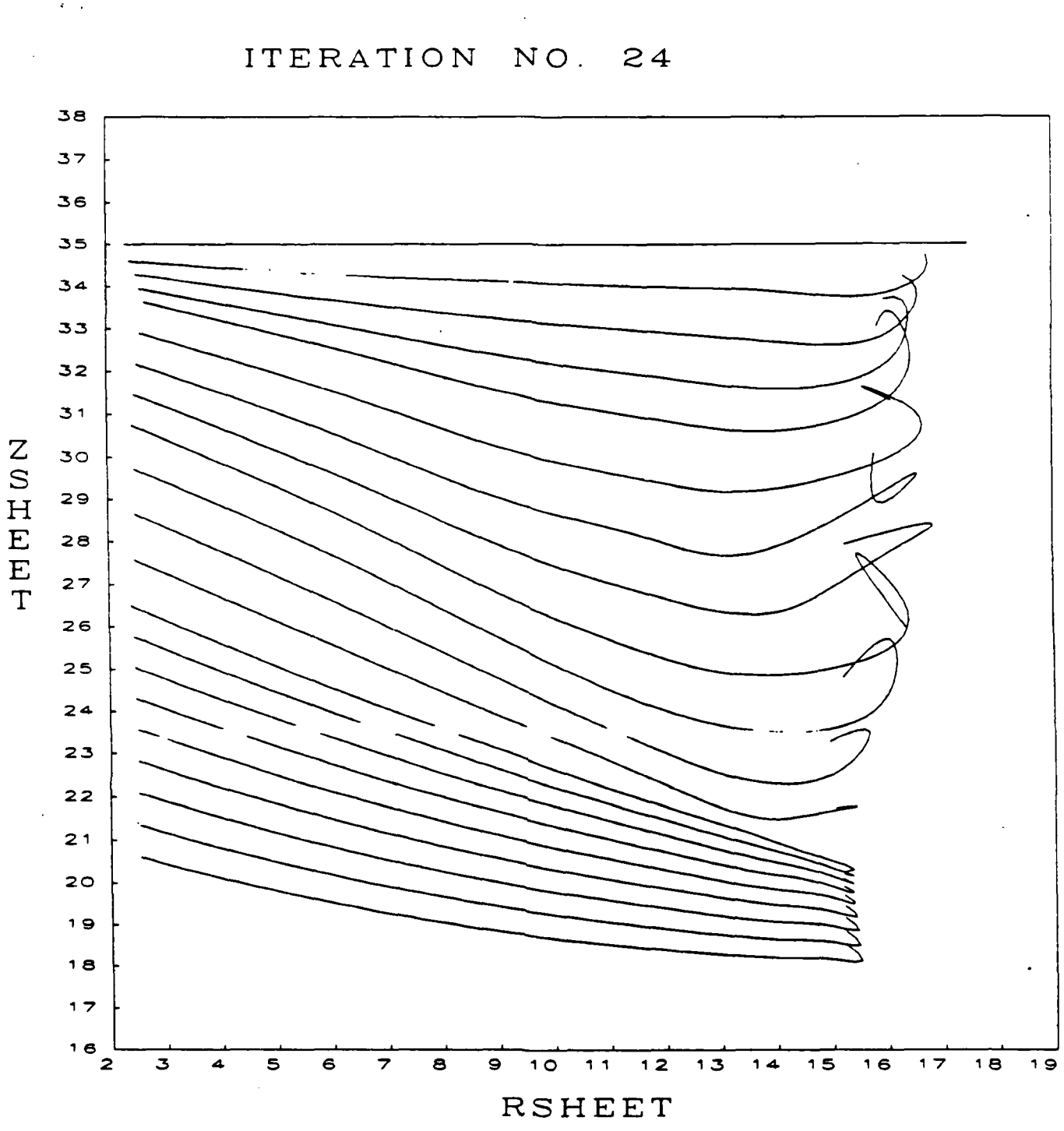

Figure 15E. Wake Geometry for Case 7

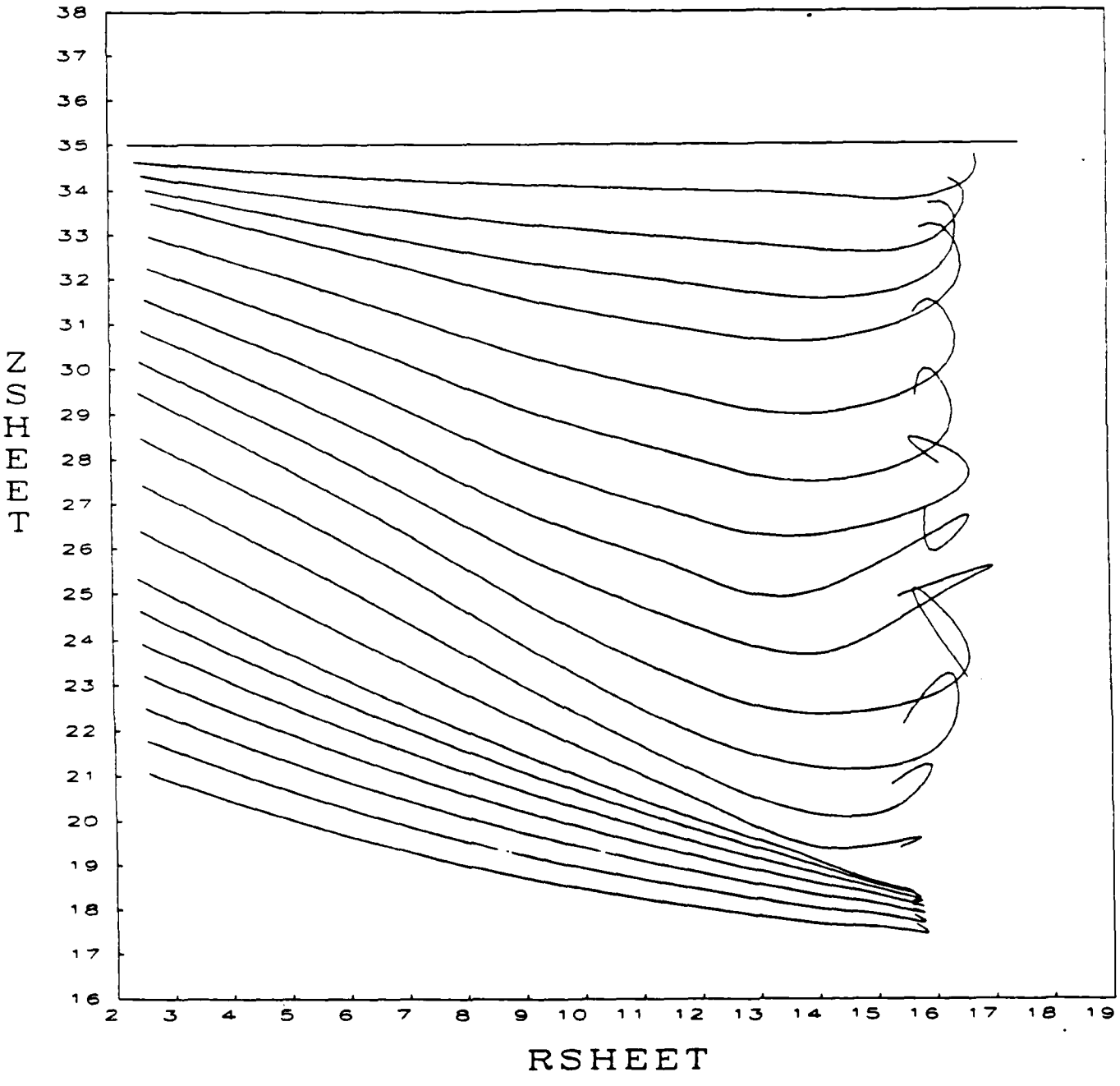

Figure 15F. Wake Geometry for Case 7

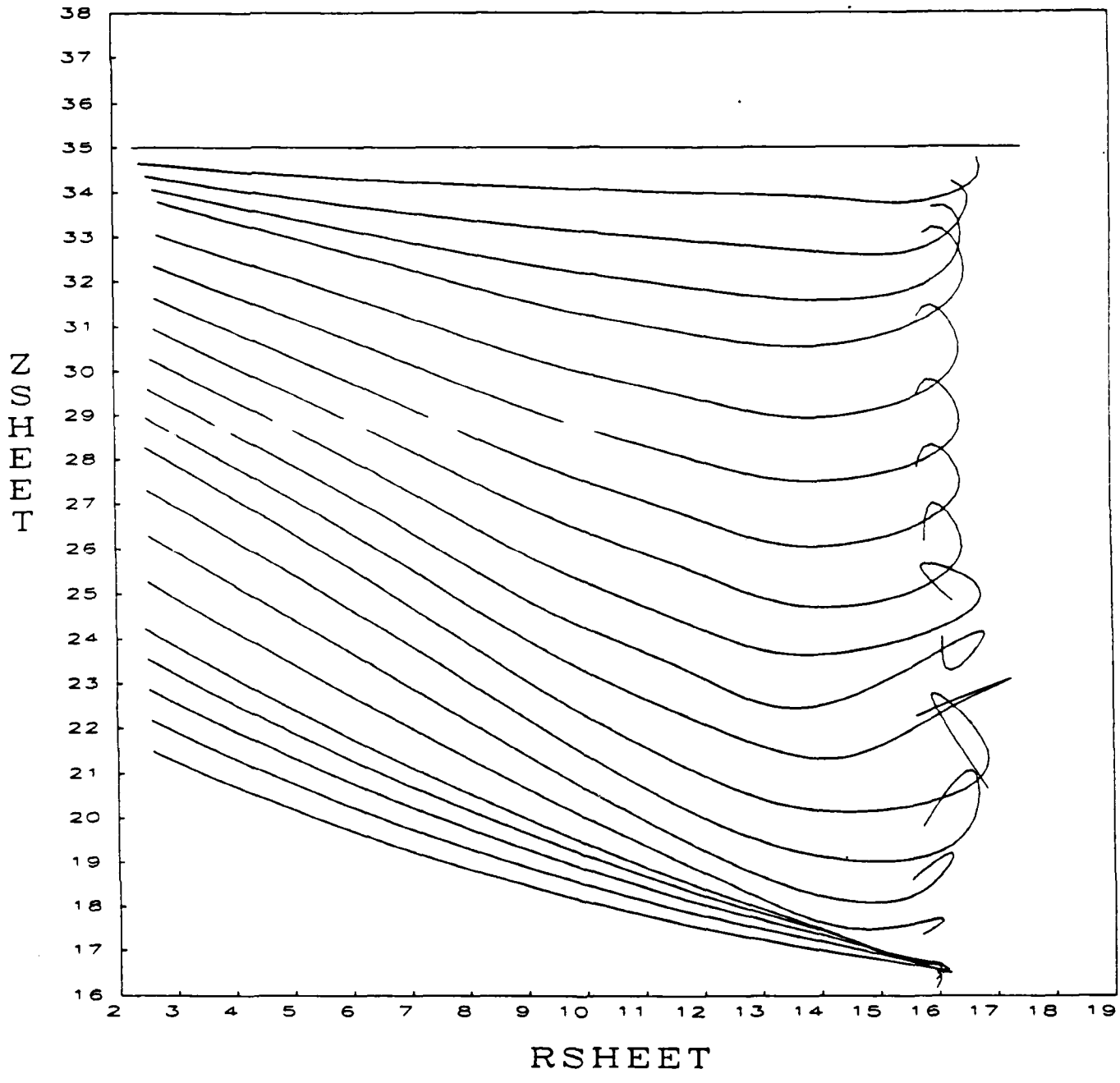

Figure 15G. Wake Geometry for Case 7

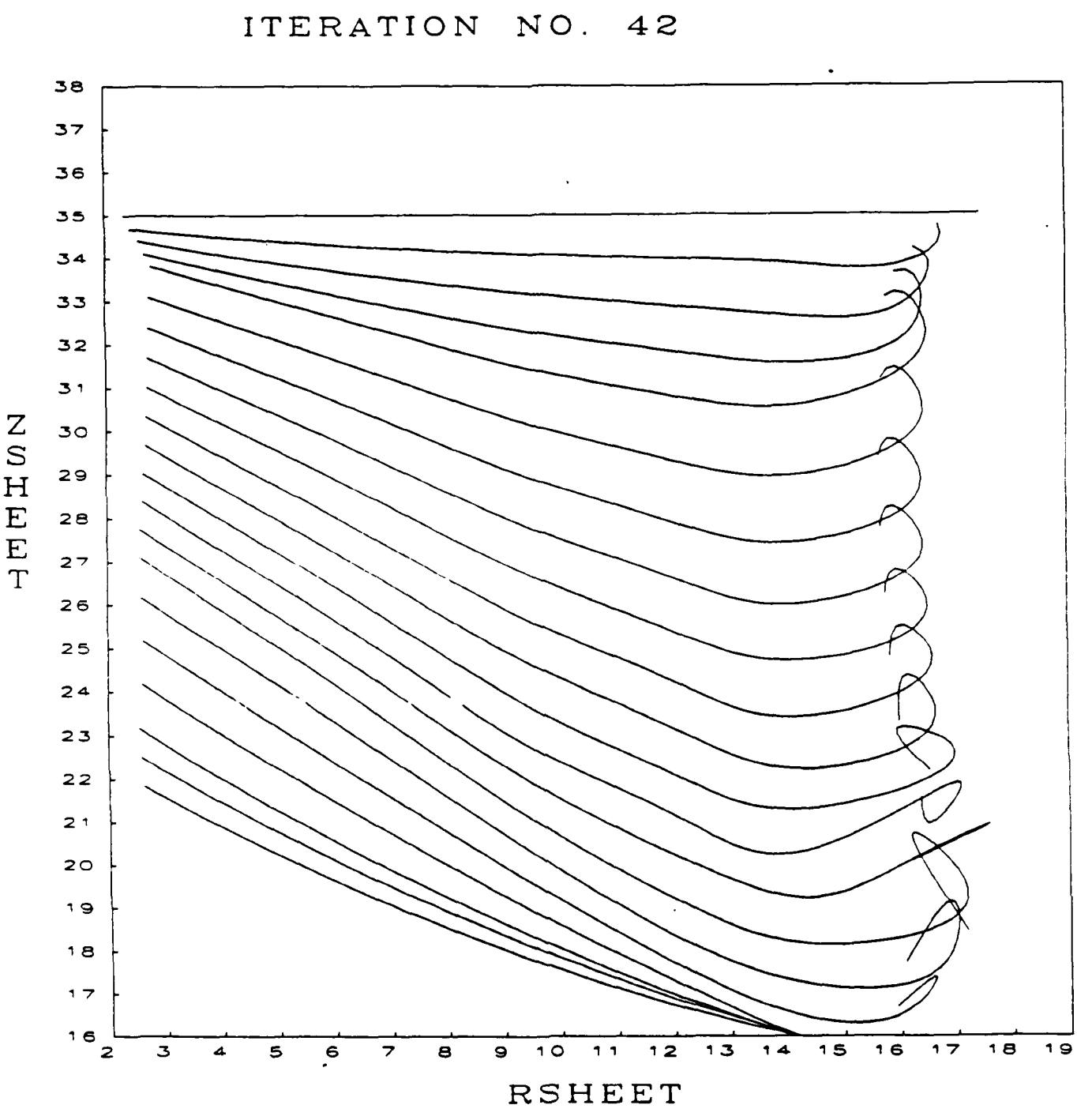

Figure 15H. Wake Geometry for Case 7

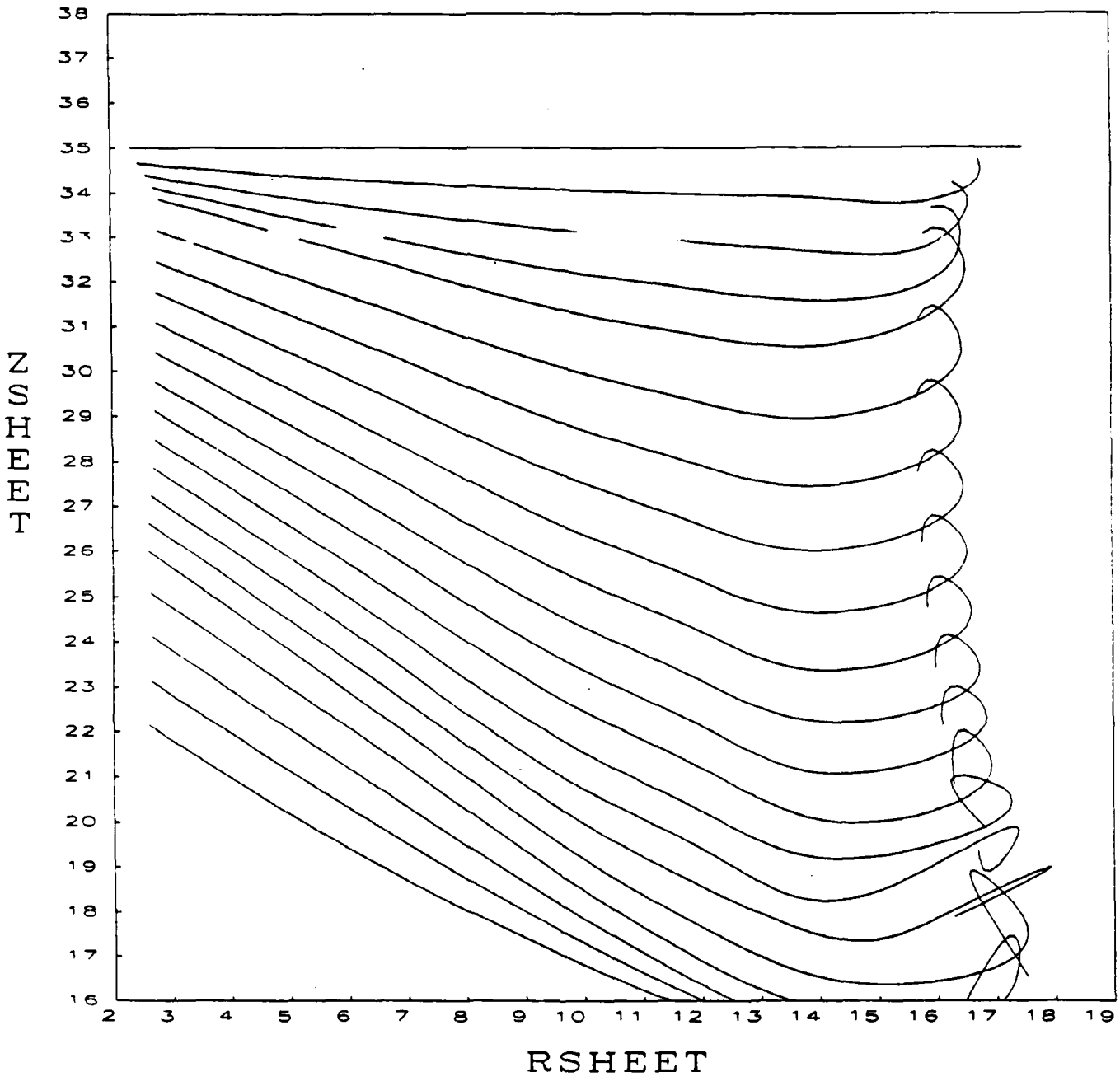

Figure 15I. Wake Geometry for Case 7

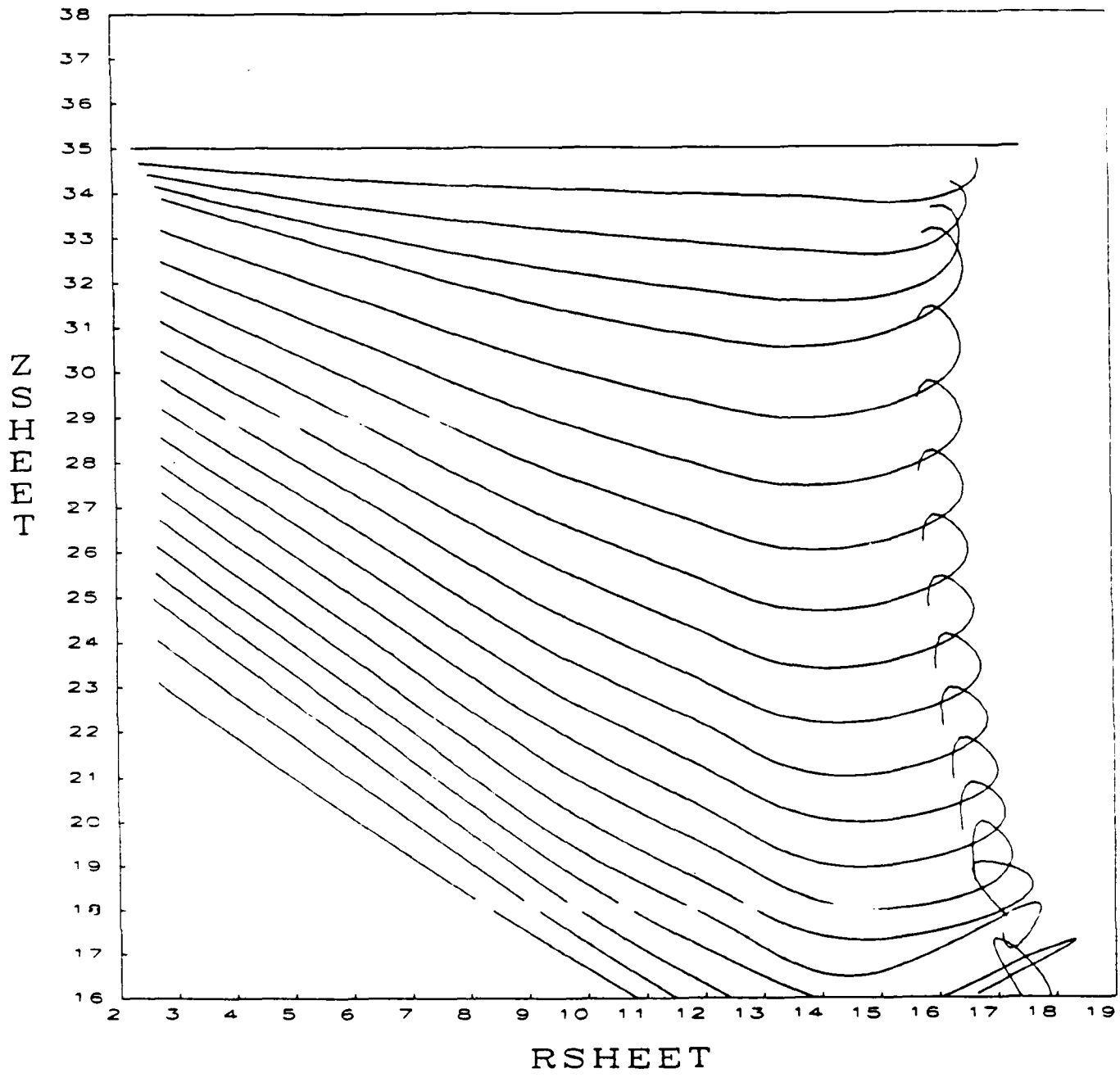

Figure 15J. Wake Geometry for Case 7

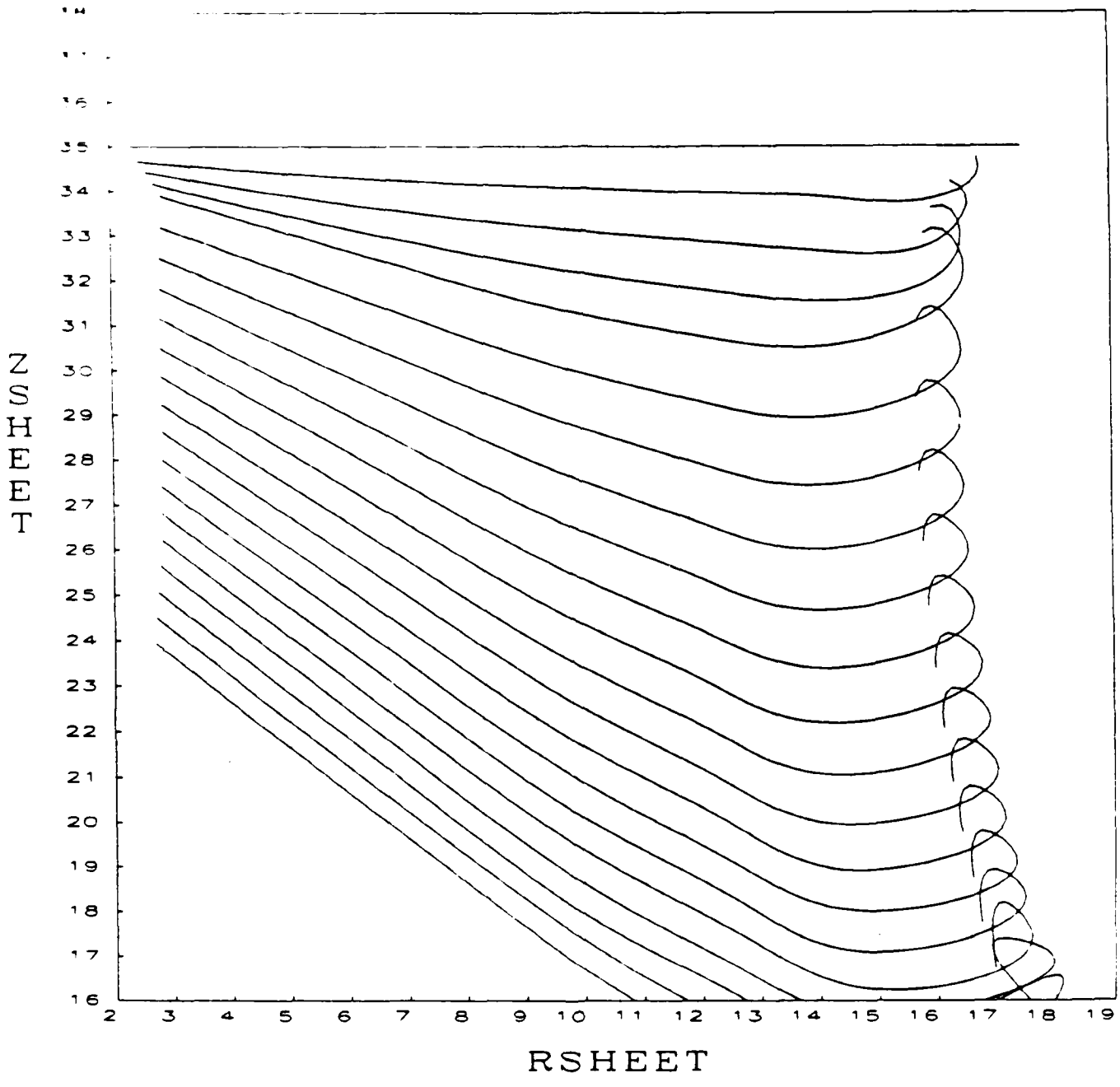

Figure 15K. Wake Geometry for Case 7

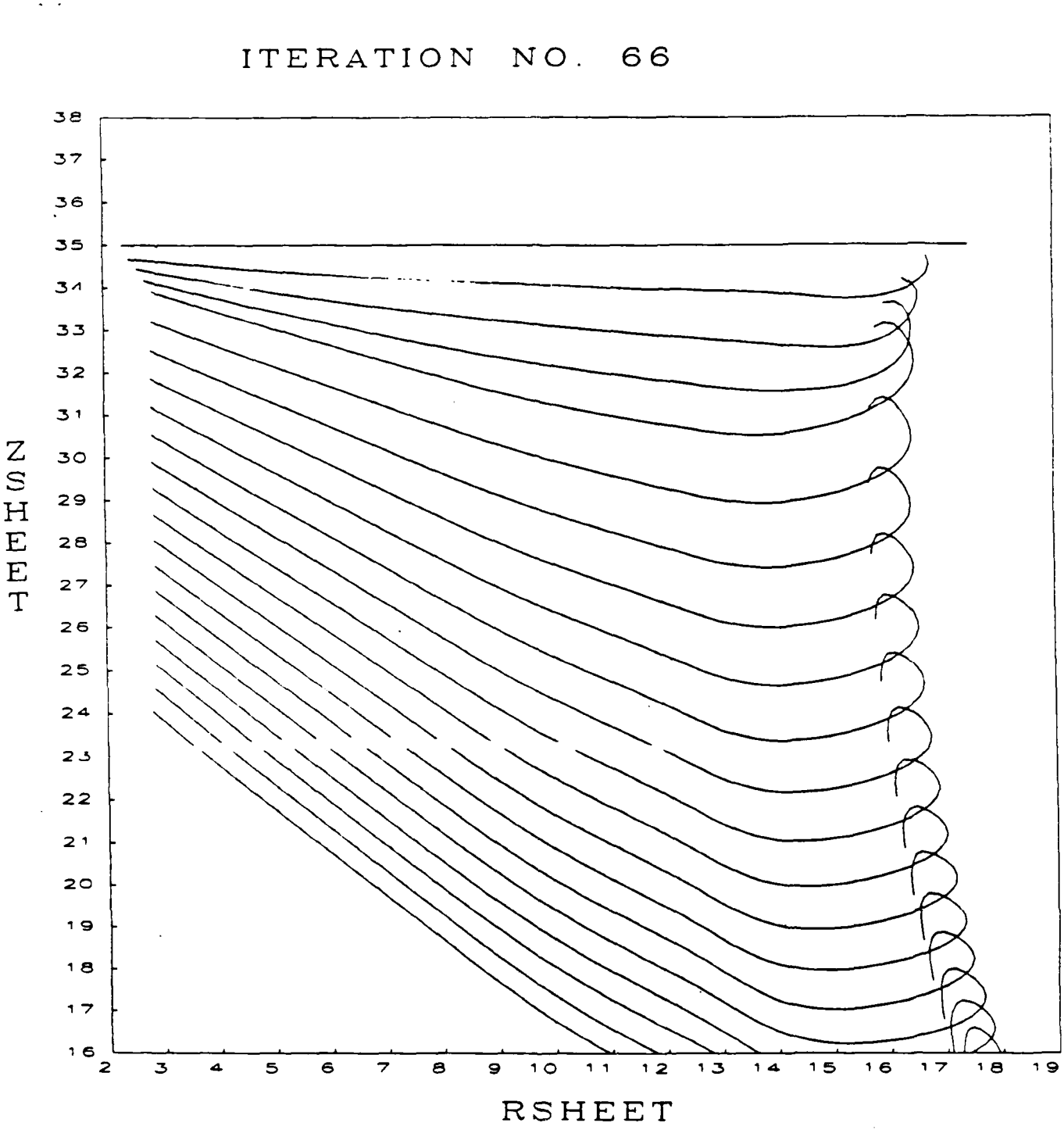

Figure 15L. Wake Geometry for Case 7

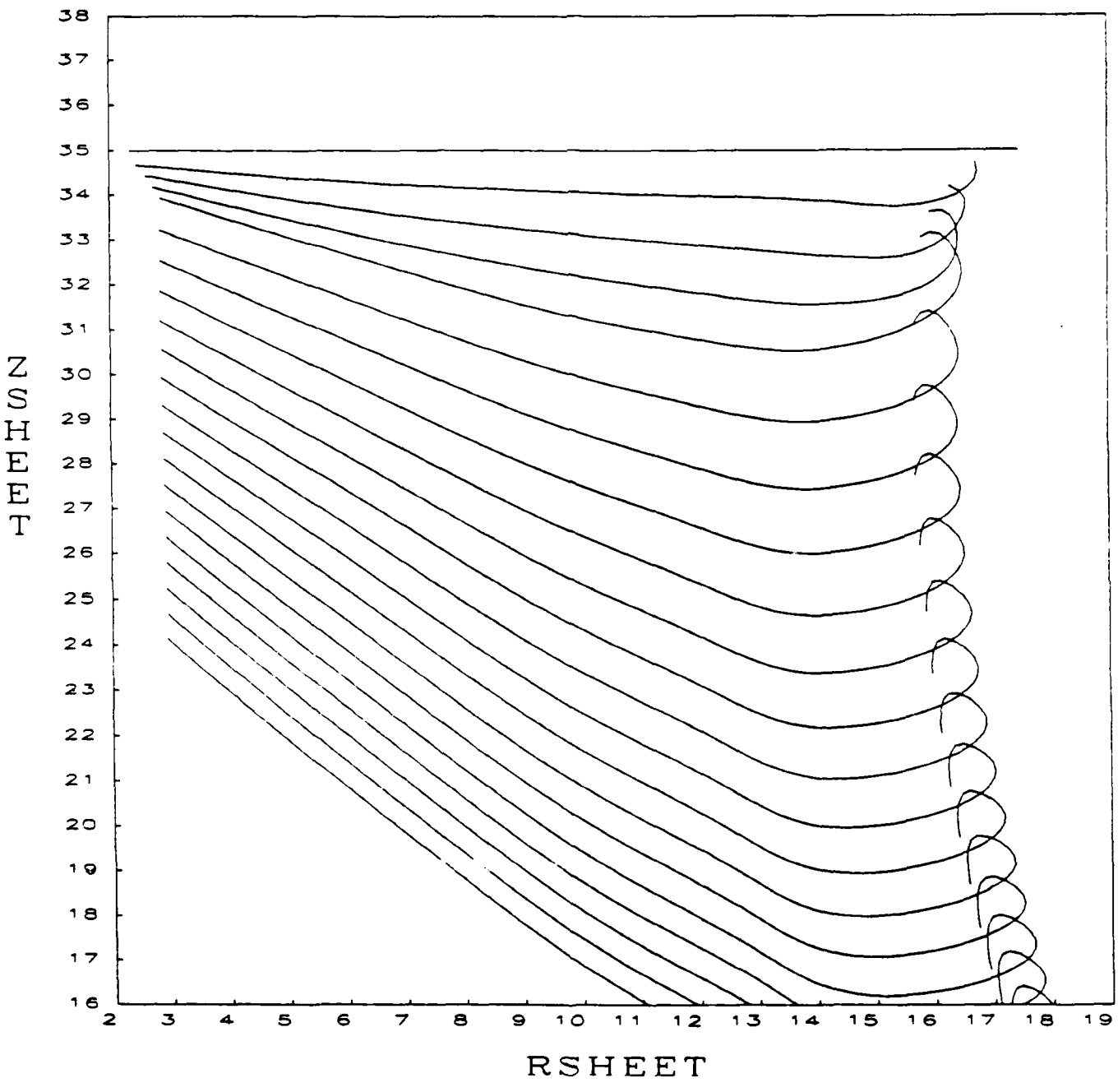

Figure 15M. Wake Geometry for Case 7

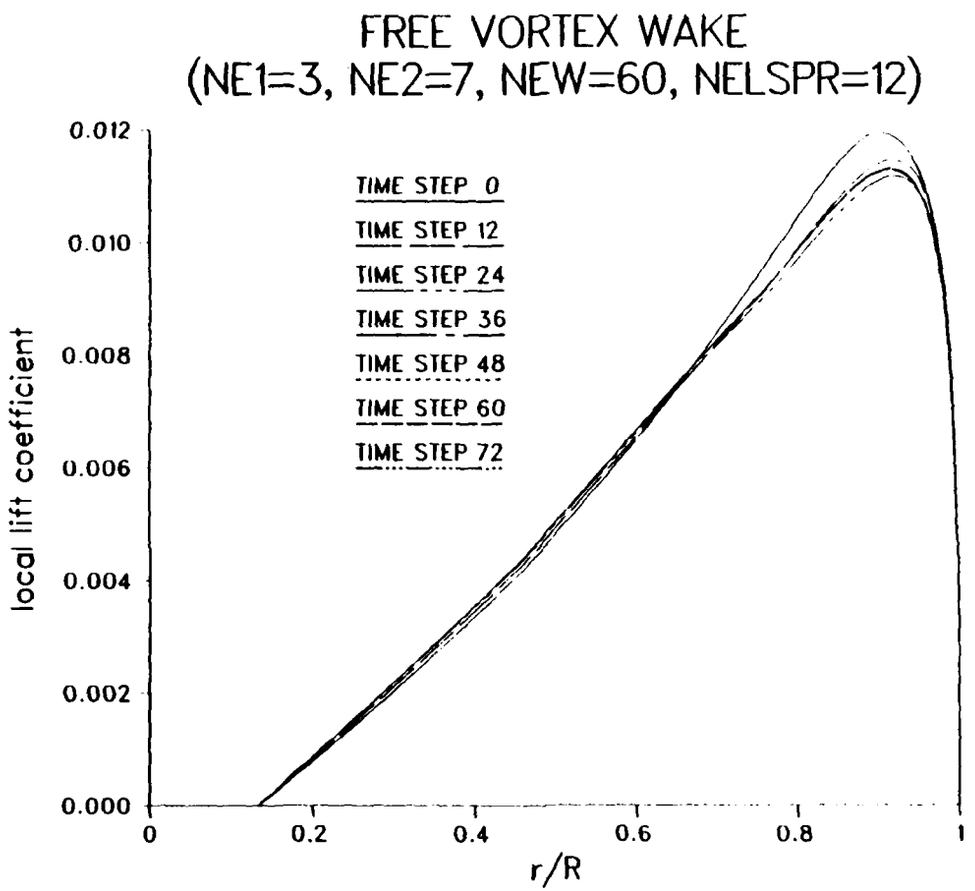

Figure 16. Sectional Lift Distribution for Case 7

END

FILMED

1-86

DTIC